

Quasi-linear regime and rare-event tails of decaying Burgers turbulence

P. Valageas

Institut de Physique Théorique, CEA Saclay, 91191 Gif-sur-Yvette, France

(Dated: November 11, 2018)

We study the decaying Burgers dynamics in d dimensions for random Gaussian initial conditions. We focus on power-law initial energy spectra, such that the system shows a self-similar evolution. This is the case of interest for the “adhesion model” in cosmology and a standard framework for “decaying Burgers turbulence”. We briefly describe how the system can be studied through perturbative expansions at early time or large scale (quasi-linear regime). Next, we develop a saddle-point method, based on spherical instantons, that allows to obtain the asymptotic probability distributions $\mathcal{P}(\eta_r)$ and $\mathcal{P}(\Theta_r)$, of the density and velocity increment over spherical cells, reached in the quasi-linear regime. Finally, we show how this approach can be extended to take into account the formation of shocks and we derive the rare-event tails of these probability distributions, at any finite time and scale. This also gives the high-mass tail of the mass function of point-like singularities (shocks in the one dimensional case).

PACS numbers: Valid PACS appear here

I. INTRODUCTION

The Burgers equation [1, 2, 3], which describes the evolution of a compressible pressureless fluid, with a non-zero viscosity, was first introduced as a simplified model of fluid turbulence, as it shares the same hydrodynamical (advective) nonlinearity and several conservation laws with the Navier-Stokes equation. It also displays strong intermittency, associated with anomalous scaling exponents for the velocity structure functions, but this arises from the formation of shocks (i.e. singular structures in the inviscid limit $\nu \rightarrow 0^+$) where energy is dissipated, whereas the structures that appear in Navier-Stokes turbulence seem to be more varied and less singular (because of pressure effects) [4]. Nevertheless, due to its greater simplicity - it can actually be explicitly integrated through the Hopf-Cole transformation [5, 6] - the Burgers dynamics retains much interest for hydrodynamical studies, particularly as a useful benchmark for approximation schemes [7]. On the other hand, the Burgers equation also appears in many physical problems, such as the propagation of nonlinear acoustic waves in non-dispersive media [8], the study of disordered systems and pinned manifolds [9], or the formation of large-scale structures in cosmology [10, 11], see [3] for a recent review. In the cosmological context, where one considers the inviscid limit without external forcing, it is known as the “adhesion model” and it provides a good description of the large-scale filamentary structure of the cosmic web [12]. Then, one is interested in the statistical properties of the dynamics, as described by the density and velocity fields, starting with a random Gaussian initial velocity [2, 13] and a uniform density. These initial conditions are the signature of quantum fluctuations generated in the primordial Universe and agree with the small Gaussian fluctuations observed on the cosmic microwave background. In the hydrodynamical context, this setup corresponds to “decaying Burgers turbulence” [13].

This problem has led to many studies, focusing on

power-law initial energy spectra (fractional Brownian motion) in one dimension, $E_0(k) \propto k^n$, especially for the two peculiar cases of white-noise initial velocity ($n = 0$) [1, 2, 14, 15] or Brownian motion initial velocity ($n = -2$) [14, 16, 17, 18]. Indeed, in these two cases the initial velocity field is built from a white-noise stochastic field (either directly or through one integration), which gives rise to Markovian processes and allows to derive many explicit analytical results. For more general n , it is not possible to obtain full explicit solutions, but several properties of the dynamics are already known [8, 13]. In particular, for $-3 < n < 1$, the system shows a self-similar evolution as shocks merge to form increasingly massive objects separated by a typical length, $L(t)$ - the integral scale of turbulence - that grows as $L(t) \sim t^{2/(n+3)}$, while the shock mass function scales as $\ln[n(> m)] \sim -m^{n+3}$ at large masses [13, 14, 19, 20]. In spite of these common scalings, the range $-3 < n < 1$ can be further split into two classes, as shocks are dense for $-3 < n < -1$ but isolated for $-1 < n < 1$ [14].

In this article, we consider the decaying Burgers dynamics in d dimensions, for random Gaussian initial conditions and power-law initial energy spectra such that the system displays a self-similar evolution. This is in particular the case of interest in the cosmological context, which shows a hierarchical evolution as increasingly large scales turn nonlinear as time goes on. Applying to the Burgers dynamics methods that have been used to study the collisionless gravitational dynamics encountered in cosmology, we present a saddle-point approximation (instanton technique) that allows to derive some properties of the velocity and density fields in two regimes, i) the quasi-linear regime associated with early times or large scales, and ii) the rare-event tails of the velocity and density distributions at any time or scale.

This article is organized as follows. We first introduce in section II the equations of motion and the initial conditions that define our system and we recall the geometrical interpretation of the Hopf-Cole solution of the

dynamics. We also define the overdensity, η_r , and the velocity divergence (i.e. spherical velocity increment), Θ_r , within spherical cells of radius r , that are the two quantities that we study in this paper. Then, we briefly describe in section III how the dynamics can be studied through perturbative expansions, that hold at early times or large scales, and we make the connection with the Zel'dovich dynamics that is equivalent from a perturbative point of view. Next, we present in section IV a saddle-point approximation that allows to derive the asymptotic probability distributions $\mathcal{P}(\eta_r)$ and $\mathcal{P}(\Theta_r)$ reached in the quasi-linear limit (i.e. at early times or large scales). Then, we show in section V how to modify this approach to take into account shocks, and we derive the rare-event tails of these probability distributions, at any fixed time and scale. This also yields the high-mass tail of the mass function of point-like objects (shocks in the one dimensional case). Finally, we conclude in section VI.

II. BURGERS DYNAMICS

A. Equations of motion and initial conditions

We consider the d -dimensional Burgers equation in the inviscid limit (with $d \geq 1$),

$$\partial_t \mathbf{u} + (\mathbf{u} \cdot \nabla) \mathbf{u} = \nu \Delta \mathbf{u}, \quad \nu \rightarrow 0^+, \quad (1)$$

for the velocity field $\mathbf{u}(\mathbf{x}, t)$, and the evolution of the density field $\rho(\mathbf{x}, t)$ generated by this dynamics, starting from a uniform density ρ_0 at the initial time $t = 0$. The latter obeys the usual continuity equation

$$\partial_t \rho + \nabla \cdot (\rho \mathbf{u}) = 0 \quad \text{and} \quad \rho(\mathbf{x}, 0) = \rho_0. \quad (2)$$

Then, since there is no external forcing in Eqs.(1)-(2), the stochasticity arises from the random initial velocity $\mathbf{u}_0(\mathbf{x})$, which we take to be Gaussian and isotropic, whence $\langle \mathbf{u} \rangle = 0$ by symmetry. Moreover, as is well-known [3], if the initial velocity is potential, $\mathbf{u}_0 = -\nabla \psi_0$, it remains so forever, so that the velocity field is fully defined by its potential $\psi(\mathbf{x}, t)$, or by its divergence $\theta(\mathbf{x}, t)$, through

$$\mathbf{u} = -\nabla \psi, \quad \theta = -\nabla \cdot \mathbf{u} = \Delta \psi. \quad (3)$$

Normalizing Fourier transforms as

$$\theta(\mathbf{x}) = \int d\mathbf{k} e^{i\mathbf{k} \cdot \mathbf{x}} \tilde{\theta}(\mathbf{k}), \quad (4)$$

the initial divergence θ_0 is taken as Gaussian, homogeneous and isotropic, so that it is fully described by its power spectrum $P_{\theta_0}(k)$ with

$$\langle \tilde{\theta}_0 \rangle = 0, \quad \langle \tilde{\theta}_0(\mathbf{k}_1) \tilde{\theta}_0(\mathbf{k}_2) \rangle = \delta_D(\mathbf{k}_1 + \mathbf{k}_2) P_{\theta_0}(k_1), \quad (5)$$

where we note δ_D the Dirac distribution. In this article we focus on the power-law initial power spectra,

$$P_{\theta_0}(k) \propto k^{n+3-d} \quad \text{with} \quad -3 < n < 1. \quad (6)$$

Thus, the initial conditions obey the scaling laws

$$\lambda > 0: \quad \tilde{\theta}_0(\lambda^{-1} \mathbf{k}) \stackrel{\text{law}}{=} \lambda^{d - \frac{n+3}{2}} \tilde{\theta}_0(\mathbf{k}), \quad (7)$$

$$\theta_0(\lambda \mathbf{x}) \stackrel{\text{law}}{=} \lambda^{-\frac{n+3}{2}} \theta_0(\mathbf{x}), \quad (8)$$

where “ $\stackrel{\text{law}}{=}$ ” means that both sides have the same statistical properties. This means that there is no preferred scale in the system and the Burgers dynamics will generate a self-similar evolution for $-3 < n < 1$, as seen in section II D. This is why we only consider the range $-3 < n < 1$ in this article. For the initial velocity and potential this yields for any $\lambda > 0$,

$$\mathbf{u}_0(\lambda \mathbf{x}) \stackrel{\text{law}}{=} \lambda^{-\frac{n+1}{2}} \mathbf{u}_0(\mathbf{x}), \quad \psi_0(\lambda \mathbf{x}) \stackrel{\text{law}}{=} \lambda^{\frac{1-n}{2}} \psi_0(\mathbf{x}). \quad (9)$$

Since we have $\tilde{\mathbf{u}}(\mathbf{k}, t) = i(\mathbf{k}/k^2) \tilde{\theta}(\mathbf{k}, t)$, the initial energy spectrum is a power law,

$$\langle \tilde{\mathbf{u}}_0(\mathbf{k}_1) \cdot \tilde{\mathbf{u}}_0(\mathbf{k}_2) \rangle = \delta_D(\mathbf{k}_1 + \mathbf{k}_2) E_0(k_1), \quad (10)$$

with

$$E_0(k) = k^{-2} P_{\theta_0}(k) \propto k^{n+1-d}. \quad (11)$$

The initial velocity correlation at distance x reads as

$$\begin{aligned} \langle \mathbf{u}_0(\mathbf{x}_1) \cdot \mathbf{u}_0(\mathbf{x}_2) \rangle &= \int d\mathbf{k} e^{i\mathbf{k} \cdot \mathbf{x}} E_0(k) \\ &= (2\pi)^{\frac{d}{2}} \int_0^\infty dk k^{d-1} \frac{J_{\frac{d}{2}-1}(kx)}{(kx)^{\frac{d}{2}-1}} E_0(k) \propto x^{-n-1}, \end{aligned} \quad (12)$$

where $\mathbf{x} = \mathbf{x}_2 - \mathbf{x}_1$ and $J_{\frac{d}{2}-1}(kx)$ is the Bessel function of the first kind of order $d/2 - 1$, whereas the initial one-point variance is

$$\langle |\mathbf{u}_0|^2 \rangle = \int d\mathbf{k} E_0(k) = \frac{2\pi^{\frac{d}{2}}}{\Gamma(d/2)} \int_0^\infty dk k^{d-1} E_0(k). \quad (13)$$

Thus, for $-1 < n < 1$ the initial velocity correlation decreases at large distance as the power law (12), in agreement with the scaling (9), while the one-point variance at $x = 0$, Eq.(13), diverges because of the contribution from high wavenumbers. Then, the initial velocity field is singular (e.g., a white noise for $d = 1$ and $n = 0$) but this ultraviolet divergence is regularized as soon as $t > 0$ by the infinitesimal viscosity [1]. For $-3 < n < -1$ the integral (13) shows an infrared divergence. In this case, the initial velocity field is no longer homogeneous and only has homogeneous increments (but the divergence θ_0 is still homogeneous) [4]. Then, to build the initial velocity from its divergence one must choose a reference point, such as the origin $\mathbf{x}_0 = 0$, with $\mathbf{u}_0(\mathbf{x}_0) = 0$, and define the initial velocity in real space as

$$\mathbf{u}_0(\mathbf{x}) = \int d\mathbf{k} (e^{i\mathbf{k} \cdot \mathbf{x}} - e^{i\mathbf{k} \cdot \mathbf{x}_0}) \tilde{\mathbf{u}}_0(\mathbf{k}), \quad \text{for} \quad -3 < n < -1. \quad (14)$$

Then, Equation (12) no longer applies but the initial second-order structure function, $\langle |\mathbf{u}_0(\mathbf{x}) - \mathbf{u}_0(\mathbf{x}_0)|^2 \rangle$,

grows as x^{-n-1} . Note that because of the nonlinear advective term in the Burgers equation (1), the increments of the velocity field are no longer homogeneous for $t > 0$, which also means that the divergence $\theta(\mathbf{x}, t)$ is no longer homogeneous either. However, at large distance from the reference point (i.e. taking the limit $|\mathbf{x}_0| \rightarrow \infty$ or $|\mathbf{x}| \rightarrow \infty$), we can expect to recover an homogeneous system (in terms of velocity increments and matter distribution), see [21] for more detailed discussions. This can be shown explicitly for the case $d = 1$ and $n = -2$, where the initial velocity field is a Brownian motion [17, 18]. On the other hand, we may add a low- k cutoff Λ to the initial power spectrum and restrict ourselves to finite times and scales where the influence of the infrared cutoff is expected to vanish for equal-time statistics.

B. Density contrast and linear mode

In order to follow the evolution of the matter distribution we define the density contrast, $\delta(\mathbf{x}, t)$, by

$$\delta(\mathbf{x}, t) = \frac{\rho(\mathbf{x}, t) - \rho_0}{\rho_0}. \quad (15)$$

Then, if we linearize the equations of motion (1)-(2) we obtain the solution

$$\tilde{\theta}_L(\mathbf{k}, t) = \tilde{\theta}_0(\mathbf{k})e^{-\nu k^2 t}, \quad \tilde{\delta}_L(\mathbf{k}, t) = \tilde{\theta}_0(\mathbf{k}) \frac{1 - e^{-\nu k^2 t}}{\nu k^2}, \quad (16)$$

where the subscript L stands for the ‘‘linear’’ mode. In the inviscid limit, $\nu \rightarrow 0^+$, this yields

$$\nu \rightarrow 0^+ : \quad \tilde{\theta}_L(\mathbf{k}, t) = \tilde{\theta}_0(\mathbf{k}), \quad \tilde{\delta}_L(\mathbf{k}, t) = t \tilde{\theta}_0(\mathbf{k}), \quad (17)$$

which could also be obtained by setting $\nu = 0$ in Eq.(1). Then, when we study the system at a finite time $t > 0$, we can as well define the initial conditions by the linear density field $\delta_L(\mathbf{x}, t)$, which is Gaussian, homogeneous and isotropic, with a power spectrum

$$-3 < n < 1 : \quad P_{\delta_L}(k, t) = t^2 P_{\theta_0}(k) \propto t^2 k^{n+3-d}, \quad (18)$$

and an equal-time two-point correlation

$$\begin{aligned} C_{\delta_L}(\mathbf{x}_1, \mathbf{x}_2) &= \langle \delta_L(\mathbf{x}_1, t) \delta_L(\mathbf{x}_2, t) \rangle \\ &= (2\pi)^{\frac{d}{2}} \int_0^\infty dk k^{d-1} \frac{J_{\frac{d}{2}-1}(kx)}{(kx)^{\frac{d}{2}-1}} P_{\delta_L}(k) \propto t^2 x^{-n-3}, \end{aligned} \quad (19)$$

where $x = |\mathbf{x}_2 - \mathbf{x}_1|$. Note that for any $n > -3$ the initial density field is homogeneous, even though the initial velocity only shows homogeneous increments when $-3 < n < -1$.

Here we may add a few comments on the initial conditions that are relevant to the cosmological context. Let us first briefly recall how the Burgers equation (1) arises in this case. In the standard cold dark matter scenario [22], about 83% of the matter content of the Universe is

in the form of a cold dark matter component, whereas ordinary baryonic matter only forms the remaining 17% (in addition, there is a dark energy component, which is consistent with a cosmological constant in the Einstein equations, which makes about 72% of the energy content of the Universe, while the previous two matter components only form the remaining 28%), see [23]. The cold dark matter has a negligible velocity dispersion (whence the label ‘‘cold’’) and it has only very weak non-gravitational interactions (whence the label ‘‘dark’’, as it has only been ‘‘seen’’ through its gravitational effects so far). Then, it is well described as a pressure-less fluid coupled to its own gravity (here we focus on the late Universe, after the end of the radiation-dominated era, about 5×10^4 years after the Big Bang, and on scales smaller than the Hubble scale, where the Newtonian approximation is valid). Therefore, the growth of matter density fluctuations is governed by the pressure-less Euler equation and the continuity equation, coupled to the Poisson equation, in an expanding background [24]. Since the gravitational force derives from the scalar gravitational potential, it does not generate any vorticity, and any primordial vorticity is diluted by the expansion of the Universe (this only holds in the linear regime, as shell-crossings can generate vorticity in a non-perturbative fashion). Then, using a rescaling of time and velocity field, that brings out the deviations from the mean Hubble flow (and also absorbs the effect of the uniform cosmological constant), and making the approximation that the velocity and gravitational potentials remain equal (this is exact in the linear regime and in one dimension, $d = 1$, before shell-crossing), one obtains the Zeldovich equation [25]. This corresponds to the Burgers equation (1) with $\nu = 0$. Then, one adds an infinitesimal viscosity, $\nu \rightarrow 0^+$, to prevent shell-crossing [10, 11]. This induces a sticking of particles within shocks, that is intended to mimic the trapping within gravitational potential wells [12].

Next, in the cosmological context, the present matter density fluctuations are assumed to arise from the growth of tiny quantum fluctuations generated during an inflationary stage in the early Universe. Moreover, these Gaussian initial fluctuations almost have a Harrison-Zeldovich power spectrum, that corresponds to $n = 1$ in Eq.(18) above (observations give $n \simeq 0.96$ [23]). The case $n = 1$ is also called ‘‘scale-invariant’’, as it gives a gravitational potential power spectrum of the form $P_{\psi_0}(k) \propto k^{n-1-d} = k^{-d}$, so that all wavenumbers contribute with the same weight and the two-point correlation is formally scale-invariant, $C_{\psi_0}(\mathbf{x}) \propto \int dk k^{d-1} P_{\psi_0}(k) W(kx)$ is independent of x (where $W(kx)$ is some filtering function on scale x). Within the inflationary scenario, this property arises from the fact that the only relevant scale is the Hubble scale, that remains roughly constant during this stage (this can also be understood from the fact that during an exponential expansion there is no genuine origin of time, i.e. the de Sitter spacetime is invariant under time translations, so that wavelengths generated at different times share the same properties). Then, since

these fluctuations have remained small until recent times they have evolved through linear theory until the matter-dominated era and the Newtonian regime. Therefore, they have remained Gaussian and different wavenumbers have evolved independently (the linearized equations of motion are diagonal in Fourier space) until a redshift $z \sim 10^3$. However, the primordial spectrum with $n \simeq 1$ has been modified in-between, during the radiation-dominated era. Indeed, during this stage, density fluctuations on scales larger than the Horizon keep growing whereas they oscillate on small scales, due to the pressure associated with the coupling to the radiation component of the Universe (photons). This implies that fluctuations $\tilde{\delta}_L(\mathbf{k})$ are multiplied by a transfer function $T(k)$ that decays as k^{-2} at high wavenumbers. Then, the ‘‘initial’’ density power spectrum $P_{\delta_0}(k)$ used to study the formation of large-scale structures in the late Universe is the primordial one, with $n \simeq 1$, multiplied by $T(k)^2$. This yields a curved cold dark matter power spectrum, with a local slope n that runs from 1 at low k to -3 at high k . Thus, today at $z = 0$ we have $n \simeq -2$ on galactic scales and $n \simeq -1$ slightly above cluster scales [24, 26]. This corresponds to the range studied in this article. Then, power-law power spectra with $-3 < n < 1$ can model the dynamics on the ranges of interest for specific purposes. On the other hand, the simplifications associated with power-law power spectra, such as the scaling laws (39)-(41) and the self-similar evolution (43) seen below, can be used to check the accuracy of numerical algorithms and to shed light on the dynamics [27].

C. Spherically symmetric statistics

In this article, in order to take advantage of the statistical isotropy of the system, we focus on two spherically symmetric quantities, the overdensity, η_r , and the mean divergence, Θ_r , within spherical cells of radius r , which we define as

$$\eta_r = \frac{m(< r)}{\rho_0 V} = \frac{\rho_r}{\rho_0} = 1 + \delta_r \quad \text{with} \quad \delta_r = \int_V \frac{d\mathbf{x}}{V} \delta(\mathbf{x}), \quad (20)$$

and

$$\Theta_r = t \int_V \frac{d\mathbf{x}}{V} \theta(\mathbf{x}) = -\frac{t}{V} \int_S d\mathbf{x} \mathbf{u}(\mathbf{x}) \cdot \hat{\mathbf{x}}, \quad (21)$$

where we used Eq.(3). Here V and S are the volume and the surface of the $(d-1)$ -sphere of radius r , $\hat{\mathbf{x}}$ the unit radial vector, and we multiplied the divergence θ by time t in the definition (21) to have a dimensionless quantity Θ_r . The moments $\langle \Theta_r^p \rangle$ can be understood as dimensionless spherical velocity structure functions, the usual longitudinal velocity structure functions being defined as $\langle [(\mathbf{u}(\mathbf{x}) - \mathbf{u}(0)) \cdot \hat{\mathbf{x}}]^p \rangle$ for a given direction $\hat{\mathbf{x}}$ and length $|\mathbf{x}|$, while in (21) we integrate over all directions. In one dimension, $d = 1$, up to a sign, Θ_r is simply the

dimensionless velocity increment over the distance $2r$,

$$d = 1 : \quad \Theta_r = -\frac{t}{2r} [u(r) - u(-r)]. \quad (22)$$

In arbitrary dimension, $-\Theta_r$ is the dimensionless velocity increment over distance $2r$ averaged over all directions about a given point. We investigate in this article the probability distributions $\mathcal{P}(\eta_r)$ and $\mathcal{P}(\Theta_r)$ in the quasi-linear regime (i.e. at large scales or early times), and their tails in any regime. The system being homogeneous we can focus on the cell that is centered on the origin, and this gives in Fourier space

$$\delta_r = \int d\mathbf{k} \tilde{\delta}(\mathbf{k}) W(kr), \quad \text{with} \quad (23)$$

$$W(kr) = \int_V \frac{d\mathbf{x}}{V} e^{i\mathbf{k} \cdot \mathbf{x}} = 2^{\frac{d}{2}} \Gamma\left(\frac{d}{2} + 1\right) \frac{J_{\frac{d}{2}}(kr)}{(kr)^{\frac{d}{2}}}. \quad (24)$$

In the linear regime we obtain from Eq.(17)

$$\delta_{Lr} = \Theta_{Lr} = -\frac{t}{V} \int_S d\mathbf{x} \mathbf{u}_0(\mathbf{x}) \cdot \hat{\mathbf{x}}. \quad (25)$$

For the initial conditions (18) the linear density contrast δ_{Lr} is Gaussian, of mean zero, $\langle \delta_{Lr} \rangle = 0$, and covariance $C_{\delta_{Lr}}(r_1, r_2)$ with

$$C_{\delta_{Lr}}(r_1, r_2) = \langle \delta_{Lr_1} \delta_{Lr_2} \rangle \quad (26)$$

$$= \frac{2\pi^{\frac{d}{2}}}{\Gamma[\frac{d}{2}]} \int_0^\infty dk k^{d-1} P_{\delta_L}(k) W(kr_1) W(kr_2) \quad (27)$$

$$\propto \frac{t^2}{(r_1 + r_2)^{n+3}} {}_2F_1\left[\frac{n+3}{2}, \frac{d+1}{2}; d+1; \frac{4r_1 r_2}{(r_1 + r_2)^2}\right] \quad (28)$$

where the last relation (28) only holds for $-3 < n < d-1$ (if $n \geq d-1$ the integral (27) diverges at high k and the correlation $C_{\delta_{Lr}}(r_1, r_2)$ is a distribution, such as a Dirac distribution for $\{n = 0, d = 1\}$).

Then, the linear variance reads as

$$n < d-2 : \quad \sigma_{\delta_{Lr}}^2 = \langle \delta_{Lr}^2 \rangle = C_{\delta_{Lr}}(r, r) \propto t^2 r^{-n-3}. \quad (29)$$

Indeed, we can note that the integral (27) converges at $k \rightarrow 0$ for any $n > -3$ but only converges at $k \rightarrow \infty$ for $n < d-2$, when $r_1 = r_2$. Therefore, in dimensions $d < 3$, the variance $\sigma_{\delta_{Lr}}^2$ shows an ultraviolet divergence for a power index in the range $d-2 \leq n < 1$ (we only consider the range $-3 < n < 1$ in this article). Of course, as soon as $t > 0$, the nonlinear evolution associated with the Burgers dynamics (shocks) makes the nonlinear variance $\langle \delta_r^2 \rangle$ finite. In such a case one could also study the density field smoothed by a Gaussian window, $\propto e^{-|\mathbf{x}|^2/(2r^2)}$, instead of the spherical top-hat (20), to obtain a finite linear variance $\sigma_{\delta_{Lr}}^2$, but we shall not investigate this alternative in this paper.

We also introduce the spherical component of the initial radial velocity, u_{0r} , which reads from Eq.(25) as

$$u_{0r} = -\frac{r}{td} \delta_{Lr}, \quad (30)$$

n	d	$C_{u_{0r}}(r_1, r_2)$	$C_{\psi_{0r}}(r_1, r_2)$	$C_{\delta_{Lr}}(r_1, r_2)$
0	1	$\delta_D(r_1 - r_2)$	r_1	$t^2 \delta_D(r_1 - r_2)/(r_1 r_2)$
0	3	r_1/r_2^2	$r_1(3r_2 - r_1)/(2r_2)$	$9t^2/r_2^3$
-1	2	r_1/r_2	$r_1^2[1 + \ln(r_2/r_1)]/2$	$4t^2/r_2^2$
-2	1	r_1	$r_1^2(3r_2 - r_1)/6$	t^2/r_2
-2	3	$r_1 - r_1^3/(5r_2^2)$	$r_1^2(r_1^2 - 5r_1 r_2 + 10r_2^2)/(20r_2)$	$9t^2[1/r_2 - r_1^2/(5r_2^3)]$
n	$d \rightarrow \infty$	$r_1 r_2 (r_1^2 + r_2^2)^{-(n+3)/2} / d^2$	$[(r_1^2 + r_2^2)^{(1-n)/2} - r_1^{1-n} - r_2^{1-n}] / (d^2(n^2 - 1))$	$t^2 (r_1^2 + r_2^2)^{-(n+3)/2}$

TABLE I: The initial velocity and potential correlations $C_{u_{0r}}(r_1, r_2)$ and $C_{\psi_{0r}}(r_1, r_2)$ of the spherical component of the initial conditions, for some values of n and d where Eqs.(27) and (33) simplify (with a dimensional normalization factor set to unity). The last column shows the covariance of the linear density contrast δ_{Lr} within radius r at time t . Here we assumed $r_1 < r_2$, except for the velocity and density correlations in the case $\{n = 0, d = 1\}$, and formulae for $r_1 > r_2$ are obtained by exchanging r_1 and r_2 . The correlations are singular at $r_1 = r_2$, except in the limit $d \rightarrow \infty$ shown in the last line (where the velocity and potential correlations also become vanishingly small as compared with the density correlation).

since $V = (r/d)S$. This is the mean initial radial velocity at radius r . As with η_r and Θ_r , for spherical components we note the dependent coordinate r as an index, to distinguish from the d -dimensional field $\mathbf{u}_0(\mathbf{x})$ (but contrary to η_r and Θ_r , u_r is the mean radial velocity at radius r , rather than within the volume V). It will also be useful to consider the spherical component of the initial velocity potential, which we define from Eq.(3) as

$$\psi_{0r} = - \int_0^r dr' u_{0r'} = \frac{1}{t d} \int_0^r dr' r' \delta_{Lr'}, \quad (31)$$

that is, we choose to normalize the initial potential by $\psi_0(0) = 0$. Then, the initial radial velocity and potential two-point correlations are

$$C_{u_{0r}}(r_1, r_2) = \frac{\partial^2}{\partial r_1 \partial r_2} C_{\psi_{0r}}(r_1, r_2) = \frac{r_1 r_2}{t^2 d^2} C_{\delta_{Lr}}(r_1, r_2), \quad (32)$$

which can be obtained from Eqs.(26)-(28), and

$$C_{\psi_{0r}}(r_1, r_2) = \frac{2^{d+1} \pi^{\frac{d}{2}} \Gamma(\frac{d}{2} + 1)^2}{\Gamma(d/2) d^2} \int_0^\infty dk k^{d-5} P_{\theta_0}(k) \times \left(\frac{J_{\frac{d}{2}-1}(kr_1)}{(kr_1)^{\frac{d}{2}-1}} - \frac{2^{1-\frac{d}{2}}}{\Gamma[\frac{d}{2}]} \right) \left(\frac{J_{\frac{d}{2}-1}(kr_2)}{(kr_2)^{\frac{d}{2}-1}} - \frac{2^{1-\frac{d}{2}}}{\Gamma[\frac{d}{2}]} \right), \quad (33)$$

with a variance

$$-3 < n < 1: \quad \sigma_{\psi_{0r}}^2 = C_{\psi_{0r}}(r, r) \propto r^{1-n}. \quad (34)$$

Note that $\sigma_{\psi_{0r}}^2$ is finite and well-defined over the whole range $-3 < n < 1$. We give in Table I the initial radial velocity and potential correlations $C_{u_{0r}}(r_1, r_2)$ and $C_{\psi_{0r}}(r_1, r_2)$ for a few low integer values of n and d where they take a simple form, as well as the limit $d \rightarrow \infty$. We also show the covariance $C_{\delta_{Lr}}(r_1, r_2)$ of the linear density contrast at time t within radius r , from Eq.(27). We can check that they satisfy Eq.(32). The formulae are written

for $r_1 < r_2$ (except for the velocity and density correlations in the case $\{n = 0, d = 1\}$) with a dimensional normalization factor set to unity. For these power-law initial power spectra, the normalizations used in Table I can always be achieved by a rescaling of spatial coordinates.

D. Hopf-Cole solution and self-similarity

As is well known, the nonlinear Burgers equation (1) can be solved through the Hopf-Cole transformation [5, 6], by making the change of variable $\psi(\mathbf{x}, t) = 2\nu \ln \Xi(\mathbf{x}, t)$. This yields the linear heat equation for $\Xi(\mathbf{x}, t)$, which leads to the solution

$$\psi(\mathbf{x}, t) = 2\nu \ln \int \frac{d\mathbf{q}}{(4\pi\nu t)^{d/2}} \exp \left[\frac{\psi_0(\mathbf{q})}{2\nu} - \frac{|\mathbf{x} - \mathbf{q}|^2}{4\nu t} \right]. \quad (35)$$

Then, in the inviscid limit $\nu \rightarrow 0^+$, a steepest-descent method gives [1, 3]

$$\psi(\mathbf{x}, t) = \max_{\mathbf{q}} \left[\psi_0(\mathbf{q}) - \frac{|\mathbf{x} - \mathbf{q}|^2}{2t} \right]. \quad (36)$$

If there is no shock, the maximum in (36) is reached at a unique point $\mathbf{q}(\mathbf{x}, t)$, which is the Lagrangian coordinate of the particle that is located at the Eulerian position \mathbf{x} at time t [1, 3]. Moreover, this particle has kept its initial velocity and we have

$$\mathbf{u}(\mathbf{x}, t) = \mathbf{u}_0(\mathbf{q}) = \frac{\mathbf{x} - \mathbf{q}(\mathbf{x}, t)}{t}. \quad (37)$$

If we have a shock at position \mathbf{x} there are several degenerate solutions to (36) and the velocity is discontinuous (as seen from Eq.(37), as we move from one solution \mathbf{q}_- to another one \mathbf{q}_+ when we go through \mathbf{x} from one side

of the shock surface to the other side) while the density is infinite. The solution (36) has a nice geometrical interpretation in terms of paraboloids [1, 3]. Thus, let us consider the family of upward paraboloids $\mathcal{P}_{\mathbf{x},c}(\mathbf{q})$ centered at \mathbf{x} and of height c , with a curvature radius t ,

$$\mathcal{P}_{\mathbf{x},c}(\mathbf{q}) = \frac{|\mathbf{q} - \mathbf{x}|^2}{2t} + c. \quad (38)$$

Then, moving down $\mathcal{P}_{\mathbf{x},c}(\mathbf{q})$ from $c = +\infty$, where the paraboloid is everywhere well above the initial potential $\psi_0(\mathbf{q})$ (this is possible for the initial conditions (6) since we have $|\psi_0(\mathbf{q})| \sim q^{(1-n)/2}$, which grows more slowly than q^2 at large distances), until it touches the surface defined by $\psi_0(\mathbf{q})$, the abscissa \mathbf{q} of this first-contact point is the Lagrangian coordinate $\mathbf{q}(\mathbf{x}, t)$. If first-contact occurs simultaneously at several points there is a shock at the Eulerian location \mathbf{x} . One can build in this manner the inverse Lagrangian map $\mathbf{x} \mapsto \mathbf{q}(\mathbf{x}, t)$.

For the initial conditions (6) that we consider in this paper, the rescaled initial velocity potential $\psi_0(\lambda\mathbf{q})$ has the same probability distribution as $\lambda^{(1-n)/2}\psi_0(\mathbf{q})$ for any $\lambda > 0$, when we normalize by $\mathbf{u}_0(0) = 0$ and $\psi_0(0) = 0$, as seen in Eq.(9). Then, the explicit solution (36) gives the scaling laws

$$\psi(\mathbf{x}, t) \stackrel{\text{law}}{=} t^{\frac{1-n}{n+3}} \psi\left(t^{\frac{-2}{n+3}}\mathbf{x}, 1\right), \quad (39)$$

$$\mathbf{u}(\mathbf{x}, t) \stackrel{\text{law}}{=} t^{\frac{-n-1}{n+3}} \mathbf{u}\left(t^{\frac{-2}{n+3}}\mathbf{x}, 1\right), \quad (40)$$

$$\mathbf{q}(\mathbf{x}, t) \stackrel{\text{law}}{=} t^{\frac{2}{n+3}} \mathbf{q}\left(t^{\frac{-2}{n+3}}\mathbf{x}, 1\right). \quad (41)$$

For the spherical overdensity η_r and the spherical velocity increment Θ_r this yields

$$\mathcal{P}(\eta_r; t) = \overline{\mathcal{P}}\left(\eta; \frac{r}{t^{2/(n+3)}}\right), \quad \mathcal{P}(\Theta_r; t) = \overline{\mathcal{P}}\left(\Theta; \frac{r}{t^{2/(n+3)}}\right), \quad (42)$$

that is, the distributions $\mathcal{P}(\eta_r; t)$ and $\mathcal{P}(\Theta_r; t)$ of the overdensity and velocity divergence at scale r and time t only depend on the ratio $r/t^{2/(n+3)}$.

These scalings mean that the dynamics is self-similar: a rescaling of time is statistically equivalent to a rescaling of distances, as

$$\lambda > 0: \quad t \rightarrow \lambda t, \quad \mathbf{x} \rightarrow \lambda^{\frac{2}{n+3}}\mathbf{x}. \quad (43)$$

Thus, the system displays a hierarchical evolution as increasingly larger scales turn nonlinear. More precisely, since in the inviscid limit there is no preferred scale for the power-law initial conditions (6), the only characteristic scale at a given time t is the so-called integral scale of turbulence, $L(t)$, which is generated by the Burgers dynamics and grows with time as in (43),

$$L(t) \propto t^{2/(n+3)}. \quad (44)$$

It measures the typical distance between shocks, and it separates the large-scale quasi-linear regime, where the energy spectrum and the density power spectrum keep

their initial power-law forms (11) and (18), $P_\delta(k, t) \propto t^2 k^{n+3-d}$, from the small-scale nonlinear regime, which is governed by shocks and point-like masses, where the density power spectrum reaches the universal white-noise behavior (i.e. $P_\delta(k, t)$ has a finite limit for $k \gg 1/L(t)$).

This self-similar evolution only holds for $n < 1$, so that $|\psi_0(\mathbf{q})|$ grows at larger scales, see for instance Eq.(34), and $n > -3$, so that $|\psi_0(\mathbf{q})|$ grows more slowly than q^2 and the solution (36) is well-defined [13]. This is the range that we consider in this paper. The persistence of the initial power law at low k for the energy spectrum, $E(k, t) \propto k^{n+1-d}$, that holds in such cases, is also called the principle of permanence of large eddies [13].

III. PERTURBATIVE EXPANSION AND ZELDOVICH DYNAMICS

Although the Burgers dynamics can be integrated through the Hopf-Cole solution (36), the computation of its statistical properties for random initial conditions remains a difficult problem for general n and d . Only in the peculiar one-dimensional cases $n = 0$ [14, 15, 28, 29, 30] and $n = -2$ [14, 16, 17, 18], with $d = 1$, where the initial velocity is a white noise or a Brownian motion, one can derive explicit analytical results, taking advantage of the Markovian character of these two specific stochastic processes. For general n and d one must resort to approximation methods, such as perturbative expansions, as with most nonlinear dynamics. In particular, at early times we may look for the solution of the equations of motion (1)-(2) as an expansion over powers of time,

$$\begin{aligned} \tilde{\delta}(\mathbf{k}, t) &= \sum_{p=1}^{\infty} t^p \int d\mathbf{k}_1 \dots d\mathbf{k}_p \delta_D(\mathbf{k}_1 + \dots + \mathbf{k}_p - \mathbf{k}) \\ &\quad \times F_p(\mathbf{k}_1, \dots, \mathbf{k}_p) \tilde{\theta}_0(\mathbf{k}_1) \dots \tilde{\theta}_0(\mathbf{k}_p), \end{aligned} \quad (45)$$

and

$$\begin{aligned} \tilde{\theta}(\mathbf{k}, t) &= \sum_{p=1}^{\infty} t^{p-1} \int d\mathbf{k}_1 \dots d\mathbf{k}_p \delta_D(\mathbf{k}_1 + \dots + \mathbf{k}_p - \mathbf{k}) \\ &\quad \times G_p(\mathbf{k}_1, \dots, \mathbf{k}_p) \tilde{\theta}_0(\mathbf{k}_1) \dots \tilde{\theta}_0(\mathbf{k}_p). \end{aligned} \quad (46)$$

The Dirac factors express the invariance through translations of the equations of motion, $F_1 = G_1 = 1$ from Eqs.(17), and the higher-order kernels F_p and G_p obey a recursion relation that is obtained by substituting the expansion (45)-(46) into the equations of motion (1)-(2). This yields in Fourier space

$$\begin{aligned} pF_p(\mathbf{k}_1, \dots, \mathbf{k}_p) - G_p(\mathbf{k}_1, \dots, \mathbf{k}_p) = \\ \sum_{\ell=1}^{p-1} \frac{\mathbf{k}_{1,p} \cdot \mathbf{k}_{1,\ell}}{|\mathbf{k}_{1,\ell}|^2} G_\ell(\mathbf{k}_1, \dots, \mathbf{k}_\ell) F_{p-\ell}(\mathbf{k}_{\ell+1}, \dots, \mathbf{k}_p), \end{aligned} \quad (47)$$

and

$$(p-1)G_p(\mathbf{k}_1, \dots, \mathbf{k}_p) = \sum_{\ell=1}^{p-1} \frac{|\mathbf{k}_{1,p}|^2 (\mathbf{k}_{1,\ell} \cdot \mathbf{k}_{\ell+1,p})}{2|\mathbf{k}_{1,\ell}|^2 |\mathbf{k}_{\ell+1,p}|^2} \times G_\ell(\mathbf{k}_1, \dots, \mathbf{k}_\ell) G_{p-\ell}(\mathbf{k}_{\ell+1}, \dots, \mathbf{k}_p), \quad (48)$$

where we note $\mathbf{k}_{i,j} = \mathbf{k}_i + \mathbf{k}_{i+1} + \dots + \mathbf{k}_j$ with $j \geq i$. This gives for $p = 2$ the kernels

$$F_2^s(\mathbf{k}_1, \mathbf{k}_2) = \frac{(\mathbf{k}_{12} \cdot \mathbf{k}_1)(\mathbf{k}_{12} \cdot \mathbf{k}_2)}{2k_1^2 k_2^2}, \quad (49)$$

and

$$G_2^s(\mathbf{k}_1, \mathbf{k}_2) = \frac{k_{12}^2(\mathbf{k}_1 \cdot \mathbf{k}_2)}{2k_1^2 k_2^2}, \quad (50)$$

where we defined $F_2^s(\mathbf{k}_1, \mathbf{k}_2) = [F_2(\mathbf{k}_1, \mathbf{k}_2) + F_2(\mathbf{k}_2, \mathbf{k}_1)]/2$ and G_2^s the symmetrized kernels. In Eqs.(45)-(50) we took the inviscid limit $\nu = 0^+$. Then, the effects of the infinitesimal viscosity (i.e. the formation of shocks) completely disappear in these perturbative expansions. This implies that taking shocks into account requires non-perturbative methods.

Note that the expansions (45)-(50) over powers of time are also expansions over powers of the initial velocity fluctuations $\theta_0(\mathbf{x})$, or equivalently over powers of the linear density mode $\delta_L(\mathbf{x}, t)$ given in Eq.(17). Since the amplitude of the linear density fluctuations decreases at large scales, as seen in Eq.(29), the perturbative expansions apply to both limits of early time or large scale. In particular, in these limits the distributions $\mathcal{P}(\eta_r)$ and $\mathcal{P}(\Theta_r)$ converge to the Gaussian of variance $\sigma_{\delta_{Lr}}^2$. Then, at early times, or when the system is smoothed over large scales, the displacements of particles are small and one recovers at leading order the linear theory of section II B, that is set by the initial conditions. A simple example is provided by the case $\{n = -2, d = 1\}$ of one-dimensional initial Brownian velocity [17, 18]. However, this only holds for $n < d - 2$, where the linear density variance $\sigma_{\delta_{Lr}}$ is well defined. For $n \geq d - 2$ it is not possible to neglect shocks as soon as $t \neq 0$, and the distributions $\mathcal{P}(\eta_r)$ and $\mathcal{P}(\Theta_r)$ remain far from Gaussian at any time and scale. This is for instance the behavior obtained in the case $\{n = 0, d = 1\}$ of one-dimensional initial white-noise velocity [15, 28, 29, 30]. We shall recover these two different behaviors in the following sections.

The perturbative approach (45)-(46) is the standard method used in cosmology to study the gravitational dynamics at large scales and early times [24, 26, 31] (in this case the equation of motion (1) gets two new linear terms, associated with the gravitational force and a friction term that comes from the expansion of the Universe and the change to comoving coordinates, but the non-linearity is the same and the perturbative expansion is similar). Indeed, in the standard cold dark matter model [22], the amplitude of the linear density fluctuations decreases at larger scales (i.e. $-3 < n < 1$ as in the present paper, with the same definition of the power-spectrum

index n for $d = 3$), and the perturbative approach allows to describe the large scale structure of the Universe (e.g. beyond the scale associated with clusters of galaxies today), that is, the cosmic web formed by voids, filaments and walls that join the nonlinear high-density objects such as galaxies or clusters of galaxies. In the hydrodynamical context, perturbative expansions over powers of time, such as (45)-(46), have been used for instance in [32, 33] to study Eulerian and Lagrangian two-point correlations. They can also serve as a basis for Padé approximants that attempt to improve the convergence of the series [33, 34].

From the point of view of the perturbative expansions (45)-(50), the Burgers dynamics (1) becomes equivalent in the inviscid limit to the Zeldovich dynamics [25], obtained by setting the right hand side in Eq.(1) to zero. This describes the free motion of collisionless particles, that always keep their initial velocity \mathbf{u}_0 and can cross each other. In a Lagrangian framework, the trajectory of the particle of initial Lagrangian coordinate $\mathbf{q} = 0$ always reads as

$$\mathbf{x}(\mathbf{q}, t) = \mathbf{q} + t \mathbf{u}_0(\mathbf{q}), \quad (51)$$

as in Eq.(37) that only held before shocks. Before orbit-crossings the conservation of matter gives for the density field

$$\rho(\mathbf{x})d\mathbf{x} = \rho_0 d\mathbf{q}, \quad \text{hence } 1 + \delta(\mathbf{x}) = \left| \det \left(\frac{\partial \mathbf{x}}{\partial \mathbf{q}} \right) \right|^{-1}. \quad (52)$$

This gives

$$1 + \delta(\mathbf{x}) = \int d\mathbf{q} \delta_D[\mathbf{x} - \mathbf{q} - t\mathbf{u}_0(\mathbf{q})], \quad (53)$$

which remains valid after orbit crossing as we integrate over all streams that pass through position \mathbf{x} at time t . In Fourier space this yields

$$\tilde{\delta}(\mathbf{k}) = \int \frac{d\mathbf{q}}{(2\pi)^d} e^{-i\mathbf{k} \cdot \mathbf{q}} \left(e^{-i\mathbf{k} \cdot t\mathbf{u}_0(\mathbf{q})} - 1 \right). \quad (54)$$

Then, expanding the exponential over \mathbf{u}_0 directly gives the symmetric kernels F_p^s associated with the expansion (45) [35],

$$F_p^s(\mathbf{k}_1, \dots, \mathbf{k}_p) = \frac{1}{p!} \frac{\mathbf{k}_{1,p} \cdot \mathbf{k}_1}{k_1^2} \dots \frac{\mathbf{k}_{1,p} \cdot \mathbf{k}_p}{k_p^2}, \quad (55)$$

which agrees with (49) for $p = 2$. From the perturbative expansions (45)-(50) we can compute the cumulants of the smoothed density contrast η_r and velocity divergence Θ_r (in the quasi-linear regime where shocks do not contribute, that is, leading-order terms at early times and large scales for $n \leq d - 3$, as discussed in section IV below). For instance, substituting the expression (45), the density three-point correlation reads in Fourier space as [26, 36]

$$\langle \delta(\mathbf{k}_1) \delta(\mathbf{k}_2) \delta(\mathbf{k}_3) \rangle_c = \delta_D(\mathbf{k}_1 + \mathbf{k}_2 + \mathbf{k}_3) \times [2P_{\delta_L}(k_1, t)P_{\delta_L}(k_2, t)F_2^s(\mathbf{k}_1, \mathbf{k}_2) + \text{cyc.} + \dots], \quad (56)$$

where ‘‘cyc.’’ stands for two terms associated with cyclic permutations over $\{\mathbf{k}_1, \mathbf{k}_2, \mathbf{k}_3\}$ of the previous term, while the dots stand for higher-order terms. Then, from Eq.(23) the cumulant of order three of the overdensity within radius r writes

$$\langle \eta_r^3 \rangle_c = 6 \int d\mathbf{k}_1 d\mathbf{k}_2 P_{\delta_L}(k_1, t) P_{\delta_L}(k_2, t) F_2^s(\mathbf{k}_1, \mathbf{k}_2) \times W(k_1 r) W(k_2 r) W(|\mathbf{k}_1 + \mathbf{k}_2| r) + \dots \quad (57)$$

Using the properties of Bessel functions, such as their addition theorem, one obtains for instance in dimension $d = 3$ [37, 38],

$$d = 3 : \quad \langle \eta_r^3 \rangle_c = (1 - n) \sigma_{\delta_{Lr}}^4 + \dots \quad (58)$$

One can use this method to derive the leading-order term of all cumulants $\langle \eta_r^p \rangle_c$ and $\langle \Theta_r^p \rangle_c$. Then, from the characteristic function $\varphi(y)$, defined from the Taylor series (64) below, one can reconstruct the distributions $\mathcal{P}(\eta_r)$ and $\mathcal{P}(\Theta_r)$ in the quasi-linear regime, $\sigma_{\delta_{Lr}} \ll 1$ [26, 38]. We shall describe in section IV below another method that directly gives the generating function $\varphi(y)$ without using the expansions (45)-(50) and that allows to go beyond the singularities associated with the Taylor series (64). Let us recall here that the previous results only hold for the case $n < d - 2$, where the linear theory is meaningful (i.e. $\sigma_{\delta_{Lr}}$ is well-defined).

IV. QUASI-LINEAR LIMIT

A. Distribution of the density within spherical cells

We consider here the probability distribution, $\mathcal{P}(\eta_r)$, of the overdensity η_r within spherical cells introduced in (20). More precisely, we investigate its asymptotic form in the quasi-linear limit, defined as $\sigma_{\delta_{Lr}} \rightarrow 0$. Therefore, we restrict ourselves to the range $n < d - 2$ (in addition to $-3 < n < 1$) so that the linear variance $\sigma_{\delta_{Lr}}^2$ is well defined, see Eq.(29). Taking advantage of the statistical isotropy of the system, we apply to the Burgers dynamics the steepest-descent method (instanton technique) that was devised in [39] for the collisionless gravitational dynamics.

1. Action $\mathcal{S}[\delta_L]$

To obtain the quasi-linear limit of the probability distribution $\mathcal{P}(\eta_r)$ it is convenient to first introduce the moment generating function $\Psi(y)$,

$$\Psi(y) = \langle e^{-y\eta_r} \rangle = \int_0^\infty d\eta_r e^{-y\eta_r} \mathcal{P}(\eta_r), \quad (59)$$

from which we can recover $\mathcal{P}(\eta_r)$ through the inverse Laplace transform

$$\mathcal{P}(\eta_r) = \int_{-i\infty}^{+i\infty} \frac{dy}{2\pi i} e^{y\eta_r} \Psi(y). \quad (60)$$

Since the system is fully defined by the Gaussian linear density field at the time of interest, $\delta_L(\mathbf{x})$ (we usually omit the time dependence as t can be seen as a mere parameter, since we only consider equal-time statistics), the average (59) can be written as the path-integral

$$\Psi(y) = (\det C_{\delta_L}^{-1})^{1/2} \int \mathcal{D}\delta_L e^{-y\eta_r[\delta_L] - \frac{1}{2}\delta_L \cdot C_{\delta_L}^{-1} \cdot \delta_L}, \quad (61)$$

where $\eta_r[\delta_L]$ is the functional that affects to the initial condition defined by the linear density field $\delta_L(\mathbf{x})$ the nonlinear overdensity η_r , built by the Burgers dynamics (1)-(2) at time t , within the spherical cell of radius r centered (for instance) on the origin $\mathbf{x} = 0$. Here and in the following we use the short-hand notation for scalar products

$$\delta_L \cdot C_{\delta_L}^{-1} \cdot \delta_L = \int d\mathbf{x}_1 d\mathbf{x}_2 \delta_L(\mathbf{x}_1) C_{\delta_L}^{-1}(\mathbf{x}_1, \mathbf{x}_2) \delta_L(\mathbf{x}_2), \quad (62)$$

where $C_{\delta_L}^{-1}$ is the inverse of the two-point correlation (19). Equation (61) is exact but the difficulty of the problem is hidden in the nonlinear functional $\eta_r[\delta_L]$. In order to make some progress, we consider the quasi-linear limit, $\sigma_{\delta_{Lr}} \rightarrow 0$, associated with large scales or early times. Then, it is convenient to rescale the moment generating function as [39]

$$\Psi(y) = e^{-\varphi(y\sigma_{\delta_{Lr}}^2)/\sigma_{\delta_{Lr}}^2}, \quad (63)$$

where $\varphi(y)$ is the cumulant generating function, which has the Taylor expansion

$$\varphi(y) = - \sum_{p=1}^{\infty} \frac{(-y)^p}{p!} \frac{\langle \eta_r^p \rangle_c}{\sigma_{\delta_{Lr}}^{2(p-1)}}. \quad (64)$$

Substituting Eq.(63) into Eq.(61) gives

$$e^{-\varphi(y)/\sigma_{\delta_{Lr}}^2} = (\det C_{\delta_L}^{-1})^{1/2} \int \mathcal{D}\delta_L e^{-\mathcal{S}[\delta_L]/\sigma_{\delta_{Lr}}^2}, \quad (65)$$

with the action $\mathcal{S}[\delta_L]$ given by

$$\mathcal{S}[\delta_L] = y\eta_r[\delta_L] + \frac{\sigma_{\delta_{Lr}}^2}{2} \delta_L \cdot C_{\delta_L}^{-1} \cdot \delta_L \quad (66)$$

The rescaling (63) allows us to derive the quasi-linear limit through a steepest-descent method, since the action $\mathcal{S}[\delta_L]$ no longer depends on the amplitude of the two-point correlation C_{δ_L} (as $\sigma_{\delta_{Lr}}^2 \propto C_{\delta_L}$) and the path-integral (65) is clearly dominated by the minimum of the action \mathcal{S} in the limit $\sigma_{\delta_{Lr}} \rightarrow 0$.

Here we may note that the use of a path-integral formalism to analyze dynamical systems such as Eqs.(1)-(2) is a standard approach, following the operator formalism of Martin-Siggia-Rose [40] or the functional method of Pithian [41, 42, 43]. In such a framework, the path-integral (61) is rewritten in terms of the nonlinear fields $\delta(\mathbf{x}, t)$ and $\theta(\mathbf{x}, t)$, so that η_r is a simple linear functional of δ as in (20), by introducing a Dirac functional such as

$\delta_D[\partial_t \mathbf{u} + (\mathbf{u} \cdot \nabla) \mathbf{u} - \nu \Delta \mathbf{u} - \xi]$ (and similarly for $\tilde{\theta}$) to enforce the equation of motion (1), where, depending on the system, $\xi(\mathbf{x}, t)$ can represent both a stochastic external forcing and the random initial conditions. Taking care of the Jacobian, which is usually equal to unity thanks to causality [44], one obtains a path integral such as (65), but over the nonlinear density field $\delta(\mathbf{x}, t)$ and its conjugate $\lambda(\mathbf{x}, t)$, rather than over $\delta_L(\mathbf{x})$, and over the velocity pair $\{\theta(\mathbf{x}, t), \mu(\mathbf{x}, t)\}$. This procedure is described in details in [34] for the Zeldovich dynamics recalled in section III above, that amounts to set the right hand side in the Burgers equation (1) to zero, see also [45] for the collisionless gravitational dynamics. For noisy dynamics, where one adds a stochastic external forcing, this method is presented for instance in [46, 47] for the forced Burgers dynamics and in [48] for the forced Navier-Stokes dynamics.

Then, one obtains a cubic action $\mathcal{S}[\delta, \theta; \lambda, \mu]$. Expanding over the cubic term gives back the perturbative results discussed in section III, as one recovers an expansion over powers of the initial power spectrum P_{δ_L} . On the other hand, this path integral can serve as a basis for other expansion schemes, such as large- N methods [34], that recover at leading order Kraichnan's direct interaction approximation when applied to the Navier-Stokes equations [49, 50].

Alternative expansion schemes, where one does not expand over powers of some coupling constant or parameter, are provided by steepest-descent methods (instanton techniques [44]) where one expands around a saddle-point of the action \mathcal{S} . If this saddle-point is non-perturbative this approach can go beyond perturbative expansions such as those described in section III, as we shall see more clearly in section V below. This approach has been applied to the forced Burgers dynamics in [46, 47] and to the forced Navier-Stokes dynamics in [48]. In particular, this allows to obtain the right exponential tail of the probability distribution of the velocity increment [46, 51] and its left power-law tail [52].

In the noiseless case, a problem that arises when one tries to apply this method to the standard action $\mathcal{S}[\delta, \theta; \lambda, \mu]$, directly obtained from the equations of motion as described above, is that this action is highly singular when there is no external forcing. Indeed, in such cases the dynamics is fully deterministic, so that the system is fully defined by the initial condition $\theta_0(\mathbf{x})$ (or by $\delta_L(\mathbf{x})$ at a given reference time). Then, one can check that this action \mathcal{S} is only finite for fields that obey the equations of motion (1)-(2) and infinite elsewhere, which simply means that the path integral only counts fields that are solutions of the dynamics, as it should. Therefore, the action is only finite over a lower dimensional subspace parameterized by $\theta_0(\mathbf{x})$, that is, the time degree of freedom of the fields $\delta(\mathbf{x}, t)$ and $\theta(\mathbf{x}, t)$ is not real. Then, the action has no finite second-derivative and the steepest-descent approach is not very well defined. Moreover, any expansion point must be an exact solution of the dynamics so that this approach does not bring much

progress.

By contrast, the path integral (65) only involves the true degrees of freedom of the system, parameterized by the linear density field $\delta_L(\mathbf{x}, t)$ at the given time of interest (i.e. we do not integrate over non-existent time degrees of freedom). Then, the action $\mathcal{S}[\delta_L]$ is finite and has a well-defined second derivative, at least close to $y = 0$ and $\delta_L = 0$, so that the steepest-descent approach rests on firm grounds. Moreover, the difficulty associated with the nonlinear functional $\eta_r[\delta_L]$ would not be overcome by using the standard action $\mathcal{S}[\delta, \theta; \lambda, \mu]$, since in this case too we would need to study exact solutions of the dynamics. Thus, the action (66) is well-suited to the application of the steepest-descent approach to deterministic dynamics, as we shall see in the following. In practice, in order to handle the term $\eta_r[\delta_L]$, one must be able to obtain saddle-points where the dynamics can be explicitly solved in simple terms. In our case, it is natural to take advantage of the statistical isotropy of the system to look for spherically symmetric solutions of the dynamics. Then, this requires to focus on spherically symmetric observables, such as η_r and Θ_r defined in Eqs.(20)-(21), so that spherical initial conditions can also be saddle-points of the action $\mathcal{S}[\delta_L]$. In fact, in such a case, a minimum of the action with respect to spherically symmetric initial conditions is automatically a saddle-point with respect to non-spherically symmetric initial conditions (but not necessarily a minimum). In our case, we shall see below in section IV A 2 that we really obtain a local minimum in the quasi-linear regime (i.e. for small y and δ_L). Then, even if there exists another local minimum reached for some non-spherical initial conditions, which requires a finite fluctuation δ_L , such a contribution is exponentially subdominant in the quasi-linear limit, $\sigma_{\delta_{L,r}} \rightarrow 0$, so that we obtain exact results in this limit, without the need to explicitly study the functional $\eta_r[\delta_L]$ over all possible non-spherical states.

Note that for non-spherically symmetric observables (for instance we could choose cubic cells to define the mean density η_r and velocity divergence Θ_r) we could apply the same approach and look for local minima with respect to spherically symmetric initial conditions. However, these would no longer be saddle-points with respect to non-spherical fluctuations, and would not be the true minima of the action. Then, one would only obtain lower bounds for the asymptotic behavior of the distribution $\mathcal{P}(X)$, where X is any observable and is not necessarily spherically symmetric, in the quasi-linear or rare-event limits. One can expect that the exponents obtained in this fashion would remain correct, but the numerical factors within exponential tails would only be approximate. The asymptotic behaviors obtained within this approximation would clearly show the same qualitative properties as those obtained for the spherical observables studied here (since one uses the same initial states). Thus, it is straightforward to obtain lower bounds for any distribution $\mathcal{P}(X)$, in the quasi-linear or rare-event limits, from the method described in this article and we restrict

ourselves to the spherically symmetric observables (20)-(21) in the following.

2. Spherical saddle-point

As explained above, and as for the gravitational dynamics [39], taking advantage of the spherical symmetry of the action (66), we can look for a spherical saddle-point. Indeed, since the first functional derivative, $\mathcal{D}\mathcal{S}/\mathcal{D}\delta_L(\mathbf{q})$, taken at a spherical linear density field $\delta_L(\mathbf{q})$, is spherically symmetric, it only depends on $|\mathbf{q}|$. Then, the first variation $\Delta\mathcal{S}$ due to a non-radial perturbation $\Delta\delta_L(\mathbf{q})$ vanishes,

$$\Delta\mathcal{S} = \int d\mathbf{q} \frac{\mathcal{D}\mathcal{S}}{\mathcal{D}\delta_L(\mathbf{q})} \Delta\delta_L(\mathbf{q}) = 0, \quad (67)$$

when

$$\delta_L(\mathbf{q}) = \delta_L(|\mathbf{q}|) \quad \text{and} \quad \int_{|\mathbf{q}|=q} d\hat{\mathbf{q}} \Delta\delta_L(\mathbf{q}) = 0, \quad (68)$$

where the second equality is the integral over angular variables at any radius q . Therefore, a saddle-point with respect to spherically symmetric states (i.e. radial degrees of freedom) is automatically a saddle-point with respect to angular degrees of freedom, whence a true saddle-point with respect to any infinitesimal perturbation $\Delta\delta_L(\mathbf{q})$. Then, we can restrict the action $\mathcal{S}[\delta_L]$ to spherically symmetric initial conditions and look for its minimum within this subspace. For such initial conditions, the action can be expressed in terms of the one-dimensional field $\delta_{Lq'}$, defined as in Eq.(20) over $0 < q' < \infty$, (we note by the letter q initial Lagrangian radii, to distinguish them from the Eulerian radii r reached at time t). This reads as

$$\mathcal{S}[\delta_{Lq'}] = y\eta_r[\delta_{Lq'}] + \frac{\sigma_{\delta_{Lr}}^2}{2} \delta_{Lq'_1} \cdot C_{\delta_{Lr}}^{-1} \cdot \delta_{Lq'_2}, \quad (69)$$

where q' is a dummy variable and $C_{\delta_{Lr}}(q'_1, q'_2)$ is the covariance introduced in Eq.(26). Then, saddle-points of the action (69) are given by the condition $\mathcal{D}\mathcal{S}/\mathcal{D}\delta_{Lq'} = 0$ over $0 < q' < \infty$, that is,

$$y \frac{\mathcal{D}\eta_r}{\mathcal{D}\delta_{Lq'}} + \sigma_{\delta_{Lr}}^2 \int_0^\infty dq'' C_{\delta_{Lr}}^{-1}(q', q'') \delta_{Lq''} = 0. \quad (70)$$

Multiplying by the operator $C_{\delta_{Lr}}$ this reads as

$$\delta_{Lq'} = \frac{-y}{\sigma_{\delta_{Lr}}^2} \int_0^\infty dq'' C_{\delta_{Lr}}(q', q'') \frac{\mathcal{D}\eta_r}{\mathcal{D}\delta_{Lq''}}. \quad (71)$$

Next, we note that if there have been no collisions (i.e. no shocks) until time t , the spherical collapse or expansion has remained well ordered, and the mass m within the radius r comes from the matter that was initially located within a Lagrangian radius q at time $t = 0$. Then, the overdensity $\eta_r = m/(\rho_0 V)$ is also given by $\eta_r = (q/r)^d$

and it only depends on the initial Lagrangian coordinate q of the shell that is located at radius r at time t . On the other hand, in the inviscid limit the Burgers dynamics (1) implies that particles that have not collided yet have kept their initial velocity \mathbf{u}_0 . Therefore, for a spherical state the initial Lagrangian radius q is related to the Eulerian radius r by $r = q + t u_{0q}$, whence

$$\eta_r = (q/r)^d = \left(1 + \frac{t u_{0q}}{q}\right)^{-d} = \mathcal{F}(\delta_{Lq}), \quad (72)$$

with

$$\mathcal{F}(\delta_{Lq}) = \left(1 - \frac{\delta_{Lq}}{d}\right)^{-d}, \quad (73)$$

where u_{0q} is the initial radial velocity at radius q and we used Eq.(30) (for spherical initial conditions we have $\mathbf{u}_0(\mathbf{x}) = u_{0x}\hat{\mathbf{x}}$). Thus, the overdensity η_r only depends on the initial velocity at the Lagrangian coordinate q , whence on the linear density contrast δ_{Lq} within the Lagrangian radius q . As a consequence, it is independent of infinitesimal perturbations to the initial profile $\delta_{Lq'}$ over inner or outer shells ($q' < q$ or $q' > q$), that only redistribute matter at smaller or larger radii. On the other hand, under an infinitesimal perturbation $\Delta\delta_{Lq'}$ the Lagrangian radius q and the overdensity η_r are modified as $q \rightarrow q + \Delta q$ and $\eta_r \rightarrow \eta_r + \Delta\eta_r$. From Eq.(72) we obtain at first order,

$$\Delta\eta_r = \mathcal{F}'(\delta_{Lq}) \left[\frac{d\delta_{Lq'}}{dq'} \Big|_q \Delta q + \Delta\delta_{Lq} \right], \quad (74)$$

$$\frac{\Delta\eta_r}{\eta_r} = d \frac{\Delta q}{q}. \quad (75)$$

This leads to $\Delta\eta_r \propto \Delta\delta_{Lq}$, which means that the functional differential $\mathcal{D}\eta_r/\mathcal{D}\delta_{Lq''}$ in Eq.(71) is a Dirac distribution centered on $q'' = q$, in agreement with the previous discussion, and we directly obtain the initial profile of the saddle-point as

$$\delta_{Lq'} \propto C_{\delta_{Lr}}(q', q) \quad \text{whence} \quad \delta_{Lq'} = \delta_{Lq} \frac{C_{\delta_{Lr}}(q', q)}{\sigma_{\delta_{Lq}}^2}. \quad (76)$$

Using Eq.(30), this also gives for the initial velocity profile

$$u_{0q'} = u_{0q} \frac{q'}{q} \frac{\delta_{Lq'}}{\delta_{Lq}} = u_{0q} \frac{C_{u_{0r}}(q', q)}{\sigma_{u_{0q}}^2}. \quad (77)$$

Next, the amplitude δ_{Lq} , or the Lagrangian coordinate q , can be determined by substituting the profile (76) into the action (69) and looking for its minimum with respect to δ_{Lq} . This reads as

$$\mathcal{S} = y\mathcal{F}(\delta_{Lq}) + \frac{\delta_{Lq}^2 \sigma_{\delta_{Lr}}^2}{2\sigma_{\delta_{Lq}}^2}. \quad (78)$$

Then, defining the variable τ and the function $\mathcal{G}(\tau)$ by

$$\tau = -\delta_{Lq} \frac{\sigma_{\delta_{Lr}}}{\sigma_{\delta_{Lq}}}, \quad \mathcal{G}(\tau) = \mathcal{F}(\delta_{Lq}) = \eta_r, \quad (79)$$

the action (78) and its derivative read as

$$\mathcal{S} = y\mathcal{G}(\tau) + \frac{\tau^2}{2}, \quad \frac{\partial \mathcal{S}}{\partial \tau} = y\mathcal{G}' + \tau. \quad (80)$$

Therefore, since at leading order in the quasi-linear limit, the cumulant generating function $\varphi(y)$ is given by the minimum of the action $\mathcal{S}[\delta_L]$ from Eq.(65), it is given by the implicit system

$$\varphi(y) = y\mathcal{G}(\tau) + \frac{\tau^2}{2} \quad \text{with} \quad \tau = -y\mathcal{G}'(\tau). \quad (81)$$

Thus, the generating function $\varphi(y)$ is also the Legendre transform of the function $-\tau(\mathcal{G})^2/2$, as defined by

$$\varphi(y) = \min_{\tau} \left[y\mathcal{G}(\tau) + \frac{\tau^2}{2} \right] = \min_{\mathcal{G}} \left[y\mathcal{G} + \frac{\tau(\mathcal{G})^2}{2} \right]. \quad (82)$$

To make sure that the solution (81) is indeed relevant, we must check that it is indeed a local minimum of the action (and not a maximum), in agreement with (82) and the original path integral (65). This directly follows from the expression (66). Indeed, for $y = 0$ the saddle-point obtained above is simply $\delta_L = 0$, i.e. $\tau = 0$, and the Hessian of the action at this point is $\sigma_{\delta_{Lr}}^2 C_{\delta_L}^{-1}$ which is strictly positive. Then, by continuity, for small y the Hessian around the saddle-point given by Eq.(81) is positive which ensures that it is a local minimum. As we shall see below in section IV A 3, for some cases it may only be a local minimum, but the global minimum associated with finite density contrasts is irrelevant in the quasi-linear limit: it corresponds to the tail of the distribution $\mathcal{P}(\eta_r)$ and it is exponentially suppressed in the limit $\sigma_{\delta_{Lr}} \rightarrow 0$.

It is clear that the procedure described above must recover the results that would be obtained for the leading-order term of the cumulants $\langle \eta_r^p \rangle_c$ (which is of order $\sigma_{\delta_{Lr}}^{2(p-1)}$) so that $\varphi(y)$ has indeed a finite quasi-linear limit in Eq.(64) from the perturbative expansion presented in section III. Indeed, in both cases we obtain an expansion over powers of $\sigma_{\delta_{Lr}}^2$ (in the steepest-descent approach subleading terms would be obtained from Eq.(65) by expanding the action around its saddle-point and performing the Gaussian integrations), as we actually start from the unperturbed solution $\delta_L = 0$. In fact, as shown for the case of the three-dimensional gravitational dynamics [53], it is possible to derive the quasi-linear generating function $\varphi(y)$ from the perturbative expansion (45)-(46), using its Taylor expansion (64) and the leading-order term of each cumulant $\langle \eta_r^p \rangle_c$. This gives back $\varphi(y)$ as the solution of the implicit system (81) for the unsmoothed case, where one has $\mathcal{G}(\tau) = \mathcal{F}(\tau)$ (so that there is no dependence on the initial conditions). Then, one can show that the same result is obtained in Lagrangian space, where the perturbative expansions are built in terms of

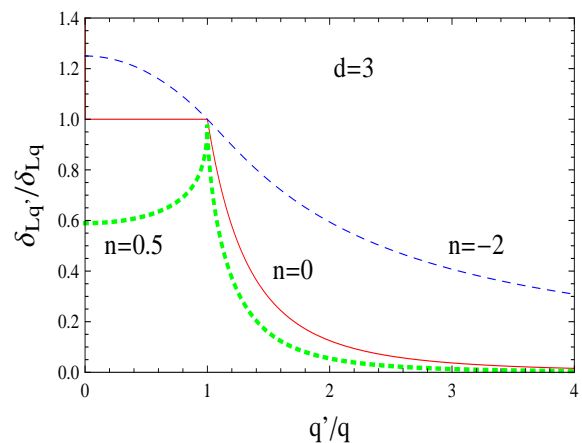


FIG. 1: (Color online) The linear density profile of the spherical saddle-point for the cases $n = -2, 0$ and 0.5 , in dimension $d = 3$. This shows the integrated linear density contrast $\delta_{Lq'}$ within the sphere of radius q' , from Eq.(83), and q is the initial Lagrangian radius of the shell that is at the radius of interest r at time t .

the Lagrangian coordinates, and the shift from $\mathcal{F}(\delta_L)$ to $\mathcal{G}(\tau)$ as in Eq.(79) is obtained through a mapping from Lagrangian to Eulerian space [54].

As shown in [39] and described above, the steepest-descent approach provides the quasi-linear generating function in a more direct fashion. In particular, the integrations over angles, as in Eq.(57), are automatically included in the spherical dynamics, and the dependence on n , associated with the mapping from Lagrangian to Eulerian coordinates (through the ratio $\sigma_{\delta_{Lr}}/\sigma_{\delta_{Lq}}$ in Eq.(79) that measures the ratio of initial power on scales r and q) is automatically provided by the form of the action $\mathcal{S}[\delta_L]$. In addition, the definition of $\varphi(y)$ as the Laplace transform (65) allows to give a meaning to $\varphi(y)$ beyond the radius of convergence of its Taylor series. Finally, as discussed below, the profile (76) of the saddle-point allows us to check the range of overdensity η_r and Laplace conjugate y to which these results apply. Indeed, they only hold as long as the saddle-point has not formed shocks yet, which can only be checked from the knowledge of Eq.(76).

For the power-law power spectra (18) the radial linear profile (76) of the saddle-point reads as

$$\frac{\delta_{Lq'}}{\delta_{Lq}} = \left(\frac{2}{1+x} \right)^{n+3} \frac{{}_2F_1\left(\frac{n+3}{2}, \frac{d+1}{2}; d+1; \frac{4x}{(1+x)^2}\right)}{{}_2F_1\left(\frac{n+3}{2}, \frac{d+1}{2}; d+1; 1\right)}, \quad (83)$$

with $x = q'/q$, see Eq.(28). This also gives the linear velocity profile through Eq.(30). We show in Figs. 1, 2, the density and velocity profiles obtained in the three-dimensional case for $n = -2, 0$ and 0.5 . For integer values of n and odd $d+n$ the hypergeometric function in Eq.(83) simplifies and we give in Table II the explicit forms obtained for some low dimensional cases. Note that the profile is singular at the Lagrangian radius q , associated

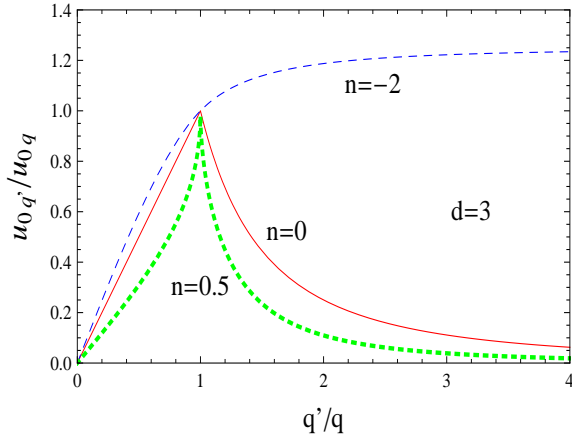


FIG. 2: (Color online) The linear velocity profile of the spherical saddle-point for the cases $n = -2, 0$ and 0.5 , in dimension $d = 3$, as in Fig. 1. This shows the initial radial velocity $u_0(q')$ at Lagrangian radius q' .

n	d	$\frac{\delta_{Lq'}}{\delta_{Lq}}$		$\frac{u_{0q'}}{u_{0q}}$	
		$x < 1$	$x > 1$	$x < 1$	$x > 1$
0	3	1	$\frac{1}{x^3}$	x	$\frac{1}{x^2}$
-1	2	1	$\frac{1}{x^2}$	x	$\frac{1}{x}$
-2	1	1	$\frac{1}{x}$	x	1
-2	3	$\frac{5-x^2}{4}$	$\frac{5x^2-1}{4x^3}$	$\frac{x(5-x^2)}{4}$	$\frac{5x^2-1}{4x^2}$
n	∞	$\left(\frac{1+x^2}{2}\right)^{-(n+3)/2}$		$x \left(\frac{1+x^2}{2}\right)^{-(n+3)/2}$	

TABLE II: The linear integrated-density and velocity profiles of the spherical saddle-point for some values of n and d , where Eq.(83) simplifies. Here $x = q'/q$, where q is the Lagrangian radius associated with the Eulerian radius of interest r . The profile is singular at $x = 1$, except in the limit of infinite dimension, $d \rightarrow \infty$, shown in the last row.

with the radius r of the Eulerian cell. We also give in the last row the simple profile obtained in the limit $d \rightarrow \infty$, where the singularity disappears. Note that in this infinite dimensional limit the profile still depends on n , in agreement with the fact that the profile (83) decays as $x^{-(n+3)}$ at large distance, independently of d .

As expected, for all values of n in the range $-3 < n < 1$ that we consider in this paper, the density contrast vanishes at large distance. For $n \leq d-3$ it is monotonically decreasing but for $n > d-3$, which corresponds to significant initial power at high wavenumbers, it shows a peak at radius q . On the other hand, the radial velocity vanishes at the center $q' = 0$, in agreement with spherical symmetry, but it only decays at large distance for $n > -2$. For $n < -2$ it keeps growing at large distance (note that the initial velocity field only shows homogeneous increments for $n < -1$, so that this growth is not

n	$\eta_r > 1, \Theta_r > 0$	$\eta_r < 1, \Theta_r < 0$
$n > d-3$	shock as soon as $t \neq 0$	
$-2 < n \leq d-3$	no shock	shock below a threshold
$-3 < n \leq -2$	no shock	no shock

TABLE III: This Table shows whether the saddle-point (76) forms a shock after a finite time, which corresponds to a finite threshold for the density η_r or the velocity divergence Θ_r . We only consider the range $-3 < n < 1$ and $d \geq 1$. If $n > d-3$ shocks form as soon as $t \neq 0$ so that the saddle-point (76) is never valid (but it should give a reasonable approximation if $n < d-2$).

surprising).

To make sure that the saddle-point obtained above is relevant we must check that no shocks have formed, so that Eq.(72) is valid. The naive Lagrangian map, $\mathbf{x} = \mathbf{q} + t\mathbf{u}_0(\mathbf{q})$, shows that a shock occurs when $\det(\partial\mathbf{x}/\partial\mathbf{q}) = 0$, that is when $1 + td u_{0q'}/dq' = 0$ for the spherical saddle-point. The profiles show a singularity at radius q of the form $|q' - q|^{d-n-2}$. Then, for $n > d-3$ the velocity has a spike at radius q with infinite left and right derivatives, so that shocks appear as soon as $t \neq 0$. For $n \leq d-3$, $|u_{0q'}|$ shows a sublinear (or linear) growth with q' hence there will be no shock, except at the center, for overdense saddle-points (particles reach the center before $du_{0q'}/dq'$ reaches $-1/t$). For underdense saddle-points, a shock appears after a finite time for $-2 < n \leq d-3$, while no shocks form for $-3 < n \leq -2$ since the radial velocity grows with radius. We summarize in Table III these behaviors associated with different ranges of the index n of the initial energy spectrum.

Since in the quasi-linear limit we only probe small density fluctuations we can use the saddle-point obtained above for $n \leq d-3$, as shocks only appear after some finite time (or never). For $n > d-3$ we should modify the saddle-point to take into account shocks. However, since for moderate times and density fluctuations this should only change the profile close to the Lagrangian radius q and give small modifications to the quasi-linear generating function $\varphi(y)$ we shall keep Eq.(81) below for $n < d-2$ (for $n \geq d-2$ where the linear variance $\sigma_{\delta_{Lr}}$ diverges it is not possible to neglect shocks). Note that for large d this problem disappears, see also the last row of Table II. For all cases shown in Table II the saddle-point obtained above is relevant in the quasi-linear regime, as can be checked from the explicit forms of the velocity profiles and in agreement with the previous discussion.

3. Cumulant generating function $\varphi(y)$

Close to the origin $y = 0$, the solution of the implicit system (81) always satisfies

$$\tau \rightarrow 0, \quad y \rightarrow 0: \quad \mathcal{G} \sim 1 - \tau, \quad y \sim \tau \quad \text{and} \quad \varphi \sim y - \frac{y^2}{2}. \quad (84)$$

Keeping only these low-order terms corresponds to the linear regime and gives back the Gaussian of variance $\sigma_{\delta_{Lr}}^2$ for the probability distribution $\mathcal{P}(\eta_r)$ on very large scales and early times. This agrees with the fact that the initial conditions are Gaussian and it means that over large scales or at early times, that is when $\sigma_{\delta_{Lr}}^2 \ll 1$ and for $|\delta_r| \ll 1$, we recover linear theory and the probability distributions are still governed by the Gaussian initial conditions. Of course, this breaks down for the cases $d - 2 < n < 1$ where the linear variance $\sigma_{\delta_{Lr}}^2$ itself is not well defined, so that even on large scales the probability distributions are strongly non-Gaussian, as seen for instance in [15, 28, 29, 30] for the case $\{n = 0, d = 1\}$.

For the case $n \leq d - 3$, where the quasi-linear regime considered in this section applies, the deviations from the Gaussian, associated with higher-order cumulants, appear for finite density contrast δ_r , that is for finite y and τ . Note that this corresponds to rare events, as expected for a steepest-descent approach to be valid. Thus, in the quasi-linear limit we are sensitive to small but finite values of $\{\delta_r, y, \tau\}$ around zero. Moreover, at leading order the moments and cumulants of the overdensity are given by the expansion (64) of $\varphi(y)$ around the origin. In particular, the solution (81) directly gives the leading order value of $\langle \eta_r^p \rangle_c$, that can also be derived from the perturbative expansion of the equations of motion (1)-(2) described in section III.

The previous results are valid for any initial energy spectrum, provided $\sigma_{\delta_{Lr}}$ is well defined. For the power-law power spectra (18), using Eq.(29), we obtain from the definition (79),

$$\tau = -\delta_{Lq} \left(\frac{r}{q} \right)^{-\frac{n+3}{2}} = -\delta_{Lq} \eta_r^{\frac{n+3}{2d}}, \quad (85)$$

whence

$$\mathcal{G}(\tau) = \mathcal{F} \left(-\tau \mathcal{G}^{-\frac{n+3}{2d}} \right) = \left(1 + \frac{\tau}{d} \mathcal{G}^{-\frac{n+3}{2d}} \right)^{-d}. \quad (86)$$

In terms of the inverse function $\tau(\mathcal{G})$ this reads as

$$\tau(\mathcal{G}) = d \left(\mathcal{G}^{\frac{n+1}{2d}} - \mathcal{G}^{\frac{n+3}{2d}} \right), \quad (87)$$

so that $\varphi(y)$ is given by the parametric representation

$$\varphi = \frac{d}{2} \left[(d-n-1) \mathcal{G}^{\frac{n+1}{d}} - 2(d-n-2) \mathcal{G}^{\frac{n+2}{d}} + (d-n-3) \mathcal{G}^{\frac{n+3}{d}} \right], \quad (88)$$

$$y = -\frac{d}{2} \mathcal{G}^{-1} \left[(n+1) \mathcal{G}^{\frac{n+1}{d}} - 2(n+2) \mathcal{G}^{\frac{n+2}{d}} + (n+3) \mathcal{G}^{\frac{n+3}{d}} \right]. \quad (89)$$

Expanding around $\tau = 0$, $y = 0$ and $\mathcal{G} = 1$, we obtain the series expansion of $\varphi(y)$. Comparing with Eq.(64) we obtain for the third and fourth-order cumulants in the quasi-linear limit,

$$\sigma_{\delta_{Lr}} \rightarrow 0: \quad S_3 = \frac{\langle \eta_r^3 \rangle_c}{\langle \eta_r^2 \rangle_c^2} = 3 \frac{d-n-2}{d}, \quad (90)$$

which agrees with (58) for $d = 3$, and

$$S_4 = \frac{\langle \eta_r^4 \rangle_c}{\langle \eta_r^2 \rangle_c^2} = \frac{83 + 16d^2 + 84n + 21n^2 - 36d(n+2)}{d^2}. \quad (91)$$

Note that although S_3 and S_4 as defined above are called the skewness and the kurtosis in the cosmological literature, they are not exactly the skewness and the kurtosis defined in standard probability theory, the latter being defined as $\langle \eta_r^3 \rangle_c / \langle \eta_r^2 \rangle_c^{3/2}$ and $\langle \eta_r^4 \rangle_c / \langle \eta_r^2 \rangle_c^2$. The reason for the use of (90)-(91) is that these quantities have a finite value in the quasi-linear limit discussed above (as seen in [30] they also have a finite value in the small-scale limit, associated with the highly nonlinear regime).

For small integer values of n and d we can obtain explicit expressions for the solution of the implicit system (88)-(89), by solving for $\mathcal{G}(y)$ and substituting into $\varphi(\mathcal{G})$. We give in Table IV our results for a few such cases. Note that from the meaning of the variable \mathcal{G} as the overdensity η_r within the radius r for the spherical saddle-point, see Eq.(79), $\varphi(y)$ is a priori determined by Eqs.(88)-(89) by letting \mathcal{G} vary over the range $0 < \mathcal{G} < \infty$. For the cases $\{n = -1, d = 2\}$ and $\{n = -2, d = 1\}$ we obtain a generating function $\varphi(y)$ that shows a singularity y_s on the negative real axis, with $y_s = -2$ or $-1/2$, and the range $y > y_s$ corresponds to the full range $\mathcal{G} > 0$. In the complex plane, there is usually a branch cut for $y < y_s$ or a pole at y_s . For the cases $\{n = 0, d = 3\}$ and $\{n = -2, d = 3\}$ it happens that the function $y(\mathcal{G})$ is no longer monotonic over $0 < \mathcal{G} < \infty$ so that the inverse $\mathcal{G}(y)$ is bivariate and $\varphi(y)$ shows two branches. We show in columns 3-5 of Table IV the quasi-linear branch, that contains the point $\{y = 0, \mathcal{G} = 1, \varphi = 0\}$ and corresponds to moderate density fluctuations. Columns 6-8 show the second branch that corresponds to large fluctuations (very low densities, $0 < \mathcal{G} < 1/8$, for $\{n = 0, d = 3\}$; very high densities, $2\sqrt{2} < \mathcal{G} < \infty$, for $\{n = -2, d = 3\}$).

For the general case, the behavior of the cumulant generating function $\varphi(y)$ defined by the implicit system (81) and the presence of singularities can be obtained from the asymptotic behaviors at large and small overdensities \mathcal{G} , using Eqs.(87)-(89). For large densities we obtain

$$\begin{aligned} \mathcal{G} \rightarrow +\infty: \quad \tau &\sim -d \mathcal{G}^{\frac{n+3}{2d}}, \quad y \sim -\frac{d(n+3)}{2} \mathcal{G}^{\frac{n+3-d}{d}}, \\ \varphi &\sim \frac{d(d-n-3)}{2} \left[\frac{-2y}{d(n+3)} \right]^{\frac{n+3}{n+3-d}}. \end{aligned} \quad (92)$$

n	d	$\varphi(y)$	y	$\mathcal{G} = \eta_r$	$\varphi(y)$	y	$\mathcal{G} = \eta_r$
0	3	$\frac{27-9\sqrt{9-6y}}{(6-\sqrt{9-6y})^2}$	$-\frac{9}{2} < y < \frac{3}{2}$	$\frac{1}{8} < \mathcal{G} < \infty$	$\frac{27+9\sqrt{9-6y}}{(6+\sqrt{9-6y})^2}$	$-\infty < y < \frac{3}{2}$	$0 < \mathcal{G} < \frac{1}{8}$
-1	2	$\frac{y}{1+y/2}$	$-2 < y < \infty$	$0 < \mathcal{G} < \infty$			
-2	1	$\sqrt{1+2y} - 1$	$-\frac{1}{2} < y < \infty$	$0 < \mathcal{G} < \infty$			
-2	3	$\frac{6^{3/2}+3\sqrt{6+16y}}{\sqrt{3+\sqrt{9+24y}}} - 9$	$-\frac{3}{8} < y < \infty$	$0 < \mathcal{G} < 2\sqrt{2}$	$\frac{6^{3/2}-3\sqrt{6+16y}}{\sqrt{3-\sqrt{9+24y}}} - 9$	$-\frac{3}{8} < y < 0$	$2\sqrt{2} < \mathcal{G} < \infty$
n	∞	$\varphi = \tau + \frac{\tau^2}{2}, y = \tau e^\tau, \mathcal{G} = e^{-\tau}; -\frac{1}{e} < y < \infty, 0 < \mathcal{G} < e; -\frac{1}{e} < y < 0, e < \mathcal{G} < \infty$					

TABLE IV: The cumulant generating function $\varphi(y)$ of the overdensity η_r , in the quasi-linear limit $\sigma_{\delta_{Lr}} \rightarrow 0$, for a few values of n and d , where explicit solutions of the system (88)-(89) can be obtained. The columns 3-5 show the quasi-linear branch, and the associated range of $\{y, \mathcal{G}\}$ that contains the point $\{0, 1\}$. The columns 6-8 show the second branch, associated with very rare events, that appears in some cases. The last row shows the infinite-dimensional limit, $d \rightarrow \infty$, which no longer depends on n but has no explicit form and shows two branches.

Thus, we have two possible behaviors for $\mathcal{G} \rightarrow +\infty$,

$$n > d - 3: \quad \tau \rightarrow -\infty, \quad y \rightarrow -\infty, \quad \varphi \rightarrow -\infty, \quad (93)$$

$$n < d - 3: \quad \tau \rightarrow -\infty, \quad y \rightarrow 0^-, \quad \varphi \rightarrow +\infty. \quad (94)$$

As explained in section IV A 2 and Table III, the saddle-point approach studied here only exactly applies to $n \leq d - 3$ as shocks form for $n > d - 3$. However, we mention the case $n > d - 3$ in (93) because this method should still provide a reasonable approximation for $d - 3 < n < d - 2$. The case $n = d - 3$ shows an intermediate behavior, as in the limit $\mathcal{G} \rightarrow +\infty$ we obtain $y \rightarrow -d^2/2$, and $\varphi \rightarrow -1$ if $d = 1$ or $\varphi \rightarrow -\infty$ if $d > 1$. Thus it is closer to the case $n > d - 3$. Then, we can see that for $n \geq d - 3$ larger densities are associated with more negative y and φ and the function $\varphi(y)$ is regular and monotonically increasing over $]-\infty, 0]$ (or $]-d^2/2, 0]$). This behavior is shown by the case $\{n = 0, d = 3\}$ in Fig. 3. For $n < d - 3$, since from (84) we have $y = 0$ at $\mathcal{G} = 1$, the limit $y \rightarrow 0^-$ for large densities implies that the function $y(\mathcal{G})$ is not monotonic over $\mathcal{G} \in [1, +\infty[$ and shows a minimum $y_s < 0$ at some value $\mathcal{G}_s > 1$. Around this point we have $y - y_s \propto (\mathcal{G} - \mathcal{G}_s)^2$. This gives rise to a square-root singularity $\sqrt{y - y_s}$ for the function $\varphi(y)$, which shows two branches going from this point. A first branch goes through the point $\{y = 0, \varphi = 0\}$, it is the branch associated with moderate fluctuations, below \mathcal{G}_s , that is most relevant in the quasi-linear limit. The second branch is associated with large overdensities above \mathcal{G}_s . This behavior is shown by the case $\{n = -2, d = 3\}$ in Fig. 3.

For low densities we obtain

$$\mathcal{G} \rightarrow 0: \quad \tau \sim d\mathcal{G}^{\frac{n+1}{2d}}, \quad y \sim -\frac{d(n+1)}{2}\mathcal{G}^{\frac{n+1-d}{d}},$$

$$\varphi \sim \frac{d(d-n-1)}{2} \left[\frac{-2y}{d(n+1)} \right]^{\frac{n+1}{n+1-d}}. \quad (95)$$

Since we assumed $n < d - 2$, so that the linear variance $\sigma_{\delta_{Lr}}^2$ is well defined, we have $n + 1 - d < -1$ and this

gives rise to the two behaviors:

$$n < -1: \quad \tau \rightarrow +\infty, \quad y \rightarrow +\infty, \quad \varphi \rightarrow +\infty, \quad (96)$$

$$n > -1: \quad \tau \rightarrow 0^+, \quad y \rightarrow -\infty, \quad \varphi \rightarrow 0^+. \quad (97)$$

Thus, for $n < -1$ the function $\varphi(y)$ is regular and monotonically increasing over $[0, +\infty[$ (case $\{n = -2, d = 3\}$ in Fig. 3) while for $n > -1$ it shows a square-root singularity at some finite value $y_s > 0$, associated with an underdensity $\mathcal{G}_s < 1$, from which two branches leave (case $\{n = 0, d = 3\}$ in Fig. 3).

In the large-dimension limit, $d \rightarrow \infty$, we obtain from Eqs.(73), (85), $\mathcal{F}(\delta_L) = e^{\delta_L}$ and $\tau = -\delta_L$. This gives the parametric representation of $\varphi(y)$ shown in the last row of Table IV. Since $0 < \mathcal{G} < \infty$ corresponds to $-\infty < \tau < \infty$ and $y(\tau)$ has a minimum at $\tau_s = -1$ this generating function $\varphi(y)$ shows two branches. The comparison with appendix A of [39] shows that in the quasi-linear limit this leads to a log-normal distribution $\mathcal{P}(\eta_r)$ (contrary to some statistical models, used to describe fully developed turbulence, this is not related to some underlying multiplicative cascade process). Note that the dependence of $\varphi(y)$ and $\mathcal{P}(\eta_r)$ on n disappears in this limit $d \rightarrow \infty$, even though the density profile of the associated saddle-point keeps a dependence on n , see last row of Table II.

As noticed in [18], it happens that in the case $\{n = -2, d = 1\}$ the quasi-linear result shown in the fourth row in Table IV actually gives the exact cumulant generating function defined as $\bar{\varphi}(y) = -\sum S_p(-y)^p/p!$, with $S_p = \langle \eta_r^p \rangle_c / \langle \eta_r^2 \rangle_c^{(p-1)}$. Note that for the quasi-linear limit we defined $\varphi(y)$ in Eq.(64) using $\sigma_{\delta_{Lr}}^2$ instead of $\langle \eta_r^2 \rangle_c$ in the coefficients S_p , which is only equivalent at leading order. In this case $\{n = -2, d = 1\}$ we actually have the exact equality $\langle \eta_r^2 \rangle_c = \sigma_{\delta_{Lr}}^2$, see [18]. For generic cases we expect the exact generating function $\bar{\varphi}(y)$ and the variance $\langle \eta_r^2 \rangle_c$ to deviate at small scales or late times from their quasi-linear limits $\varphi(y)$ and $\sigma_{\delta_{Lr}}^2$.

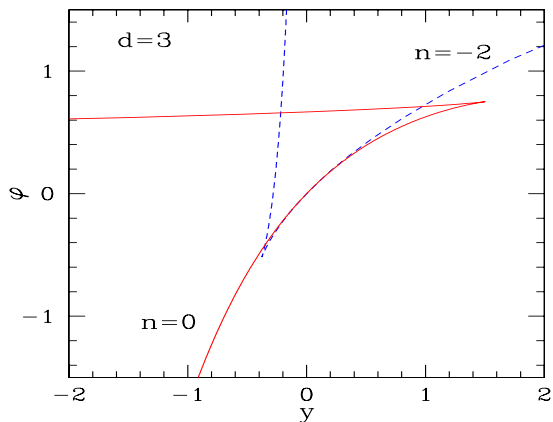


FIG. 3: (Color online) The density cumulant generating function $\varphi(y)$ in dimension $d = 3$ for the power indices $n = 0$ (solid line) and $n = -2$ (dashed line), from rows 2 and 5 of Table IV. In both cases there is a singularity on the real axis, with $y_s = 3/2$ for $n = 0$ and $y_s = -3/8$ for $n = -2$. The branch that runs through the origin is associated with moderate density fluctuations and is the relevant one for the expansion (64) in terms of cumulants at leading order in the quasi-linear limit.

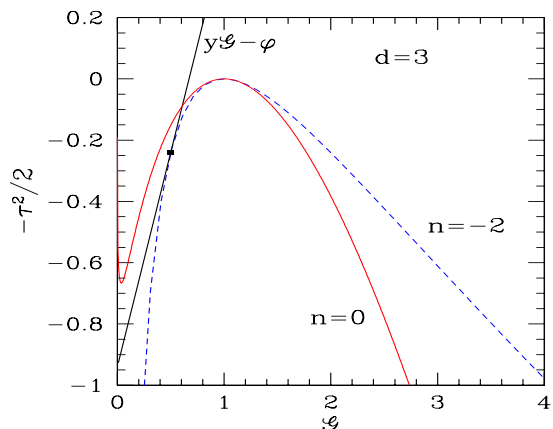


FIG. 4: (Color online) The Legendre transformation (82) of the curve $-\tau^2(\mathcal{G})/2$, which gives the generating function $\varphi(y)$. The first-contact line $y\mathcal{G} + c$, of fixed slope y and height c decreasing from $+\infty$, with the curve $-\tau^2(\mathcal{G})/2$, intersects the vertical axis at $(0, -\varphi)$ (i.e. for $c = -\varphi$). We show the cases $n = 0$ and $n = -2$ in three dimensions.

We display in Fig. 3 the cumulant generating function $\varphi(y)$ that we obtain in dimension $d = 3$ for the two indices $n = 0$ and $n = -2$. This provides an illustration of all the behaviors (93)-(97). The appearance of these singular behaviors can also be seen from the geometrical construction of the Legendre transform (82), that we show in Fig. 4 for these three-dimensional cases, $n = 0$ and $n = -2$. For a given y , $-\varphi$ is obtained as the intercept on the vertical axis of the first-contact straight line

$y\mathcal{G} + c$, of slope y , with the curve $-\tau^2(\mathcal{G})/2$, decreasing its height c from $+\infty$. Thus, the Legendre transform (82) follows the concave hull of the function $-\tau^2(\mathcal{G})/2$ and it is regular if the latter is concave over $0 < \mathcal{G} < \infty$. Note that this is obviously the case in the linear regime where $\tau = 1 - \mathcal{G}$.

For $n = 0$ we have $\tau(0) = 0$ (the curve $-\tau^2(\mathcal{G})/2$ shows a steep up-turn at very low \mathcal{G} in Fig. 4) so that for $y > 0$ the global minimum is $\tau = 0$: the point in the range $\mathcal{G}_s < \mathcal{G} < 1$ with a tangent of slope $y > 0$ is only a local minimum and there is a local maximum in the range $0 < \mathcal{G} < \mathcal{G}_s$. The local minimum corresponds to the regular branch in Fig. 3 and Table IV, that runs through $\varphi(0) = 0$, while the local maximum corresponds to the second branch in Fig. 3 and Table IV. For $n = -2$ we have $\tau(\mathcal{G})^2 \propto \mathcal{G}^{1/3}$ at large overdensities, from Eq.(92). Then, for $y_s < y < 0$ we again have a local minimum, with $1 < \mathcal{G} < \mathcal{G}_s$, and a local maximum, with $\mathcal{G} > \mathcal{G}_s$.

In the quasi-linear limit, $\sigma_{\delta_{Lr}} \rightarrow 0$, such large density fluctuations are exponentially suppressed by a term of order $e^{-\tau^2/(2\sigma_{\delta_{Lr}}^2)}$, as seen in Eq.(99) below, so that it is sufficient to define the generating function by the branch that runs through the origin.

4. Probability distribution $\mathcal{P}(\eta_r)$

Finally, from the cumulant generating function $\varphi(y)$ we obtain through an inverse Laplace transform the probability distribution $\mathcal{P}(\eta_r)$ in the quasi-linear limit. Using Eqs.(60),(63), we have

$$\mathcal{P}(\eta_r) = \int_{-i\infty}^{+i\infty} \frac{dy}{2\pi i \sigma_{\delta_{Lr}}^2} e^{[y\eta_r - \varphi(y)]/\sigma_{\delta_{Lr}}^2}. \quad (98)$$

It is best to compute the integral (98) exactly, using the branch of $\varphi(y)$ that runs through $\varphi(y) = 0$ in case this function is multivalued (then it only applies to some range of overdensities η_r around unity). However, in the quasi-linear limit at fixed η_r , it is again possible to evaluate the distribution $\mathcal{P}(\eta_r)$ from a steepest-descent method. The saddle-point of the exponent in (98) is given by $\eta_r = \varphi'(y)$. On the other hand, from (81) we have $\varphi'(y) = \mathcal{G}$, whence $\mathcal{G} = \eta_r$. Therefore, as expected the probability distribution $\mathcal{P}(\eta_r)$ at point η_r is governed by the saddle-point described in section IV A 2 such that its overdensity \mathcal{G} is equal to η_r , and we obtain from Eqs.(81), (79),

$$\mathcal{P}(\eta_r) \sim e^{-\tau(\eta_r)^2/(2\sigma_{\delta_{Lr}}^2)} = e^{-\delta_{Lq}^2/(2\sigma_{\delta_{Lq}}^2)}. \quad (99)$$

Thus, in the saddle-point approximation associated with the quasi-linear limit there is a precise correspondence between the overdensity η_r and its Laplace conjugate y , and the variable τ expresses the Gaussian weight of the initial velocity (or linear density contrast) as shown by Eq.(99). The nontrivial relation $\tau(\eta_r)$ describes both the evolution (72) of the density of a Lagrangian region,

n	d	$\ln \mathcal{P}(\eta_r)$	η_r
0	3	$-\frac{r^3}{2t^2} \left(\eta_r^{1/6} - \eta_r^{1/2} \right)^2$	$\eta_r > (2/3)^3$
-1	2	$-\frac{r^2}{2t^2} \left(1 - \eta_r^{1/2} \right)^2$	$\eta_r > 1/4$
-2	1	$-\frac{r}{2t^2} \left(\eta_r^{-1/2} - \eta_r^{1/2} \right)^2$	$\eta_r > 0$
-2	3	$-\frac{5r}{8t^2} \left(\eta_r^{-1/6} - \eta_r^{1/6} \right)^2$	$\eta_r > 0$
n	∞	$-\frac{(2r^2)^{\frac{n+3}{2}}}{2t^2} \ln^2(\eta_r)$	

TABLE V: Asymptotic behavior of the probability distribution $\mathcal{P}(\eta_r)$ in the quasi-linear regime $\sigma_{\delta_{Lr}} \rightarrow 0$ (i.e. $t \rightarrow 0$ or $r \rightarrow \infty$), for the initial conditions of Table I. The last column shows the range of overdensities η_r where these results apply. If the lower threshold is not zero (i.e. $-2 < n \leq d-3$, see Table III), it means that the spherical saddle-point forms shocks for lower densities.

which only depends on the dimension d , and the effect (79), (85), of the change of size from q to r , which involves the initial power-spectrum index n through the dependence of initial power on scale. In particular, for the power-law power spectra (18), using Eq.(87), Eq.(99) reads as

$$\sigma_{\delta_{Lr}} \rightarrow 0 : \ln \mathcal{P}(\eta_r) \sim -\frac{d^2}{2\sigma_{\delta_{Lr}}^2} \left(\eta_r^{\frac{n+1}{2d}} - \eta_r^{\frac{n+3}{2d}} \right)^2. \quad (100)$$

In the large dimensional limit, $d \rightarrow \infty$, we have seen that $\tau(\eta_r) = -\ln(\eta_r)$ (last row of Table IV), whence

$$d \rightarrow \infty, \sigma_{\delta_{Lr}} \rightarrow 0 : \ln \mathcal{P}(\eta_r) \sim -\frac{\ln^2(\eta_r)}{2\sigma_{\delta_{Lr}}^2}. \quad (101)$$

Note however that Eqs.(100)-(101) only hold for densities η_r such that the saddle-point (76) has not formed shocks yet. As discussed in section IV A 2 and summarized in Table III, this implies $n \leq d-3$ and it gives a lower bound for η_r if $n > -2$. These lower bounds are given by the last column in Table V and they will be obtained in section V B below.

As seen from the last expression (99), the tails of the probability distribution $\mathcal{P}(\eta_r)$ are simply governed at leading order by the initial Gaussian weight $e^{-\delta_{Lq}^2/(2\sigma_{\delta_{Lq}}^2)}$ of the associated initial fluctuation δ_{Lq} at the Lagrangian scale q . In fact, Eq.(99) could be directly obtained from a Lagrange multiplier method, without introducing the generating function $\varphi(y)$. Indeed, in the rare-event limit we may write

$$\text{rare events : } \mathcal{P}(\eta) \sim \max_{\{\delta_L[\mathbf{q}]|\eta_r[\delta_L]=\eta\}} e^{-\frac{1}{2}\delta_L \cdot C_L^{-1} \cdot \delta_L}. \quad (102)$$

That is, $\mathcal{P}(\eta)$ is governed by the maximum of the Gaussian weight $e^{-(\delta_L \cdot C_L^{-1} \cdot \delta_L)/2}$ subject to the constraint

$\eta_r[\delta_L] = \eta$ (assuming there are no degenerate maxima). Then, we can obtain this maximum by minimizing the action $\mathcal{S}[\delta_L]/\sigma_{\delta_{Lr}}^2$ of Eq.(66), where y plays the role of a Lagrange multiplier. This gives the saddle-point (76), and the amplitude δ_{Lq} and the radius q are directly obtained from the constraint $\eta = \mathcal{F}(\delta_{Lq})$, as in Eq.(72). Then, we do not need the explicit expression of the Lagrange multiplier y , as this is sufficient to obtain the last expression of the asymptotic tail (99). Nevertheless, it is useful to introduce the generating function $\varphi(y)$, which makes it clear that the Lagrange multiplier y is also the Laplace conjugate of the nonlinear overdensity η as in Eq.(59), since it is also of interest by itself, as it yields the density cumulants through the expansion (64). Moreover, it is easier to check through the action \mathcal{S} and the generating function $\varphi(y)$ that the path integral (65) is indeed dominated by a saddle-point. On the other hand, as noticed above, in the quasi-linear regime it is best to compute the distribution $\mathcal{P}(\eta_r)$ from the integral (98), expressed in terms of $\varphi(y)$, as the property $\varphi(0) = 0$ automatically ensures that the probability distribution is properly normalized to unity (in the case of the gravitational dynamics this has been seen to give a good match with numerical results [26, 39]).

We can note that at this order the nonlinear distribution $\mathcal{P}(\eta_r)$ could be described by a spherical-dynamics model, where one makes the approximation $\mathcal{P}(\eta_r)d\eta_r = \mathcal{P}_L(\delta_{Lq})d\delta_{Lq}$ with $\eta_r = \mathcal{F}(\delta_{Lq})$ and \mathcal{P}_L is the initial distribution of the linear density contrast, as developed for instance in [55] for the collisionless gravitational dynamics. Note that such a phenomenological model can be readily extended to non-Gaussian initial conditions. However, one needs the steepest-descent framework described in the previous sections to justify the behavior (99) for the rare-event tails. Moreover, in cases where collisions (shocks) take place, such a phenomenological model becomes ambiguous, while the saddle-point approach remains valid and allows to derive exact results, as we shall describe in section V B below.

We show in Table V the asymptotic behaviors (100) obtained for the initial conditions given in Table I, as well as the lower bound η_* below which the saddle-point (76) forms shocks. The value of η_* will be derived in section V below, where we take into account shocks. Note that it is not related to the value \mathcal{G}_s where the cumulant generating function is singular, which was given in Table IV.

We show the distribution $\mathcal{P}(\eta_r)$ in Fig. 5 for a linear variance $\sigma_{\delta_{Lr}}^2 = 0.5$ and the cases $n = 0$ and $n = -2$ in $d = 3$. For finite $\sigma_{\delta_{Lr}}$ it is better to use the integral (98), rather than the asymptotic result (99), as it ensures that the distribution is normalized to unity and captures the asymmetry of the distribution with the shift of its peak. Note that in the case $\{n = -2, d = 1\}$ the inverse Laplace transform (98) of the quasi-linear generating function given in the fourth row of Table IV gives

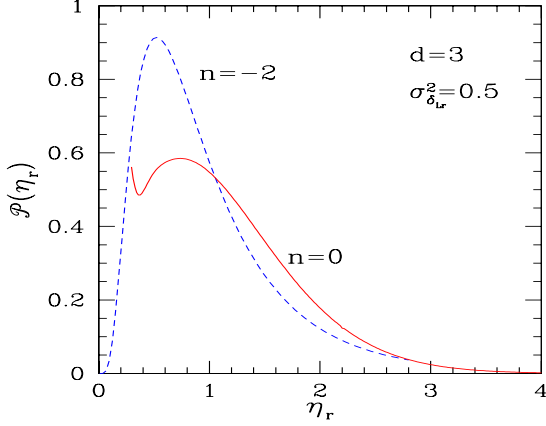


FIG. 5: (Color online) The probability distribution $\mathcal{P}(\eta_r)$ in the quasi-linear limit from Eq.(98). We show the cases $n = 0$ and $n = -2$ in three dimensions, for a linear variance $\sigma_{\delta_{Lr}}^2 = 0.5$.

the explicit expression

$$n = -2, d = 1: \mathcal{P}(\eta_r) = \frac{\eta_r^{-3/2}}{\sqrt{2\pi}\sigma_{\delta_{Lr}}} e^{-(\sqrt{\eta_r} - \frac{1}{\sqrt{\eta_r}})^2 / (2\sigma_{\delta_{Lr}}^2)}. \quad (103)$$

Again, as seen in [18], it happens that in this case the result (103) is actually exact. In generic cases, deviations from the quasi-linear limiting distribution should appear at small scales and late times.

From the geometrical construction described in Fig. 4 we can see that singularities for the function $\varphi(y)$ occur at inflexion points of the curve $-\tau^2(\mathcal{G})/2$. In particular, in agreement with the analysis of Eqs.(92)-(94), at large densities a singularity appears as soon as $\tau^2/\mathcal{G} \rightarrow 0$ for $\mathcal{G} \rightarrow \infty$, which implies that $-\tau^2(\mathcal{G})/2$ is no longer concave at large \mathcal{G} . From Eq.(99) this simply corresponds to a sub-exponential large-density tail of the form $\sim e^{-\eta_r^\alpha}$ with $\alpha < 1$. Then, it is clear that the integral (59) is divergent for $y < 0$ so that the exact cumulant generating function has a branch cut on the negative real axis, $y < 0$, even though the cumulants of all orders may be finite. In this case, the singularity at $y_s < 0$ and the two branches observed on $y_s < y < 0$ are related to this branch cut and to this sub-exponential large-density tail.

For the low-density tail, this construction shows that when $\tau(\mathcal{G})$ and $\tau'(\mathcal{G})$ remain finite for $\mathcal{G} \rightarrow 0$, a singularity appears on the positive real axis, $y_s > 0$, or $\varphi(y)$ is restricted to a finite range $y < y_s$. Thus, singularities on the positive real axis are generically associated with distributions that do not vanish in the limit $\eta_r \rightarrow 0$.

In any case, in the quasi-linear limit the large-fluctuation regime associated with the second branch of $\varphi(y)$ is irrelevant, as it is exponentially suppressed by a factor of the form $e^{-1/\sigma_{\delta_{Lr}}^2}$, see Eq.(99). Therefore, we only plot in Fig. 5 the range associated with the quasi-linear branch of $\varphi(y)$, that is, $\eta_r < 2\sqrt{2}$ for $n = -2$,

see Table IV. For $n = 0$, this would require $\eta_r > 1/8$, but as shown in Table V and explained in section VB7 below, shocks appear before this threshold, as soon as $\eta_r < (2/3)^3$, below which Eq.(100) is no longer valid. Therefore, in the case $\{n = 0, d = 3\}$, we only plot the result (98), obtained from the quasi-linear generating function, above this lower-density bound, $\eta_r > (2/3)^3$. In the limit $\sigma_{\delta_{Lr}} \rightarrow 0$ the weight associated with such low-density regions decays exponentially as $e^{-1/\sigma_{\delta_{Lr}}^2}$ (disregarding the numerical factor), but at $\sigma_{\delta_{Lr}}^2 = 0.5$ this region is already non-negligible. Note that the upturn at low density shown in Fig. 5 is not necessarily a signature of the breakdown of the quasi-linear limit in this domain at $\sigma_{\delta_{Lr}}^2 = 0.5$. Indeed, as discussed in section VB7, the distribution $\mathcal{P}(\eta_r)$ does not decay exponentially at low density, see also Table IX, and it may even grow as a power law. As shown in [30], this is for instance what happens for the case $\{n = 0, d = 1\}$, where at low density the probability distribution shows an inverse square root tail, $\mathcal{P}(\eta_r) \propto 1/\sqrt{\eta_r}$.

B. Velocity divergence (i.e. spherical velocity increment)

We now consider the probability distribution, $\mathcal{P}(\Theta_r)$, of the mean velocity divergence Θ_r , defined in Eq.(21), that is also the velocity increment over distance $2r$ averaged over all directions (up to a normalization factor). Following the method described in section IV A for the spherical overdensity η_r , we can also obtain the quasi-linear limit of $\mathcal{P}(\Theta_r)$ by a steepest-descent approach. Thus, we again define the moment and cumulant generating functions $\Psi(y)$ and $\varphi(y)$ as in Eqs.(59)-(64), which can be expressed as a path integral (65) with an action $\mathcal{S}[\delta_L]$ as in (66), where the nonlinear functional $\eta_r[\delta_L]$ is replaced by $\Theta_r[\delta_L]$. The action still being spherically symmetric, we can also look for a spherical saddle-point. If particles on the sphere S have not been shocked yet they have kept their initial velocity \mathbf{u}_0 , so that Θ_r only depends on the initial radial velocity \mathbf{u}_{0q} of the particles at the Lagrangian radius q that have moved to radius r at time t . Then, by the same reasoning as for the overdensity, we obtain as expected the same profile (76) for the saddle-point, but a different function $\mathcal{F}(\delta_{Lq})$. Indeed, since the radii q and r are related by $r = q + t u_{0q}$ we have from Eq.(21)

$$\Theta_r = -\frac{d}{r} t u_r(t) = -\frac{d}{r} t u_{0q} = d \left(\frac{q}{r} - 1 \right). \quad (104)$$

Note that Eq.(104) shows that for spherical dynamics the quantity Θ_r obeys

$$\Theta_r \geq -d. \quad (105)$$

This lower bound corresponds to very fast expansion, so that the particles observed at radius r come from the center $\mathbf{q} = 0$. Note that this requires the initial velocity field

to be singular at the origin, whence $n > -1$, in agreement with the exponential falloff (129), (134), obtained at low densities for $n < -1$, as shown in section V below. In such cases, where rarefaction regions can appear (i.e. truly empty regions), it may happen that the cell of radius r is within a larger empty domain, so that there are no particles on the sphere S . However, in the quasi-linear limit, where we consider small values of $|\Theta_r|$, we do not consider this case. Next, from Eq.(30) the linear density contrast is given by

$$\delta_{Lq} = -d \frac{t u_{0q}}{q} = d \left(1 - \frac{r}{q}\right), \quad (106)$$

whence

$$\Theta_r = \mathcal{F}(\delta_{Lq}) \quad \text{with} \quad \mathcal{F}(\delta_{Lq}) = -d + \frac{d}{1 - \frac{\delta_{Lq}}{d}}. \quad (107)$$

Again, since the function \mathcal{F} simply describes the spherical Burgers dynamics it only depends on the dimension d and not on the initial power spectrum. Then, we obtain the expression (78) with this new function \mathcal{F} , and we can define the associated variables τ and \mathcal{G} as in (79), so that the cumulant generating function $\varphi(y)$ is given by the relations (81) and (82). The spherical saddle-point being identical to the one obtained in section IV A 2, the profile (83) still applies for power-law power spectra, as well as Figs. 1, 2. In particular, if $n > d - 3$ shocks appear as soon as $t \neq 0$ so that this saddle-point is no longer exact in such cases. As in section IV A we shall not consider the modifications that appear in such cases, as they should remain small in the quasi-linear regime (with $d - 3 < n < d - 2$), and we focus on cases such that $n \leq d - 3$.

Close to the origin, since by symmetry we have $\langle \mathbf{u} \rangle = 0$, whence $\langle \Theta_r \rangle = 0$, we always have (compare with (84))

$$\tau \rightarrow 0, \quad y \rightarrow 0: \quad \mathcal{G} \sim -\tau, \quad y \sim \tau \quad \text{and} \quad \varphi \sim -\frac{y^2}{2}, \quad (108)$$

and keeping only these low-order terms gives back the linear Gaussian of variance $\sigma_{\delta_{Lr}}^2$. For the power-law initial power spectra (6) we obtain from Eqs.(79), (104),

$$\tau = -\delta_{Lq} \left(\frac{r}{q}\right)^{-\frac{n+3}{2}} = -\delta_{Lq} \left(1 + \frac{\Theta_r}{d}\right)^{\frac{n+3}{2}}, \quad (109)$$

which leads to

$$\tau(\mathcal{G}) = d \left(1 + \frac{\mathcal{G}}{d}\right)^{\frac{n+1}{2}} - d \left(1 + \frac{\mathcal{G}}{d}\right)^{\frac{n+3}{2}}, \quad (110)$$

and to the parametric representation of $\varphi(y)$,

$$\varphi = -dy - \frac{d^2}{2} \left[n \left(1 + \frac{\mathcal{G}}{d}\right)^{n+1} - 2(n+1) \left(1 + \frac{\mathcal{G}}{d}\right)^{n+2} + (n+2) \left(1 + \frac{\mathcal{G}}{d}\right)^{n+3} \right], \quad (111)$$

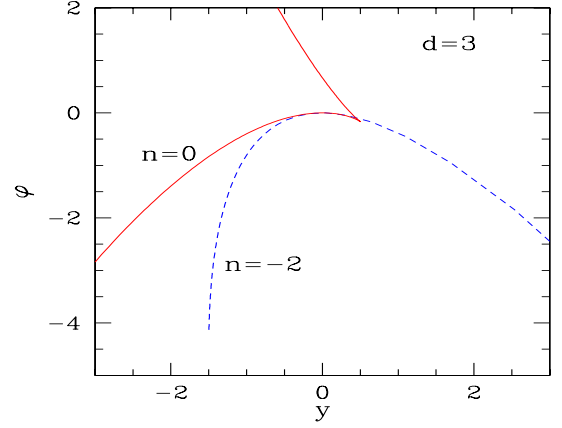


FIG. 6: (Color online) The cumulant generating function $\varphi(y)$ for the velocity divergence Θ_r , in dimension $d = 3$ for the power indices $n = 0$ (solid line) and $n = -2$ (dashed line), from rows 2 and 4 of Table VI. In both cases there is a singularity on the real axis, with $y_s = 1/2$ for $n = 0$ and $y_s = -3/2$ for $n = -2$, but only one branch for $n = -2$. The branch that runs through the origin is associated with moderate velocity fluctuations and is the relevant one for the expansion in terms of cumulants in the quasi-linear limit.

$$y = -\frac{d}{2} \left(1 + \frac{\mathcal{G}}{d}\right)^{-1} \left[(n+1) \left(1 + \frac{\mathcal{G}}{d}\right)^{n+1} - 2(n+2) \left(1 + \frac{\mathcal{G}}{d}\right)^{n+2} + (n+3) \left(1 + \frac{\mathcal{G}}{d}\right)^{n+3} \right] \quad (112)$$

We can see that, contrary to the Eqs.(88)-(89) associated with the density contrast, the dependence on d of the system (111)-(112) simplifies as $d^{-2}\varphi(dy)$ no longer depends on the dimension d . This implies for the probability distribution the scaling

$$\mathcal{P}_d(\Theta_r; \sigma_{\delta_{Lr}}^2) = \frac{1}{d} \mathcal{P}_1 \left(\frac{\Theta_r}{d}; \frac{\sigma_{\delta_{Lr}}^2}{d^2} \right), \quad (113)$$

where we noted $\mathcal{P}_d(\Theta_r; \sigma_{\delta_{Lr}}^2)$ the quasi-linear probability density of Θ_r in dimension d when the linear variance is $\sigma_{\delta_{Lr}}^2$. Thus, in the quasi-linear limit the change of dimension is fully absorbed by a rescaling of the velocity divergence Θ_r and of the linear variance $\sigma_{\delta_{Lr}}^2$. Therefore, contrary to the case of the overdensity studied in section IV A, the properties of $\varphi(y)$ and $\mathcal{P}(\Theta_r)$, such as the presence of singularities and sub-exponential tails, only depend on n and not on the dimension d .

Expanding near the origin, we obtain for the third and fourth-order cumulants in the quasi-linear limit:

$$\sigma_{\delta_{Lr}} \rightarrow 0: \quad S_3 = \frac{\langle \Theta_r^3 \rangle_c}{\langle \Theta_r^2 \rangle_c^2} = -3 \frac{n+1}{d}, \quad (114)$$

$$S_4 = \frac{\langle \Theta_r^4 \rangle_c}{\langle \Theta_r^2 \rangle_c^3} = \frac{3(n+1)(7n+9)}{d^2}. \quad (115)$$

n	$\varphi(y)$	y	$\mathcal{G} = \Theta_r$	$\varphi(y)$	y	$\mathcal{G} = \Theta_r$
0	$\frac{d^2}{27} - \frac{dy}{3} - \frac{d^2}{27} \left(1 - \frac{6y}{d}\right)^{3/2}$	$-\infty < y < \frac{d}{6}$	$-\frac{d}{3} < \mathcal{G} < \infty$	$\frac{d^2}{27} - \frac{dy}{3} + \frac{d^2}{27} \left(1 - \frac{6y}{d}\right)^{3/2}$	$-\frac{d}{2} < y < \frac{d}{6}$	$-d < \mathcal{G} < -\frac{d}{3}$
-1	$-\frac{y^2}{2}$	$-\infty < y < d$	$-d < \mathcal{G} < \infty$			
-2	$-d^2 - dy + d^2 \sqrt{1 + \frac{2y}{d}}$	$-\frac{d}{2} < y < \infty$	$-d < \mathcal{G} < \infty$			
$d = \infty$	$-\frac{y^2}{2}$	$-\infty < y < \infty$	$-\infty < \mathcal{G} < \infty$			

TABLE VI: The cumulant generating function $\varphi(y)$ of the velocity divergence Θ_r , in the quasi-linear limit $\sigma_{\delta_{Lr}}^2 \rightarrow 0$, for integer values of n and arbitrary dimension d , where explicit solutions of the system (111)-(112) can be obtained. The columns 2-4 show the quasi-linear branch, and the associated range of $\{y, \mathcal{G}\}$ that contains the point $\{0, 0\}$. The columns 5-7 show the second branch, associated with very rare events, that appears in some cases (here only for $n = 0$). The last row shows the infinite-dimensional limit, $d \rightarrow \infty$, which no longer depends on n and corresponds to the Gaussian.

As discussed below (21) this also gives the cumulants associated with the third and fourth-order spherical velocity structure functions in the quasi-linear limit. As for Eqs.(90)-(91), these quantities are not the standard skewness and kurtosis, and the powers in the denominators are such that they have a finite non-zero quasi-linear limit.

For integer values of n we can also derive explicit solutions to Eqs.(111)-(112), which we show in Table VI. As for the density studied in section IV A 3, the quasi-linear generating function $\varphi(y)$ can show two branches when the function $y(\mathcal{G})$ is not monotonic over $\mathcal{G} \in]-d, +\infty[$ (the variable \mathcal{G} now covers the range $]-d, +\infty[$, as seen from Eq.(105)). This occurs for $n = 0$, shown in the second row in Table VI, while for $n = -1$ and $n = -2$ there is only one branch.

In dimension $d = 1$ we have from Eqs.(104), (72),

$$d = 1 : \quad \Theta_r = \frac{q}{r} - 1 = \eta_r - 1, \quad (116)$$

so that the distributions $\mathcal{P}_1(\eta_r)$ and $\mathcal{P}_1(\Theta_r)$ are identical up to a shift of unity. Then, we can check that the results shown in Tables IV and VI for the case $\{n = -2, d = 1\}$ are consistent. In particular, the generating function given in the fourth row of Table VI yields the probability distribution

$$n = -2 : \quad \mathcal{P}(\Theta_r) = \frac{1}{\sqrt{2\pi}\sigma_{\delta_{Lr}}} \left(\frac{\Theta_r}{d} + 1\right)^{-3/2} \times \exp \left[-\frac{d^2}{2\sigma_{\delta_{Lr}}^2} \left(\sqrt{\frac{\Theta_r}{d} + 1} - \frac{1}{\sqrt{\frac{\Theta_r}{d} + 1}} \right)^2 \right]. \quad (117)$$

We can check that this agrees with relation (116) and Eq.(103) for $d = 1$. Moreover, in dimension $d = 1$ this result (117) again happens to be exact [18].

For $n = -1$ we simply obtain the Gaussian (third row

in Table VI)

$$n = -1 : \quad \varphi(y) = -\frac{y^2}{2}, \quad \mathcal{P}(\Theta_r) = \frac{1}{\sqrt{2\pi}\sigma_{\delta_{Lr}}} e^{-\Theta_r^2/(2\sigma_{\delta_{Lr}}^2)}. \quad (118)$$

Thus, the effects of the nonlinear evolution (107) and of the change of scale $q \rightarrow r$ (encoded in the change from \mathcal{F} to \mathcal{G}) compensate in such a way that at leading order in the quasi-linear limit the cumulants $\langle \Theta_r^p \rangle_c$ vanish, whence $\langle \Theta_r^p \rangle_c \ll \sigma_{\delta_{Lr}}^{2(p-1)}$ for $\sigma_{\delta_{Lr}} \rightarrow 0$ and $p \geq 3$, in agreement with Eqs.(114)-(115). However, note that the distribution (118) differs from the linear Gaussian in the sense that Θ_r is restricted to $\Theta_r \geq -d$, from Eq.(105). Of course, the weight associated with this lower bound becomes exponentially small in the quasi-linear limit, so that it cannot be seen in the leading-order value of the cumulants $\langle \Theta_r^p \rangle_c$, whence in the quasi-linear generating function $\varphi(y)$.

On the other hand, in the limit of large dimension, $d \rightarrow \infty$, we obtain $\mathcal{G}(\tau) = -\tau$ which gives back the linear Gaussian of Eq.(118), again in agreement with Eqs.(114)-(115). However, contrary to the distribution (118) associated with $n = -1$ at finite d , in the limit $d \rightarrow \infty$ the Gaussian extends down to $-\infty$, since the lower bound (105) is repelled to $-\infty$. Note that this was not the case for the overdensity η_r , where the probability distribution did not tend to the Gaussian but to a lognormal distribution for $d \rightarrow \infty$, see the last row in Table IV and Eqs.(90)-(91).

We show in Fig. 6 the quasi-linear cumulant generating function $\varphi(y)$, obtained in three dimensions for $n = 0$ and $n = -2$. Although there is a singularity on the real axis for both cases, there is only one branch for $n = -2$.

Next, the quasi-linear probability distribution $\mathcal{P}(\Theta_r)$ is obtained from the cumulant generating function $\varphi(y)$ by an inverse Laplace transform, as in Eq.(98). In the quasi-linear limit, as for the overdensity η_r , it obeys the asymptotic behavior (99). Then, using Eq.(110) we ob-

n	d	$\ln \mathcal{P}(\Theta_r)$	Θ_r
0	3	$-\frac{r^3}{2t^2} \left[\left(1 + \frac{\Theta_r}{3}\right)^{1/2} - \left(1 + \frac{\Theta_r}{3}\right)^{3/2} \right]^2$	$\Theta_r > -1$
-1	2	$-\frac{r^2}{8t^2} \Theta_r^2$	$\Theta_r > -1$
-2	1	$-\frac{r}{2t^2} \left[\left(1 + \Theta_r\right)^{-1/2} - \left(1 + \Theta_r\right)^{1/2} \right]^2$	$\Theta_r > -1$
-2	3	$-\frac{5r}{8t^2} \left[\left(1 + \frac{\Theta_r}{3}\right)^{-1/2} - \left(1 + \frac{\Theta_r}{3}\right)^{1/2} \right]^2$	$\Theta_r > -3$
n	∞	$-\frac{(2r^2)^{\frac{n+3}{2}}}{2t^2} \Theta_r^2$	

TABLE VII: Asymptotic behavior of the probability distribution $\mathcal{P}(\Theta_r)$ in the quasi-linear regime, for a few integer values of n and d , using the normalization of Table I for the initial conditions. The last column shows the range of spherical velocity increment Θ_r where these results apply. If the lower threshold is not equal to $-d$ (i.e. $-2 < n < d-3$), it means that the spherical saddle-point forms shocks for lower Θ_r .

tain

$$\sigma_{\delta_{Lr}} \rightarrow 0: \ln \mathcal{P}(\Theta_r) \sim \frac{-d^2}{2\sigma_{\delta_{Lr}}^2} \left[\left(1 + \frac{\Theta_r}{d}\right)^{\frac{n+1}{2}} - \left(1 + \frac{\Theta_r}{d}\right)^{\frac{n+3}{2}} \right]^2 \quad (119)$$

and in the large dimensional limit, where $\tau = -\Theta_r$,

$$d \rightarrow \infty, \sigma_{\delta_{Lr}} \rightarrow 0: \ln \mathcal{P}(\Theta_r) \sim -\frac{\Theta_r^2}{2\sigma_{\delta_{Lr}}^2}, \quad (120)$$

which only hold for $n < d-3$ and above a low- Θ_r threshold if $n > -2$, see Table III. Note that Eq.(119) may be directly obtained from the asymptotic tail (100) derived for the density distribution, $\mathcal{P}(\eta_r)$, by substituting

$$\Theta_r = d(\eta_r^{1/d} - 1), \quad \eta_r = \left(1 + \frac{\Theta_r}{d}\right)^d. \quad (121)$$

This relation follows from Eqs.(72), (104), that express both η_r and Θ_r in terms of the Lagrangian radius q of the saddle-point, so that there is a unique correspondence between η_r and Θ_r for these spherical saddle-points.

We show in Table VII the asymptotic behaviors (119) obtained for the initial conditions given in Table I, as well as the lower bound Θ_* below which the saddle-point (76) forms shocks, which will be derived in section V below where we take into account shocks. Again, the value (and the existence) of Θ_* is not related to the value (and the existence) of \mathcal{G}_s where the cumulant generating function is singular, which was given in Table VI.

We show in Fig. 7 our results for $\mathcal{P}(\Theta_r)$ for the cases $n = 0$ and $n = -2$ in three dimensions, for a linear variance $\sigma_{\delta_{Lr}}^2 = 0.5$, as in Fig. 5. Again, we only plot the distribution over the range associated with the quasi-linear branch of $\varphi(y)$. For $n = -2$ this actually covers the whole range $\Theta_r > -d$, but for $n = 0$ this corresponds to

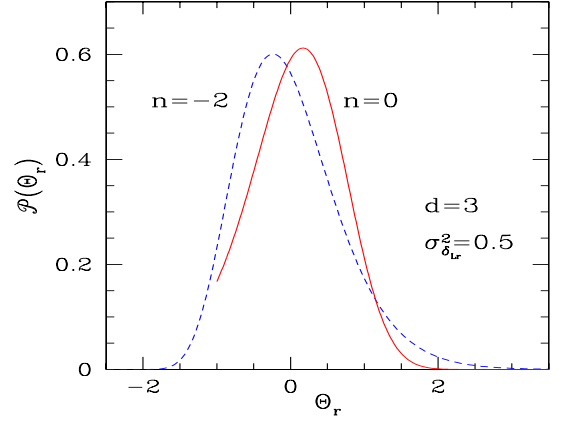


FIG. 7: (Color online) The probability distribution $\mathcal{P}(\Theta_r)$ of the velocity divergence Θ_r (spherical velocity increment) in the quasi-linear limit. We show the cases $n = 0$ and $n = -2$ in three dimensions, for a linear variance $\sigma_{\delta_{Lr}}^2 = 0.5$.

$\Theta_r > -d/3$, see Table VI. Note that in the latter case this lower bound happens to coincide with the lower bound Θ_* where shocks appear (for $d = 3$). The comparison between Figs. 7 and 5 shows that the distribution of the velocity divergence Θ_r remains closer to the Gaussian than the distribution of the overdensity η_r . This can also be seen from the fact that the singularities y_s are farther from the origin $y = 0$ (compare Tables VI and IV and Figs. 6 and 3). On the other hand, in agreement with (114), we can see that the skewness has opposite signs for $n = 0$ and $n = -2$, as the peak of the distribution shifts to either side of $\Theta_r = 0$, while the skewness of the density was always positive for $n < d-2$, see Eq.(90), which covers the range where $\sigma_{\delta_{Lr}}^2$ is well defined.

V. ASYMPTOTIC TAILS

The results obtained in section V applied to the quasi-linear limit, $\sigma_{\delta_{Lr}} \rightarrow 0$, for the case $n \leq d-3$, so that $\sigma_{\delta_{Lr}}$ is well defined and shocks only appear after a finite time (if $d-3 < n < d-2$ shocks appear as soon as $t \neq 0$ but $\sigma_{\delta_{Lr}}$ is still well defined and these results should provide a reasonable approximation). We now consider the limit of rare events, that is very large density and velocity fluctuations at fixed linear variance $\sigma_{\delta_{Lr}}^2$, or at fixed $\sigma_{\psi_{0r}}^2$ if $\sigma_{\delta_{Lr}}^2$ is divergent. Thus we study the tails of the probability distributions $\mathcal{P}(\eta_r)$ and $\mathcal{P}(\Theta_r)$, for any value of $\sigma_{\delta_{Lr}}$ or $\sigma_{\psi_{0r}}$. As in section IV we can use a steepest-descent approach and look for the minimum of the action \mathcal{S} , defined as in (66). This will give the tails of the probability distribution through Eq.(99).

A. Saddle-point without shocks

1. Rare density fluctuations

For $n \leq d - 3$ we can use the same action $\mathcal{S}[\delta_L]$ as in (66) and we obtain the same saddle-point defined by Eqs.(76) and (82) provided no shocks have formed. As discussed in section IV A 2, this constraint is satisfied for overdensities if $n \leq d - 3$ and for underdensities if $-3 < n \leq -2$. Therefore, in such cases Eq.(99) remains valid, where $\tau(\eta_r)$ is still given by Eq.(87), provided the saddle-point approximation is justified. Thus, we must show that as we consider very large density fluctuations the Laplace transform $\Psi(y)$ and the distribution $\mathcal{P}(\eta_r)$ are dominated by an increasingly narrow region around this saddle-point. We no longer have a fixed action $\mathcal{S}[\delta_L]$ multiplied by a prefactor that goes to infinity, as was the case in the quasi-linear regime for (65), with $1/\sigma_{\delta_{Lr}}^2 \rightarrow \infty$. Therefore, the analysis is more complicated as we should study the Hessian of the action at the saddle-point, which requires second-order perturbation theory around this saddle-point, taking into account angular degrees of freedom. Here we shall simply show that the steepest-descent approximation is well justified for $\Psi(y)$ (i.e. $\varphi(y)$) with respect to the family of initial states (76)-(77), parameterized by the overdensity \mathcal{G} within radius r .

In this subspace, the action $\mathcal{S}[\delta_L]$ is an ordinary function $\mathcal{S}(\mathcal{G})$, given by Eq.(80) as $\mathcal{S}(\mathcal{G}) = y\mathcal{G} + \tau(\mathcal{G})^2/2$. Thus, at the saddle-point the first and second derivative read as

$$\frac{d\mathcal{S}}{d\mathcal{G}} = 0, \quad \frac{d^2\mathcal{S}}{d\mathcal{G}^2} = \frac{d^2}{d\mathcal{G}^2} \left(\frac{\tau(\mathcal{G})^2}{2} \right). \quad (122)$$

Let us first consider the case of large underdensities, $\mathcal{G} \rightarrow 0$, with $-3 < n \leq -2$. Then, from Eq.(87) we have

$$\mathcal{G} \rightarrow 0: \quad \frac{d^2\mathcal{S}}{d\mathcal{G}^2} \sim \frac{(n+1)(n+1-d)}{2} \mathcal{G}^{\frac{n+1}{d}-2}. \quad (123)$$

Then, over this subspace, disregarding prefactors associated with changes of variables, we write the analog of (65) as

$$e^{-\varphi(y)/\sigma_{\delta_{Lr}}^2} \sim \int d\mathcal{G} e^{-\mathcal{S}(\mathcal{G})/\sigma_{\delta_{Lr}}^2}, \quad (124)$$

and expanding the action around the saddle-point \mathcal{G}_c , defined by the condition $d\mathcal{S}/d\mathcal{G} = 0$, we find that only values sufficiently close to \mathcal{G}_c contribute to the integral, with

$$|\mathcal{G} - \mathcal{G}_c| \sim \frac{1}{\sqrt{\mathcal{S}''(\mathcal{G})}} \sim \mathcal{G}_c^{1-\frac{n+1}{2d}}, \quad (125)$$

whence (since $-3 < n \leq -2$)

$$\mathcal{G}_c \rightarrow 0: \quad \frac{|\mathcal{G} - \mathcal{G}_c|}{\mathcal{G}_c} \sim \mathcal{G}_c^{-(n+1)/(2d)} \rightarrow 0. \quad (126)$$

Since $\mathcal{S}(\mathcal{G})$ behaves as a power law, Eq.(126) implies that higher-order terms beyond the Gaussian around \mathcal{G}_c are subdominant. Thus, at large positive y , which corresponds to $\mathcal{G}_c \rightarrow 0$, see (96), the Laplace transform $\varphi(y)$ is dominated by its saddle-point (if we only consider the subspace described by the profile (76)). Then, assuming that this remains true when we take into account other degrees of freedom, and that there is no deeper minimum associated with strong deviations from spherical symmetry, we recover at large y the behavior (95) obtained in section IV A 3 where we studied the quasi-linear regime. Next, the distribution $\mathcal{P}(\eta_r)$ is still given by the inverse Laplace transform (98), and it only remains to show that this integral is again dominated by its saddle-point, in the limit $\eta_r \rightarrow 0$. As noticed in section IV A 4, the saddle-point y_c of the exponential satisfies $\eta_r = \varphi'(y_c)$, whence $\eta_r = \mathcal{G}_c$ where \mathcal{G}_c is related to y_c through the Legendre transformation (81). Thus, in the limit $\eta_r \rightarrow 0$ we obtain $y_c \rightarrow +\infty$ and from the previous results the behavior (95). Next, expanding the exponential around y_c , we find that contributions to $\mathcal{P}(\eta_r)$ come from the range

$$|y - y_c| \sim \frac{1}{\sqrt{-\varphi''(y_c)}} \sim y_c^{1-\frac{n+1}{2(n+1-d)}}, \quad (127)$$

where we used the large- y behavior (95). This yields

$$y_c \rightarrow \infty: \quad \frac{|y - y_c|}{y_c} \sim y_c^{-\frac{n+1}{2(n+1-d)}} \rightarrow 0, \quad (128)$$

which again ensures that the integral (98) is dominated by the Gaussian integration around its saddle-point in the limit $\eta_r \rightarrow 0$. Therefore, the steepest-descent approximation is legitimate at very low densities, whatever the value of $\sigma_{\delta_{Lr}}$, and we recover the rare-event tail (99). As in (100), this yields the low-density tail

$$-3 < n \leq -2, \quad \eta_r \rightarrow 0: \quad \mathcal{P}(\eta_r) \sim e^{-d^2\eta_r^{\frac{n+1}{d}}/(2\sigma_{\delta_{Lr}}^2)}. \quad (129)$$

We can apply the same procedure for large overdensities, $\eta_r \rightarrow +\infty$. Here, a subtlety arises from the fact that for $n < d - 3$ large densities are associated with the second branch (94) of $\varphi(y)$ discussed in section IV A 3. As recalled in section IV A 4, this simply corresponds to cases where the high-density tail of the distribution $\mathcal{P}(\eta_r)$ shows a sub-exponential decay, such as $e^{-\eta_r^\alpha}$ with $\alpha < 1$. From the definition (59) we can see at once that in such cases the Laplace transform $\Psi(y)$, whence $\varphi(y)$, diverge for negative y : they generically have a branch cut along the negative real axis. Then, the saddle-point in the path integral (65) becomes a local maximum but one can still apply the steepest-descent method, using an appropriate deformation of the integration contours in the complex plane. This is discussed in details in section 3.6 and appendices A and B of [39] hence we do not give further comments on this point here, see also the chapter on instanton contributions in [44]. Then, as for underdensities, we can check that for large overdensities the contributions to $\varphi(y)$ come from an increasingly narrow

range of \mathcal{G} , when we restrict to the subspace parameterized by the profile (76), as in (124). Thus, using again Eq.(87), we now find that the range of overdensities that contribute to $\varphi(y)$ behaves as

$$\mathcal{G}_c \rightarrow +\infty : \frac{|\mathcal{G} - \mathcal{G}_c|}{\mathcal{G}_c} \sim \mathcal{G}_c^{-(n+3)/(2d)} \rightarrow 0, \quad (130)$$

so that $\varphi(y)$ is still governed by the saddle-point (assuming there are no larger contributions associated with strong deviations from spherical symmetry), and we recover the behavior (94). Then, the range of y that contributes to the large-density tail is

$$y_c \rightarrow 0^- : \frac{|y - y_c|}{|y_c|} \sim |y_c|^{\frac{n+3}{2(d-n-3)}} \rightarrow 0. \quad (131)$$

Therefore, the steepest-descent approximation is again legitimate at very high densities, whatever the value of $\sigma_{\delta_{Lr}}$, and we recover the rare-event tail (99). As in (100), this yields the high-density tail

$$n \leq d - 3, \quad \eta_r \rightarrow \infty : \mathcal{P}(\eta_r) \sim e^{-d^2 \eta_r^{\frac{n+3}{d}} / (2\sigma_{\delta_{Lr}}^2)}. \quad (132)$$

We can check that in the case $\{n = -2, d = 1\}$ both asymptotics (129), (132), agree with the exact distribution (103).

In the large dimensional limit, $d \rightarrow \infty$, we still obtain Eq.(101), which applies to both rare overdensities and underdensities, but only if $n \leq -2$ in the latter case.

In fact, the saddle-point approximation is valid as long as we consider the limit of rare events, which corresponds either to the quasi-linear limit, $\sigma_{\delta_{Lr}} \rightarrow 0$ (i.e. $r^{n+3}/t^2 \rightarrow \infty$) at fixed density η_r and velocity increment Θ_r , or to the limit of extreme densities, $\eta_r \rightarrow 0$ or $\eta_r \rightarrow \infty$, and extreme velocities, $\Theta_r \rightarrow -d$ or $\Theta_r \rightarrow \infty$, at fixed time and scale (i.e. at finite $\sigma_{\delta_{Lr}}$). Of course, the range of density fluctuations to which these results apply is a priori repelled to increasingly large fluctuations, $\eta_r \rightarrow \infty$ or $\eta_r \rightarrow 0$, as $\sigma_{\delta_{Lr}}$ grows (since they correspond to rare events, $\mathcal{P} \ll 1$). In such regimes, integrals such as (65) are governed at leading order by the minimum of the action \mathcal{S} , which shows a steep dependence on the initial conditions. This legitimates the steepest-descent approximation in these cases.

We can note that an exception to this behavior occurs when the action happens to be singular at its minimum, that is the initial conditions where \mathcal{S} is close to its minimum form a subspace of measure zero. For ordinary integrals such as (124), this corresponds to cases where the function $\mathcal{S}(\mathcal{G})$ is discontinuous at the point \mathcal{G}_c , with $\mathcal{S}(\mathcal{G}_c)$ being strictly smaller than both left and right limits, $\mathcal{S}(\mathcal{G}_c^-)$ and $\mathcal{S}(\mathcal{G}_c^+)$. This possibility actually appears for the case of the collisionless gravitational dynamics [56], where at large positive densities a strong radial orbit instability appears (associated with the extreme sensitivity of the trajectories, that actually diverges, as particles move through the center of the object). This problem does not appear in the Burgers dynamics, since in any

case particles that would reach the center would stick there. Thus, the infinitesimal viscosity regularizes the dynamics and makes the sensitivity to non-spherical perturbations finite. This well-behaved dependence on the initial conditions clearly appears through the Hopf-Cole solution recalled in section II D.

If we are only interested in the exponents that appear in the expressions (129), (132), disregarding the numerical factors and using Eq.(29) they read at leading order as

$$n \leq d - 3, \quad \eta_r \rightarrow \infty : \ln \mathcal{P}(\eta_r) \propto -r^{n+3} \eta_r^{\frac{n+3}{d}} / t^2 \quad (133)$$

$$-3 < n \leq -2, \quad \eta_r \rightarrow 0 : \ln \mathcal{P}(\eta_r) \propto -r^{n+3} \eta_r^{\frac{n+1}{d}} / t^2 \quad (134)$$

We give in Table VIII the explicit expressions of the tails (129), (132), for the initial conditions normalized as in Table I, and we mark as ‘‘shock’’ the cases where the saddle-point discussed above gives rise to shocks. This agrees with Table V where we only keep the leading term for $\eta_r \rightarrow \infty$ or $\eta_r \rightarrow 0$.

2. Rare velocity fluctuations

The discussion of $\mathcal{P}(\eta_r)$ in the previous section directly extends to the tails of the distribution $\mathcal{P}(\Theta_r)$ of the mean divergence Θ_r (spherical velocity increment), defined in (21). Thus, for the same cases as in section V A 1 where the saddle-point does not form shocks, the rare-event tails are still given at leading order by the first exponential in Eq.(99), where $\tau(\Theta_r)$ is given by Eq.(110), whence by Eq.(119). This yields

$$n \leq d - 3, \quad \Theta_r \rightarrow \infty :$$

$$\ln \mathcal{P}(\Theta_r) \sim -\frac{d^2}{2\sigma_{\delta_{Lr}}^2} \left(\frac{\Theta_r}{d}\right)^{n+3} \propto -\frac{r^{n+3} \Theta_r^{n+3}}{t^2}, \quad (135)$$

and

$$-3 < n \leq -2, \quad \Theta_r \rightarrow -d :$$

$$\ln \mathcal{P}(\Theta_r) \sim \frac{-d^2}{2\sigma_{\delta_{Lr}}^2} \left(1 + \frac{\Theta_r}{d}\right)^{n+1} \quad (136)$$

$$\propto -\frac{r^{n+3}}{t^2} \left(1 + \frac{\Theta_r}{d}\right)^{n+1}. \quad (137)$$

In the large dimension limit we still have Eq.(120), which holds for $\Theta_r \rightarrow \infty$ for any n , but for $\Theta_r \rightarrow -\infty$ only if $n \leq -2$. We also give these results in Table VIII.

Note that the appearance of a second branch for $\varphi(y)$ is not simultaneous for η_r and Θ_r , as noticed in section IV B and as can be seen from the comparison of Tables IV and VI. Since for spherical initial conditions η_r and Θ_r are related by (121), it is clear that the subtlety associated with the second branch of $\varphi(y)$, that is, the branch cut of the exact Laplace transform, is only a mathematical difficulty due to a sub-exponential tail but has no physical effect. Thus, in cases where only

n	d	$\ln \mathcal{P}(\eta_r)$ for $\eta_r \rightarrow \infty$	$\ln \mathcal{P}(\eta_r)$ for $\eta_r \rightarrow 0$	$\ln \mathcal{P}(\Theta_r)$ for $\Theta_r \rightarrow \infty$	$\ln \mathcal{P}(\Theta_r)$ for $\Theta_r \rightarrow -d$
0	3	$-r^3 \eta_r / (2t^2)$	shock	$-r^3 \Theta_r^3 / (54t^2)$	shock
-1	2	$-r^2 \eta_r / (2t^2)$	shock	$-r^2 \Theta_r^2 / (8t^2)$	shock
-2	1	$-r \eta_r / (2t^2)$	$-r / (2t^2 \eta_r)$	$-r \Theta_r / (2t^2)$	$-r / [2t^2 (1 + \Theta_r)]$
-2	3	$-5 r \eta_r^{1/3} / (8t^2)$	$-5 r / (8t^2 \eta_r^{1/3})$	$-5 r \Theta_r / (24t^2)$	$-15 r / [8t^2 (3 + \Theta_r)]$
n	∞	$-\frac{(2r^2)^{\frac{n+3}{2}}}{2t^2} \ln^2(\eta_r)$	$-\frac{(2r^2)^{\frac{n+3}{2}}}{2t^2} \ln^2(\eta_r)$ if $n \leq -2$	$-\frac{(2r^2)^{\frac{n+3}{2}}}{2t^2} \Theta_r^2$	$-\frac{(2r^2)^{\frac{n+3}{2}}}{2t^2} \Theta_r^2$ if $n \leq -2$

TABLE VIII: The tails of the distributions $\mathcal{P}(\eta_r)$ and $\mathcal{P}(\Theta_r)$ for a few integer values of n and d where the relevant saddle-point is regular (i.e. does not induce shocks), from Eqs.(129), (132). The initial conditions are those given in Table I (i.e. with the same normalization). Cases marked as “shock” correspond to saddle-points that give rise to shocks, so that the normalization factors in Eqs.(129), (132), and (135)-(136), are no longer valid. They are analyzed in section VB (this includes the case $\{n = 0, d = 1\}$ for both large and small densities). For $d \rightarrow \infty$ the expressions given at low densities and velocity divergences only hold for $n \leq -2$ ($n > -2$ gives rise to shocks).

the density quasi-linear generating function $\varphi(y)$ shows a second branch, we can first compute the high- Θ_r tail of $\mathcal{P}(\Theta_r)$, which only involves local minima of the action and does not require a deformation of integration contours, and next use the relation (121) to derive the high-density tail of $\mathcal{P}(\eta_r)$. More generally, as noticed in [39], in order to avoid the complications associated with sub-exponential tails, we can simply compute the rare-event tail of the quantity $X = \eta_r^\beta$, with a small enough β so that $\mathcal{P}(X)$ shows a super-exponential decay, and next derive $\mathcal{P}(\eta_r)$ from $\mathcal{P}(X)$ through a simple change of variable. On the other hand, we could directly obtain Eqs.(135)-(137) from Eqs.(129), (132), by using the relation (121).

B. Saddle-point with shocks

1. Paraboloid construction and action $\mathcal{S}[\psi_0]$

For cases where the constraints in (129), (132), are not satisfied, that is when shocks cannot be ignored, we can no longer rely on the regular saddle-point of the previous section V A. However, we can use the exact solution (36), and the geometrical construction (38), to study solutions of the equations of motion that contain shocks. In particular, following the approach used in the previous sections, we can look for saddle-points of an appropriate action, that include shocks, to obtain the tails of the distribution $\mathcal{P}(\eta_r)$. However, to use (36) it is more convenient to work with the velocity potential ψ_0 , rather than with its Laplacian, $\theta_0 = \delta_L/t$, that we used in section IV. Thus, we now write the Laplace transform (59) as

$$\Psi(y) = (\det C_{\psi_0}^{-1})^{1/2} \int \mathcal{D}\psi_0 e^{-y\eta_r[\psi_0] - \frac{1}{2}\psi_0 \cdot C_{\psi_0}^{-1} \cdot \psi_0}, \quad (138)$$

where $\eta_r[\psi_0]$ is now the functional that affects to the initial condition ψ_0 the nonlinear overdensity η_r , built at

time t within the cell of radius r centered on the origin, $\mathbf{x} = 0$; and $C_{\psi_0}(\mathbf{x}_1, \mathbf{x}_2)$ is the two-point correlation of the initial potential. Although this is no longer essential (since we do not consider here the limit $\sigma_{\psi_{0r}} \rightarrow 0$) we rescale the transform $\Psi(y)$ in a fashion similar to Eq.(63),

$$\Psi(y) = e^{-\varphi(y\sigma_{\psi_{0r}}^2)/\sigma_{\psi_{0r}}^2}, \quad (139)$$

so as to obtain an action $\mathcal{S}[\psi_0]$ that is similar to Eq.(66),

$$\mathcal{S}[\psi_0] = y \eta_r[\psi_0] + \frac{\sigma_{\psi_{0r}}^2}{2} \psi_0 \cdot C_{\psi_0}^{-1} \cdot \psi_0, \quad (140)$$

where $\sigma_{\psi_{0r}}$ is the variance of the initial radial potential ψ_{0r} at radius r , defined in Eq.(34).

As in section IV we can look for spherical saddle-points. Then, we can look for the minimum of the action $\mathcal{S}[\psi_0]$ within the subspace of spherically symmetric initial conditions, where $\psi_0(\mathbf{q}) = \psi_{0q}$ with $q = |\mathbf{q}|$, and the restriction of the action to this subspace reads as

$$\mathcal{S}[\psi_{0q'}] = y \eta_r[\psi_{0q'}] + \frac{\sigma_{\psi_{0r}}^2}{2} \psi_{0q'_1} \cdot C_{\psi_{0r}}^{-1} \cdot \psi_{0q'_2}, \quad (141)$$

where $C_{\psi_{0r}}(q'_1, q'_2)$ is the radial covariance introduced in Eq.(33).

2. Regular saddle-point without shocks

Let us first check that in the case where there is no shock, we recover from (141) the results obtained in section IV. As in Eq.(71), a saddle-point of the action (141) is characterized by

$$\psi_{0q'} = \frac{-y}{\sigma_{\psi_{0r}}^2} \int_0^\infty dq'' C_{\psi_{0r}}(q', q'') \frac{\mathcal{D}\eta_r}{\mathcal{D}\psi_{0q''}}. \quad (142)$$

Following the discussion below Eq.(73), since η_r only depends on the initial velocity at the Lagrangian radius q , and $u_{0q} = -d\psi_{0q}/dq$, the functional differential

$\mathcal{D}\eta_r/\mathcal{D}\psi_{0q''}$ is zero for $q'' \neq q$. However, it is no longer a Dirac, $\delta_D(q'' - q)$, but its first derivative, $\delta'_D(q'' - q)$. Indeed, from the geometrical construction (38), the Lagrangian radius q is obtained as the first-contact point of the paraboloid $\mathcal{P}_{\mathbf{x},c}(\mathbf{q})$ with the initial potential $\psi_0(\mathbf{q})$. Using the spherical symmetry this corresponds to the first-contact point of the parabola $\mathcal{P}_{r,c}(q)$ with the curve ψ_{0q} , which is characterized by the two equations (for contact and tangent slopes)

$$\psi_{0q} = \frac{(q-r)^2}{2t} + c, \quad \psi'_{0q} = \frac{q-r}{t}. \quad (143)$$

Then, as we change the initial potential by an infinitesimal perturbation $\Delta\psi_{0q'}$, both c and q are modified by amounts Δc and Δq , and the second Eq.(143) gives

$$\Delta q = \left(\frac{1}{t} - \psi''_{0q} \right)^{-1} \Delta \psi'_{0q} \quad (144)$$

Then, since $\eta_r = (q/r)^d$ as in Eq.(72), we have $\Delta\eta_r \propto \Delta q \propto \Delta\psi'_{0q}$, whence

$$\frac{\mathcal{D}\eta_r}{\mathcal{D}\psi_{0q''}} \propto \delta'_D(q'' - q). \quad (145)$$

Thus, in agreement with the previous discussion, the derivative (145) vanishes for $q'' \neq q$, but it is now the first derivative of the Dirac distribution. Substituting into Eq.(142) gives the linear profiles of the saddle-point as

$$\psi_{0q'} \propto \frac{\partial}{\partial q} C_{\psi_{0r}}(q', q), \quad (146)$$

$$u_{0q'} \propto \frac{\partial^2}{\partial q' \partial q} C_{\psi_{0r}}(q', q) \propto C_{u_{0r}}(q', q), \quad (147)$$

where we used Eq.(32). Then, the comparison with Eq.(77) shows that we have obtained the same spherical saddle-point as in section IV A 2. This means that we recover the results of section IV in the quasi-linear limit (here $\sigma_{\psi_{0r}} \rightarrow 0$), and of section V A in the appropriate rare-event limits ($\eta_r \rightarrow 0$ or $\eta_r \rightarrow \infty$). In particular, the tail of the probability distribution reads at leading order as

$$\mathcal{P}(\eta_r) \sim e^{-\frac{1}{2}\psi_0(\mathbf{q}_1) \cdot C_{\psi_0}^{-1} \cdot \psi_0(\mathbf{q}_2)} = e^{-\frac{1}{2}\psi_{0q_1} \cdot C_{\psi_{0r}}^{-1} \cdot \psi_{0q_2}}, \quad (148)$$

where the exponent is evaluated at the saddle-point, as in Eq.(99) to which it is equivalent.

3. Taking shocks into account

The advantage of the formulation (141) in terms of the potential ψ_0 is that we can now handle cases where shocks must be taken into account. Note that this applies in particular to the cases $n \geq d - 2$ where the variance σ_{Lr}^2 of the linear density contrast is divergent. To this

order, we generalize the previous configuration, with a unique first-contact point between $\mathcal{P}_{r,c}(q)$ and ψ_{0q} , to states where the initial potential follows the parabola over a finite range $[q_-, q_+]$, and remains below it elsewhere. This corresponds in particular to a shock at radius r that contains all the matter that was initially located within Lagrangian radii q_- and q_+ (all this matter merging at position r at time t). Then, the nonlinear overdensity η_r is not modified by infinitesimal perturbations $\Delta\psi_{0q}$ over $q \notin [q_-, q_+]$ (since they do not affect the first-contact parabola) and Eq.(142) implies

$$q \geq 0: \quad \psi_{0q} = \int_{q_-}^{q_+} dq' C_{\psi_{0r}}(q, q') f(q'), \quad (149)$$

with some kernel $f(q')$ to be determined (in the case of a unique contact point, i.e. no shock, we have seen above in Eq.(146) that we have $f(q') \propto \delta'_D(q' - q_+)$ and $q_- = q_+$). Let us note $\overline{C}_{\psi_{0r}}$ the restriction of the kernel $C_{\psi_{0r}}(q_1, q_2)$ to the interval $[q_-, q_+]$. Then, since $\psi_{0q} = \mathcal{P}_{r,c}(q)$ over the range $[q_-, q_+]$, Eq.(149) implies over this interval:

$$q_- \leq q \leq q_+: \quad \mathcal{P}_{r,c} = \overline{C}_{\psi_{0r}} \cdot f, \quad \text{whence } f = \overline{C}_{\psi_{0r}}^{-1} \cdot \mathcal{P}_{r,c} \quad (150)$$

Moreover, substituting Eq.(149) into the action (141) yields

$$\mathcal{S} = y\eta_r + \frac{\sigma_{\psi_{0r}}^2}{2} \int_{q_-}^{q_+} dq_1 dq_2 f(q_1) C_{\psi_{0r}}(q_1, q_2) f(q_2) \quad (151)$$

$$= y\eta_r + \frac{\sigma_{\psi_{0r}}^2}{2} \int_{q_-}^{q_+} dq_1 dq_2 \mathcal{P}_{r,c}(q_1) \overline{C}_{\psi_{0r}}^{-1}(q_1, q_2) \mathcal{P}_{r,c}(q_2) \quad (152)$$

$$= y\eta_r + \frac{\sigma_{\psi_{0r}}^2}{2} \int_{q_-}^{q_+} dq f(q) \mathcal{P}_{r,c}(q). \quad (153)$$

Next, since η_r and $\overline{C}_{\psi_{0r}}^{-1}$ only depend on q_- and q_+ , minimizing the action (152) with respect to the height c of the parabola $\mathcal{P}_{r,c}$ gives

$$\frac{\partial \mathcal{S}}{\partial c} = \sigma_{\psi_{0r}}^2 \int_{q_-}^{q_+} dq_1 dq_2 \overline{C}_{\psi_{0r}}^{-1}(q_1, q_2) \mathcal{P}_{r,c}(q_2) = 0, \quad (154)$$

whence, using Eq.(150),

$$\int_{q_-}^{q_+} dq f(q) = 0. \quad (155)$$

Thus, in order to minimize the action $\mathcal{S}[\psi_0]$ over the spherically symmetric initial conditions that show a shock at radius r we proceed in two steps. First, the minimum of \mathcal{S} over the class of profiles ψ_0 that follow their first-contact parabola over a finite range $[q_-, q_+]$, to be determined afterwards, is obtained by solving Eqs.(150) and (155). This gives the kernel f and the parabola height c as a function of the parameters q_- and q_+ . Second, substituting into the action (153) we minimize \mathcal{S} over q_- and q_+ . This provides the minimum of the action (141) over all spherical states such that the Eulerian radius r maps to a continuous Lagrangian range

$[q_-, q_+]$, provided the saddle-point obtained in this fashion remains strictly below the parabola $\mathcal{P}_{r,c}$ outside of the interval $[q_-, q_+]$, which we must check afterwards since we have not imposed the constraint $\psi_0 \leq \mathcal{P}_{r,c}$ in the previous derivation. A priori it could happen that the minimum of the action is reached for initial configurations that touch the first-contact parabola over disjoint regions. Then, this would be seen by noticing that the minimum obtained through the previous procedure touches or crosses the parabola $\mathcal{P}_{r,c}$ somewhere outside of the range $[q_-, q_+]$. In such a case, one would need to generalize the approach described above to initial states that follow their first-contact parabola over k several disjoint intervals $[q_-^{(i)}, q_+^{(i)}]$, $i = 1, \dots, k$. Starting with the case $k = 1$ discussed above, one could add a new contact interval in a series of steps, until the minimizing profile remains below the first-contact parabola everywhere outside of the k contact intervals. Note that this method also includes the case where some intervals are reduced to a point, which corresponds to the limit $q_+^{(i)} - q_-^{(i)} \rightarrow 0$. Thus, this covers the case where the parabola would only have two (or a few) isolated first-contact points.

Finally, we must specify the relation between the overdensity η_r and the Lagrangian coordinates q_- and q_+ . We must separate the cases of large overdensities and underdensities as

$$\eta_r > 1: \quad \eta_r = \left(\frac{q_+}{r}\right)^d, \quad \eta_r < 1: \quad \eta_r = \left(\frac{q_-}{r}\right)^d. \quad (156)$$

Indeed, since we have a shock at radius r , with a finite mass $m^{\text{shock}} \propto (q_+^d - q_-^d)$, the density within radius r and the enclosed mass are ambiguous. It is actually discontinuous at r , going from m_- to m_+ with $m_+ - m_- = m^{\text{shock}}$. This also means that the minimum discussed above is unstable, in the sense that an infinitesimal perturbation will move this mass inward or outward, so that $m(< r)$ goes to m_- or m_+ . Then, if we consider rare and large overdensities, the probability $\mathcal{P}(\eta_r)$ will be governed by the initial conditions close to the previous minimum such that $m(< r) \simeq m_+$, which leads to the first Eq.(156). Similarly, for extreme underdensities we obtain the second Eq.(156). Note that this also shows that the action \mathcal{S} is not regular at the minimum obtained above and going beyond the leading term given by the exponential as in Eq.(148) would require a careful analysis. However, this discontinuity is not of the same kind as the one encountered for collisionless gravitational collapse, associated with radial orbit instability and recalled in section V A 1 above, since by using (156) we simply consider the left or right limit of \mathcal{S} (with respect to any degree of freedom) and not an isolated point of zero measure.

4. Computation of the saddle-point

In practice, it can be difficult to solve Eq.(150) for the kernel f , and we did not obtain a general solution. However, for the power-law power spectra (6) with low integer

values of n and d , where the radial potential correlation $C_{\psi_{0r}}(q_1, q_2)$ takes the simple forms given in Table I, it is possible to derive explicit expressions for $f(q)$ from Eq.(150). It is convenient to first write $f(q)$ as a derivative,

$$f(q) = \frac{dg}{dq} \quad \text{and} \quad g(q_+) = g(q_-) = 0. \quad (157)$$

In the second equality we used Eq.(155), which yields $g(q_+) = g(q_-)$, and the fact that $g(q)$ being defined up to an additive constant we can choose $g(q_-) = 0$. Next, substituting into the first Eq.(150), integrating by parts and derivating once, we obtain

$$q_- \leq q \leq q_+ : \quad \frac{r-q}{t} = \int_{q_-}^{q_+} dq' C_{u_{0r}}(q, q') g(q'), \quad (158)$$

where we used the first relation (32). Then, we can devise a systematic procedure to solve Eq.(158) when $d - n$ is an odd integer, that is for

$$d = n + 1 + 2\ell \quad \text{with} \quad \ell \in \mathbb{N}. \quad (159)$$

Indeed, from Eqs.(32) and (27) we have, with a normalization factor D ,

$$C_{u_{0r}}(q_1, q_2) = D \int_0^\infty dk k^n \Phi_k(q_1) \Phi_k(q_2), \quad (160)$$

where we introduced the eigenfunctions on $[0, \infty[$ of the linear operator \mathcal{L} ,

$$q \geq 0 : \quad \Phi_k(q) = \frac{J_{d/2}(kq)}{(kq)^{d/2-1}}, \quad \mathcal{L} \cdot \Phi_k = k^2 \Phi_k, \quad (161)$$

with

$$\mathcal{L} = -\frac{d^2}{dq^2} + \frac{1-d}{q} \frac{d}{dq} + \frac{d-1}{q^2}. \quad (162)$$

On the other hand, we note from standard properties of Bessel functions (i.e. Hankel transforms) that

$$\int_0^\infty dk k^{d-1} \Phi_k(q_1) \Phi_k(q_2) = q_1^{1-d} \delta_D(q_1 - q_2). \quad (163)$$

Therefore, noting \mathcal{L}^\dagger the adjoint of \mathcal{L} ,

$$\mathcal{L}^\dagger = -\frac{d^2}{dq^2} + \frac{d-1}{q} \frac{d}{dq}, \quad (164)$$

we have when condition (159) is satisfied, for $q_- \leq q \leq q_+$,

$$\begin{aligned} & \int_{q_-}^{q_+} dq' C_{u_{0r}}(q, q') \left(\mathcal{L}^{\dagger \ell} q'^{d-1} \frac{r-q'}{Dt} \right) \\ &= \int_{q_-}^{q_+} dq' \int_0^\infty dk k^n \Phi_k(q) (\mathcal{L}^\ell \Phi_k(q')) q'^{d-1} \frac{r-q'}{t} + \text{b.t.} \\ &= \frac{r-q}{t} + \text{b.t.} \end{aligned} \quad (165)$$

where we used Eqs.(161), (163), and ‘‘b.t.’’ stands for boundary terms at $q' = q_{\pm}$ generated by the integrations by parts over q' . Thus, we obtain the solution of Eq.(158) as

$$g(q) = \mathcal{L}^{\dagger \ell} q^{d-1} \frac{r-q}{Dt} + \text{b.t.} \quad (166)$$

where the boundary terms are of the Dirac type, such as $\delta_D(q-q_{\pm})$ and its derivatives, localized on the boundaries q_{\pm} . Using the relation (159) this yields

$$\ell = 0 : g(q) \propto q^n \frac{r-q}{t}, \quad \ell \geq 1 : g(q) \propto \frac{q^n r}{t} + \text{b.t.} \quad (167)$$

Then, the kernel $f(q)$ can be obtained from Eq.(157). However, from Eq.(149) we can see that $g(q)$ directly gives the velocity profile of the saddle-point as

$$u_{0q} = \int_{q-}^{q+} dq' C_{u_{0r}}(q, q') g(q'), \quad (168)$$

which follows the linear slope (158) in the interval $[q-, q+]$, while the action (153) writes

$$\mathcal{S} = y\eta_r + \frac{\sigma_{\psi_{0r}}^2}{2} \int_{q-}^{q+} dq g(q) \frac{r-q}{t}. \quad (169)$$

Since the second equality (157) has already fulfilled the constraint (155), associated with the minimization with respect to the parabola height c , we only need to minimize \mathcal{S} over q_- and q_+ to complete the derivation of the saddle-point and of the rare-event tails of the distribution $\mathcal{P}(\eta_r)$ (after we check that this minimum does not give rise to other shocks). In fact, from Eq.(169), in the present case the analog of Eqs.(99) and (148) reads as

$$\mathcal{P}(\eta_r) \sim e^{-\frac{1}{2} \int_{q-}^{q+} dq g(q) \frac{r-q}{t}}. \quad (170)$$

Thus, for overdensities q_+ is defined as a function of η_r from the first Eq.(156), and we only need to minimize \mathcal{S} over q_- to determine the saddle-point and the high-density tail (170). For underdensities q_- is set by the second Eq.(156) and we must minimize \mathcal{S} over q_+ to obtain the low-density tail.

Again, this approach only holds for the rare-event tails, in both limits of large scale/early time at fixed density, and of extreme density at fixed scale and time, where the probability (170) is much smaller than unity. In such regimes, the expression (170) gives the asymptotic tail of the probability distribution at leading order.

5. Tails of the velocity divergence distribution

The method described in the previous section can also be applied to the distribution of the velocity divergence, $\mathcal{P}(\Theta_r)$. As for the quasi-linear regime studied in section IV B the only difference as we go from the overdensity to the velocity divergence is to replace η_r by Θ_r in the

action \mathcal{S} . In particular, we recover the same saddle-point and the same rare-event tail (170), and we only need to specify the relation between Θ_r and the Lagrangian radii q_- and q_+ . Applying the discussion below Eq.(156) to Θ_r , which is given by Eq.(104) for regular points, we now write

$$\Theta_r > 0 : \quad \Theta_r = d \left(\frac{q_+}{r} - 1 \right), \quad (171)$$

$$\Theta_r < 0 : \quad \Theta_r = d \left(\frac{q_-}{r} - 1 \right). \quad (172)$$

This gives back the relation (121), so that the tails of the distribution $\mathcal{P}(\Theta_r)$ can again be obtained (at leading order) from the tails of $\mathcal{P}(\eta_r)$ by substituting the second Eq.(121).

6. Case $n = 0, d = 1$: white-noise initial velocity

Let us describe how this procedure works for the case $\{n = 0, d = 1\}$ (whence $\ell = 0$ in Eq.(159)), where the variance $\sigma_{\delta_{Lr}}^2$ of the linear density contrast is actually divergent, so that shocks must always be taken into account. Using the initial velocity correlation given in Table I, we immediately obtain the solution of Eq.(158),

$$q_- < q < q_+ : g(q) = \frac{r-q}{t}, \quad g(q_{\pm}) = 0, \quad (173)$$

which gives the linear velocity profile

$$q \in [q-, q+] : u_{0q} = \frac{r-q}{t}, \quad q \notin [q-, q+] : u_{0q} = 0. \quad (174)$$

Note that $g(q)$ is singular (discontinuous) at q_{\pm} , since $g(q_{\pm}) = 0$, which gives Dirac terms $\delta_D(q - q_{\pm})$ for the kernel $f(q)$. Then, the action (169) writes

$$\mathcal{S} = y\eta_r + \frac{\sigma_{\psi_{0r}}^2}{6t^2} [(q_+ - r)^3 + (r - q_-)^3]. \quad (175)$$

For overdensities, $\eta_r > 1$, the upper boundary q_+ is given by (156), $q_+ = r\eta_r$, whereas q_- is determined by minimizing \mathcal{S} . This gives $q_- = r$, since $q_- > r$ is excluded as it would give further shocks over the range $[r, q_-]$: we must check that the profile ψ_{0r} does not cross the parabola $\mathcal{P}_{r,c}$ outside of $[q-, q+]$, that is, that the velocity profile does not create a larger shock. For the simple profile (174) we do not need to consider ψ_{0r} to check that no shocks appear beyond $[q-, q+]$. Thus, the system is motionless over $[0, r[$ and $]q_+, +\infty[$, and particles in the range $]r, q_+[$ have the linear initial profile (174) and simultaneously merge at radius r at time t . Note that there appears a rarefaction interval (empty region) over $]r, q_+[$ as the initial velocity is discontinuous at q_+ . This is due to the large power at high k of the initial white-noise energy spectrum (11). We can see that there are no other shocks over disjoint regions that modify the density within radius r at time t , so that we have obtained the

true minimum over symmetric initial conditions. Then, Eq.(170) gives

$$\eta_r > 1 : \mathcal{P}(\eta_r) \sim e^{-r^3(\eta_r-1)^3/(6t^2)}. \quad (176)$$

For underdensities, we obtain by a similar reasoning $q_- = r\eta_r$, $q_+ = r$, and

$$\eta_r < 1 : \mathcal{P}(\eta_r) \sim e^{-r^3(1-\eta_r)^3/(6t^2)}. \quad (177)$$

From Eq.(121) we obtain at once for the velocity divergence Θ_r , which is also the dimensionless velocity increment (22), the tails

$$\mathcal{P}(\Theta_r) \sim e^{-r^3|\Theta_r|^3/(6t^2)}. \quad (178)$$

Since the case $\{n = 0, d = 1\}$ of white-noise one-dimensional initial velocity can actually be solved [15, 30], we can compare the results (176)-(177) with the exact distribution $\mathcal{P}(\eta_r)$. Using the notations of [30], it is known to display the asymptotic behaviors at large scales,

$$X \gg 1, \quad |\eta_r - 1| \gg X^{-1}, \quad \eta_r \gg X^{-3} : \\ \mathcal{P}(\eta_r) \sim e^{-\omega_1 X |\eta_r - 1| - X^3 |\eta_r - 1|^3/12}, \quad (179)$$

and at small scales,

$$X \ll 1, \quad \eta_r \gg X^{-1} : \mathcal{P}(\eta_r) \sim e^{-\omega_1 X \eta_r - X^3 \eta_r^3/12}, \quad (180)$$

where we did not write power-law prefactors, and $-\omega_1$ is the zero of the Airy function $\text{Ai}(x)$ closest to the origin ($\omega_1 \simeq 2.338$). Here X is the dimensionless length of the interval $[-r, r]$ of radius r , whence of size $x = 2r$,

$$X = \frac{2r}{(2Dt^2)^{1/3}} = \frac{2r}{(4t^2)^{1/3}}, \quad \text{hence} \quad \frac{X^3}{12} = \frac{r^3}{6t^2}, \quad (181)$$

since the normalization used in the present paper corresponds to $D = 2$ [61]. Thus, we can check that for large overdensities our saddle-point result (176) agrees with the exact results (179)-(180) at leading order, at both large and small scales. Of course, this only applies to the rare-event tail, which is repelled to larger densities, $\eta_r \gg 1/X$, at small scales in the highly nonlinear regime. For large underdensities, we also recover the exact result (179) at leading order, that applies to large scales. It cannot give the low-density tail in the highly nonlinear regime because this no longer corresponds to rare events. Indeed, as described in [30], at low densities the distribution $\mathcal{P}(\eta_r)$ shows an inverse square root tail, $\propto 1/\sqrt{\eta_r}$, and a Dirac contribution, $\delta_D(\eta_r)$, that both have a weight, of order $e^{-\omega_1 X - X^3/12}$ at large scales, that becomes of order unity at small scales. In fact, on small scales most cells of radius r are actually empty, so that there no longer exists a rare-underdensities tail. Note that this feature can actually be seen on the saddle-point result (177), as we can see that for $r < t^{2/3}$ the exponential becomes of order unity for $\eta_r = 0$. This shows that

empty or almost empty regions are no longer rare, and that the distribution $\mathcal{P}(\eta_r)$ over this range cannot be obtained by a saddle-point approach of the type described in this article.

Finally, it is interesting to note that Eq.(176) agrees with the behavior that would be obtained by a naive extension of Eq.(133) to $\{n = 0, d = 1\}$, even though the derivation of Eq.(132) does not apply to this case (the variance $\sigma_{\delta_{Lr}}^2$ is even divergent). On the other hand, for underdensities Eq.(134) would give $\ln \mathcal{P}(\eta_r) \sim -t^{-2} r^3 \eta_r \rightarrow 0$ for $\eta_r \rightarrow 0$. This shows at once that this cannot give the low-density part of the probability distribution, since we do not find a rare-event tail ($\ln \mathcal{P}(\eta_r) \not\rightarrow -\infty$) but a probability of order unity, which a saddle-point approach cannot describe. As discussed above, this is not a failure of Eq.(134), since there is no rare low-density tail as empty regions occur with a finite probability, that goes to unity at small scales.

Of course, the discussion above also applies to the distribution $\mathcal{P}(\Theta_r)$. Thus, the tail (178) agrees with the exact result for large positive Θ_r in all regimes, and for negative Θ_r in the quasi-linear regime, while on small scales, in the highly nonlinear regime, cells with $\Theta_r \simeq -1$ (associated with almost empty domains) are no longer rare and cannot be described by the method used here. Again, the scalings obtained in the exponential (178) agree with a naive extension of Eq.(135) while the extension of Eq.(137) correctly signals the absence of rare low- Θ_r tail.

7. Case $n = 0, d = 3$

We now consider the case $\{n = 0, d = 3\}$, which gives $\ell = 1$ in Eq.(159). From Eq.(167) the regular part of $g(q)$ is proportional to r/t , and we find for the solution of Eq.(158) with the normalization of $C_{u_{0r}}$ given in Table I,

$$g(q) = \frac{2r}{3t} + \frac{rq_-}{3t} \delta_D(q - q_-) + \frac{2rq_+ - 3q_+^2}{3t} \delta_D(q - q_+). \quad (182)$$

Here the Dirac terms should be understood as $\delta_D[q - (q_{\pm} \mp \epsilon)]$ with $\epsilon \rightarrow 0^+$ (i.e. they have an integral weight of unity within $[q_-, q_+]$). This gives the linear velocity profile

$$q < q_- : u_{0q} = \frac{q(r - q_-)}{tq_-}, \quad q \in [q_-, q_+] : u_{0q} = \frac{r - q}{t}, \\ q > q_+ : u_{0q} = \frac{q_+^2(r - q_+)}{tq^2}, \quad (183)$$

and the action

$$S = y\eta_r + \frac{\sigma_{\psi_{0r}}^2}{6t^2} (4r^2q_+ - 6rq_+^2 + 3q_+^3 - r^2q_-). \quad (184)$$

For overdensities, $\eta_r > 1$, the minimization over q_- gives $q_- = q_+$. Indeed, contrary to the previous case, $\{n = 0, d = 1\}$, it is now possible to have $q_- > r$ without

building a larger shock, as already seen from Fig. 2, since we actually recover the saddle-point of section V A without shocks, as $q_- = q_+$ (i.e. an isolated contact point between the parabola $\mathcal{P}_{r,c}(q)$ and ψ_{0q}). Then, Eq.(170) writes as $\mathcal{P}(\eta_r) \sim e^{-r^3(\eta_r^{1/6} - \eta_r^{1/2})^2/(2t^2)}$, in agreement with Eq.(100) and Table V, and we recover the tail (132) and Table VIII. Indeed, the constraint in (132) is satisfied, so that we already knew that we had to recover that regular saddle-point.

For underdensities, $\eta_r < 1$, the minimization over q_+ gives $q_+ = 2r/3$, so that we only have a shock (i.e. $q_- < q_+$) for $q_- < 2r/3$, that is for low densities below $\eta_* = (2/3)^3$. This agrees with the discussion in section IV A 2 and Table III, where we found that the regular saddle-point (76) only develops a shock after a finite time, that is below a nonzero density contrast threshold. In the quasi-linear limit, $r^3/t^2 \gg 1$, where the range $\eta_* < \eta_r < 1$ already corresponds to large density fluctuations, we can also use the method described in section IV and we obtain the result of Table V. The analysis described above from the action (184) provides the density threshold $\eta_* = (2/3)^3$ written in that Table. From the relation (121), this also gives the velocity divergence threshold $\Theta_* = -1$, above which the quasi-linear distribution $\mathcal{P}(\Theta_r)$ is given by Table VII.

For larger underdensities, $0 < \eta_r < \eta_*$, we have $q_- < q_+$ and we must use the action (184) that takes shocks into account, since we can check that the profile (183) is valid (there are no other shocks that modify the density within radius r). Then, Eq.(170) gives

$$0 < \eta_r < (2/3)^3 : \ln \mathcal{P}(\eta_r) \sim -\frac{r^3}{6t^2} \left(\frac{8}{9} - \eta_r^{1/3} \right). \quad (185)$$

Of course, we can check that at point $\eta_r = \eta_*$ Eq.(185) is equal to the result (100), shown in Table V, which is provided by the regular saddle-point. We can see that below this threshold the dependence on η_r of $\mathcal{P}(\eta_r)$ is modified by shocks. Thus, Eq.(185) provides the very low density tail of $\mathcal{P}(\eta_r)$ in the quasi-linear limit, $r^3/t^2 \gg 1$.

In the nonlinear regime, $r^3/t^2 \ll 1$, the result (185) becomes of order unity over the range $0 \leq \eta_r < \eta_*$. Note that this agrees with the naive extension of Eq.(134), which also yields the correct exponents of r, t and η_r . Then, as for the case $\{n = 0, d = 1\}$ studied in the previous section V B 6, there is no rare underdensities tail, and empty or almost empty regions are not rare. More precisely, there is no exponential decay of $\mathcal{P}(\eta_r)$ at low η_r , but power-law prefactors associated with subleading order terms may give either a power-law growth or falloff at $\eta_r \rightarrow -d$. However, the precise behavior of the distribution $\mathcal{P}(\eta_r)$ for $\eta_r \simeq 0$ cannot be derived through a saddle-point method since there is no rare tail and one should take into account many possible initial configurations.

The previous results directly extend to the distribution $\mathcal{P}(\Theta_r)$. Thus, for large Θ_r we recover the saddle-point of section V A and the tail (135), which applies to both

quasi-linear and highly nonlinear regimes. For low Θ_r , Eq.(185) gives

$$-3 < \Theta_r < -1 : \ln \mathcal{P}(\Theta_r) \sim \frac{r^3}{18t^2} \left(\frac{1}{3} + \Theta_r \right). \quad (186)$$

Again, this provides the very low- Θ_r tail in the quasi-linear regime, which disappears in the highly nonlinear regime where there is no longer a rare-event low- Θ_r tail, and this behavior can also be seen in the naive extension of Eq.(137).

8. Case $n = -1, d = 2$

We now turn to the case $\{n = -1, d = 2\}$. As seen from Table VIII, shocks should only appear for underdensities, as in the previous case $\{n = 0, d = 3\}$. The extension of Eq.(134) gives a vanishing power of η_r , so we can expect a logarithmic dependence on η_r (or a finite asymptote) for $\ln \mathcal{P}(\eta_r)$ at low densities. We again have $\ell = 1$ in Eq.(159), so that the regular part of $g(q)$ is obtained from Eq.(167) as $\propto r/(tq)$, and we find

$$g(q) = \frac{r}{2tq} + \frac{r}{2t} \delta_D(q - q_-) + \frac{r - 2q_+}{2t} \delta_D(q - q_+), \quad (187)$$

and

$$\begin{aligned} q < q_- : u_{0q} &= \frac{q(r - q_-)}{tq_-}, & q \in [q_-, q_+] : u_{0q} &= \frac{r - q}{t}, \\ q > q_+ : u_{0q} &= \frac{q_+(r - q_+)}{tq}, \end{aligned} \quad (188)$$

while the action writes

$$\mathcal{S} = y\eta_r + \frac{\sigma_{\psi_{0r}}^2}{4t^2} \left(r^2 \ln \frac{q_+}{q_-} + 2r^2 - 4rq_+ + 2q_+^2 \right). \quad (189)$$

As expected, for overdensities we recover $q_- = q_+$ (i.e. the regular saddle-point without shock) and $\mathcal{P}(\eta_r) \sim e^{-r^2(\sqrt{\eta_r} - 1)^2/(2t^2)}$, in agreement with Eq.(100) and Table V, and we also recover the tail (132) and Table VIII.

For underdensities we obtain $q_+ = r/2$, so that we only have a shock below $\eta_* = 1/4$, which provides the density threshold written in Table V. Thus, as for the case $\{n = 0, d = 3\}$ and in agreement with section IV A 2, in the quasi-linear regime for rare underdensities in the range $\eta_* < \eta_r < 1$ the distribution $\mathcal{P}(\eta_r)$ is obtained from the method described in section IV, which gives the result of Table V. In terms of the velocity divergence Θ_r , this also provides the threshold $\Theta_* = -1$ of Table VII, and above this threshold the distribution $\mathcal{P}(\Theta_r)$ is given by Eq.(119) and Table VII in the quasi-linear limit.

For lower densities, in the range $0 < \eta_r < \eta_*$, we obtain from Eq.(189)

$$0 < \eta_r < 1/4 : \ln \mathcal{P}(\eta_r) \sim -\frac{r^2}{8t^2} [1 - \ln(4\eta_r)], \quad (190)$$

$$\text{whence } \mathcal{P}(\eta_r) \sim (4\eta_r)^{r^2/(8t^2)} e^{-r^2/(8t^2)}. \quad (191)$$

n	d	$\ln \mathcal{P}(\eta_r)$ for $\eta_r > 1$	$\ln \mathcal{P}(\eta_r)$ for $\eta_r < 1$	$\ln \mathcal{P}(\Theta_r)$ for $\Theta_r > 0$	$\ln \mathcal{P}(\Theta_r)$ for $\Theta_r < 0$
0	1	$-\frac{r^3}{6t^2} (\eta_r - 1)^3$	$-\frac{r^3}{6t^2} (1 - \eta_r)^3$	$-\frac{r^3}{6t^2} \Theta_r^3$	$-\frac{r^3}{6t^2} (-\Theta_r)^3$
0	3	no shock	$-\frac{r^3}{6t^2} \left(\frac{8}{9} - \eta_r^{1/3} \right)$ for $\eta_r < \frac{8}{27}$	no shock	$\frac{r^3}{18t^2} \left(\frac{1}{3} + \Theta_r \right)$ for $\Theta_r < -1$
-1	2	no shock	$-\frac{r^2}{8t^2} [1 - \ln(4\eta_r)]$ for $\eta_r < \frac{1}{4}$	no shock	$-\frac{r^2}{8t^2} [1 - 2 \ln(2 + \Theta_r)]$ for $\Theta_r < -1$

TABLE IX: The tails of the distributions $\mathcal{P}(\eta_r)$ and $\mathcal{P}(\Theta_r)$ for the initial conditions of Table I, in cases where shocks appear. These results also hold for the quasi-linear limit, $t \rightarrow 0$ or $r \rightarrow \infty$, at fixed η_r or Θ_r , but only below the thresholds given in this Table for the last two rows (higher densities and velocity divergences are described by Tables V, VII). For $\{n = 0, d = 1\}$, these results hold in the quasi-linear limit for any $\eta_r \neq 1$ and $\Theta_r \neq 0$. In the highly nonlinear limit, $r \rightarrow 0$ or $t \rightarrow \infty$, the rare-event tails at low η_r and Θ_r disappear as low densities and velocity divergences are no longer rare ($\ln \mathcal{P}$ in this Table becomes of order unity and these formulae are no longer valid). Cases marked as “no shock” correspond to saddle-points that do not give rise to shocks, so that the results of Tables V, VII and VIII are valid.

Again, at the transition $\eta_r = \eta_*$ Eq.(190) is equal to Eq.(100) shown in Table V. Thus, we obtain as expected a logarithmic dependence over η_r for $\ln \mathcal{P}(\eta_r)$, in agreement with (134). In the quasi-linear regime, $r^2/t^2 \gg 1$, Eq.(191) means that the low-density tail has a power-law behavior $\mathcal{P}(\eta_r) \sim \eta_r^\alpha$, with an exponent $\alpha \sim r^2/(8t^2)$ that grows at large scales and early times, so that the low-density falloff is increasingly sharp. However, because there could be a power-law prefactor in Eq.(191) due to sub-leading corrections to the steepest-descent approximations, this is unlikely to give the exact exponent α but only its behavior at large r and small t . Then, in the nonlinear regime, $r^2/t^2 \ll 1$, Eq.(191) is not sufficient to give the behavior of $\mathcal{P}(\eta_r)$ for $\eta_r \rightarrow 0$, as these prefactors may either give a positive or negative exponent. This limiting configuration between the cases $n > -1$, where empty or almost empty regions have a finite probability at small scales, and $n < -1$, where low densities exhibit an exponential tail of the form (134), requires a finer analysis in the nonlinear regime.

For large velocity divergence Θ_r we recover the tail (135) associated with the regular saddle-point while for low Θ_r Eqs.(190) and (121) yield

$$-2 < \Theta_r < -1 : \ln \mathcal{P}(\Theta_r) \sim \frac{-r^2}{8t^2} [1 - 2 \ln(2 + \Theta_r)], \quad (192)$$

$$\text{whence } \mathcal{P}(\Theta_r) \sim (2 + \Theta_r)^{r^2/(4t^2)} e^{-r^2/(8t^2)}. \quad (193)$$

This only gives the behavior at low Θ_r in the quasi-linear regime, $r^2/t^2 \gg 1$, as in the nonlinear regime power-law prefactors may lead either to a growth or decay of $\mathcal{P}(\Theta_r)$, but in both cases there is no rare-event tail (i.e. no exponential falloff).

9. Summary for low integer n and d

We summarize in Table IX the results obtained from the approach developed in the previous sections for the tails of the distributions $\mathcal{P}(\eta_r)$ and $\mathcal{P}(\Theta_r)$, for the initial

n	d	$\ln[n(m)]$ for $m \rightarrow \infty$
0	1	$-m^3/(48t^2 \rho_0^3)$
0	3	$-3m/(8\pi t^2 \rho_0)$
-1	2	$-m/(2\pi t^2 \rho_0)$
-2	1	$-m/(4t^2 \rho_0)$
-2	3	$-\frac{5}{8t^2} [3m/(4\pi \rho_0)]^{1/3}$

TABLE X: Large-mass tail of the mass function $n(m)$ of point-like objects, for the initial conditions of Table I, from Eq.(196).

conditions of Table I where shocks cannot be neglected. This complements the Table VIII that applies to cases where the saddle-point does not form shocks.

These rare-event tails apply to the large fluctuation limits, $\eta_r \rightarrow \infty$ and $\eta_r \rightarrow 0$, or $\Theta_r \rightarrow \infty$ and $\Theta_r \rightarrow -d$, at fixed time and scale, whatever the value of the variance $\sigma_{\delta_{Lr}}^2$ or $\sigma_{\psi_{0r}}^2$.

They also apply to the quasi-linear limit, $\sigma_{\delta_{Lr}} \rightarrow 0$ or $\sigma_{\psi_{0r}} \rightarrow 0$, that is at early times or large scales, at fixed η_r and Θ_r , below some finite thresholds η_* and Θ_* in the two cases $\{n = 0, d = 3\}$ and $\{n = -1, d = 2\}$, and for any $\eta_r \neq 1$ and $\Theta_r \neq 0$ in the case $\{n = 0, d = 1\}$.

For these three cases, in the highly nonlinear regime, $r \rightarrow 0$ or $t \rightarrow \infty$, the rare-event tail at low η_r and Θ_r disappears as these results predict that $\ln \mathcal{P}$ becomes of order unity. Then, low densities and velocity divergences are no longer rare (but the probability distribution might still decay as a power law) and cannot be described by a saddle-point approach.

C. Mass function of point-like singularities

As the density and velocity fields evolve through the nonlinear Burgers dynamics, starting from the scale-free initial conditions (6), the system displays an intricate self-similar progression from smaller to larger scales. In particular, collisions between particles create discontinuities (shocks) of dimension $d-1$, $d-2$, ..., down to 0, lower dimensional objects arising at the intersection of higher-dimension structures. For instance, if $d = 3$, once particles have formed a two-dimensional sheet of finite surface density, orthogonal to the direction of the largest eigenvalue of the initial tidal tensor, they keep moving within this surface and form critical lines and nodes. Then, the typical distance between such objects increases as $L(t)$, as in (44), and their mass grows accordingly. The mass and the overdensity within radius r about a point \mathbf{x} , contained in such a D -dimensional structure, scale as

$$r \rightarrow 0 : m(< r) \sim \mu r^D, \quad (194)$$

$$\eta_r = \frac{m(< r)}{\rho_0 V} \sim r^{D-d}. \quad (195)$$

Thus, at small scales we can see that very large densities are associated with the lowest-dimension objects, $D = 0$, and the contribution of these point-like masses to the probability distribution $\mathcal{P}(\eta_r)$ reads as

$$r \rightarrow 0, \eta_r \rightarrow \infty : \mathcal{P}(\eta_r)d\eta_r \sim Vn(m)dm, \quad (196)$$

where V is the volume of the sphere of radius r and $n(m)$ is the mass function of point-like masses, that is, $n(m)dmd\mathbf{x}$ is the mean number of such objects of 0-dimension, with a mass in the range $[m, m + dm]$, within the volume element $d\mathbf{x}$. Then, from Eq.(133) we obtain for the high-mass tail

$$m \rightarrow \infty : \ln[n(m)] \propto -\frac{m^{(n+3)/d}}{t^2}. \quad (197)$$

Indeed, we have seen in section VB that the scaling (133), that was derived in section VA1 for $n \leq d-3$, actually extends to the full range $-3 < n < 1$, but the proportionality factor is no longer set by Eq.(132). However, in the range $n \leq d-3$, this numerical factor is given by Eq.(132), while for $d-3 < n < 1$ it can be obtained from the analysis described in section VB, and from Table IX for the associated integer values $n = 0$ and $d = 1$. We show our results in Table X for the high-mass tail of the mass function $n(m)$ of point-like objects, for the initial conditions of Table I.

Of course, as for the density and velocity distributions, these results agree with the exact expressions that can be obtained in the two cases $\{n = 0, d = 1\}$ and $\{n = -2, d = 1\}$ [14, 15, 16, 17, 18, 29, 30]. For more general cases, the scaling (197) was already conjectured in [11, 14], from numerical simulations and heuristic arguments, and proved in [19] for $-1 < n < 1$ with $d = 1$ (with upper and lower bounds for the proportionality factor).

D. Pre-shock singularities

Before we conclude, we should add a few comments on the comparison of this work with studies of pre-shock singularities [3]. As shown in [57], for smooth initial conditions large densities are localized near “kurtoparabolic” singularities residing on space-time manifolds of codimension two. They lead to universal density tails $\mathcal{P}(\eta) \sim \eta^{-7/2}$ in any dimension. In one dimension, this corresponds to pre-shocks [58, 59], that is, when a shock forms the Lagrangian potential changes from a single extremum to three extrema and at the transition, where its second derivative vanishes, one can see through a Taylor expansion that the Eulerian density field behaves as $x^{-2/3}$ close to the singularity. Then, the contribution from the neighborhood of such events (both in space and time) yields a power-law tail $\mathcal{P}(\eta) \sim \eta^{-7/2}$. This can also be extended to higher dimensions [3, 57]. These results apply to the unsmoothed density field for smooth initial conditions. By contrast, in the present article we study the smoothed density and velocity fields, that is we always consider the mean density and velocity increment over a finite radius r , for non-smooth initial conditions described by the power-law power spectra (18). Thus, these are two very different regimes. In particular, this explains why we obtain probability distributions that depend on both the dimension d and the slope n of the initial power spectrum (over the range $-3 < n < 1$), rather than universal tails. We can note from Eq.(133) that in the regime studied here the probability distribution $\mathcal{P}(\eta_r)$ shows a large-density exponential tail with a characteristic cutoff $\eta_r \sim r^{-d}$ that goes to infinity as $r \rightarrow 0$. Then, at very small scales (i.e. in the highly nonlinear regime) an intermediate power-law regime can develop below this upper cutoff. However, this power law is not universal either, since the exact results obtained in [18, 30] show that for $d = 1$ we have $\mathcal{P}(\eta_r) \sim \eta_r^{-3/2}$ if $n = -2$, see also Eq.(103), and $\mathcal{P}(\eta_r) \sim \eta_r^{-1/2}$ if $n = 0$.

We can note that for the forced Burgers equation similar universal power-law tails can be obtained using instanton methods (i.e. looking for relevant saddle-points, that correspond to shocks) [52], although there is some debate on the exact value of the exponent, which might depend on the influence of the boundary conditions [59, 60]. Again, these results consider a smooth forcing so that the exponent is set by the dynamics of a single shock and is universal. For singular forcing (i.e. with significant power at high wavenumbers) one might obtain non-universal results for the density and velocity increments over finite radius r , in a fashion similar to the free case studied here. However, this goes beyond the scope of this article.

VI. CONCLUSION

We have studied in this article some asymptotic properties of decaying Burgers turbulence in d dimensions. Focussing on the case of random Gaussian initial velocities and a uniform initial density, we considered power-law initial energy spectra such that the evolution is self-similar. Thus, the system displays a hierarchical evolution and the integral scale of turbulence, $L(t)$, that is generated by the Burgers dynamics and separates the large-scale quasi-linear regime from the small-scale highly nonlinear regime, grows with time as a power law, $L(t) \propto t^{2/(n+3)}$. Then, in order to take advantage of the statistical homogeneity and isotropy of the system (once we have taken care of the infrared divergence if $n \leq -1$), we have defined the spherical quantities, η_r and Θ_r , that are the overdensity and the velocity increment over a sphere of radius r . This allows to preserve the statistical isotropy of the problem and to handle the case of large dimensions $d > 1$.

We have first recalled how such a nonlinear dynamics can be studied through standard perturbative expansions. Here this corresponds to expansions over powers of time, or equivalently over powers of the initial velocity fluctuations. This approach is quite flexible, as it does not require any symmetry, but it becomes very heavy at high orders. It can be somewhat simplified when one focusses on spherically symmetric quantities such as η_r and Θ_r , defined through a real-space top-hat filter, but it remains cumbersome for arbitrary dimensions. We have pointed out that from a perturbative point of view the Burgers dynamics in the inviscid limit is equivalent to the Zeldovich dynamics. This means that shocks are not taken into account and require non-perturbative methods.

Next, we have described how to derive the asymptotic probability distributions $\mathcal{P}(\eta_r)$ and $\mathcal{P}(\Theta_r)$ reached in the quasi-linear regime from a saddle-point approximation. This method allows to obtain at once the asymptotic cumulant generating function $\varphi(y)$, the Taylor expansion of which provides the leading-order term for each cumulant $\langle \eta_r^p \rangle_c$, that would be obtained from the previous perturbative expansion truncated at order $p - 1$. In addition, the generating function $\varphi(y)$ being obtained directly through a steepest-descent computation, one can go beyond its apparent singularities (associated with large high-order cumulants and slowly decaying tails for the probability distributions) and make sense of possible secondary branches, that are found when this function appears to be multivalued. This approach takes advantage of the spherical symmetry of the observables η_r and Θ_r to reduce the problem to a one-dimensional system, as the relevant saddle-point (instanton) is also spherically symmetric. This allows to derive simple results for arbitrary dimension d , provided this instanton has not formed shocks yet.

Then, from the radial profile of this saddle-point, we have found that these results only apply to the range of

initial energy spectrum index $-3 < n \leq d - 3$ (within $-3 < n < 1$), and only above a nonzero underdensity if $-2 < n \leq d - 3$. For $n \geq d - 2$ the quasi-linear regime does not really exist. More precisely, the overdensity and velocity divergence η_r and Θ_r are already divergent at linear order and their distributions do not converge towards a Gaussian at early time or large scale, in spite of the Gaussianity of the initial conditions. Thus, the system is always dominated by shocks. For $d - 3 < n < d - 2$ the linear theory is well defined, so that one recovers Gaussian distributions at very early times or large scales, but the saddle-point forms shocks as soon as $t > 0$. Then, the qualitative results obtained from this steepest-descent approach should remain valid and still provide a reasonable quantitative approximation, as shocks appear over a limited range of radii, but they are expected to be modified by prefactors of order unity.

Thus, in order to describe the cases $d - 3 < n < 1$, as well as very large underdensities for $-2 < n \leq d - 3$, it is necessary to take into account shocks. We have shown how to modify this saddle-point method, taking advantage of the geometrical interpretation of the Hopf-Cole solution in terms of first-contact paraboloids, to handle these cases. This allows us to find out the instantons, which contain shocks, that provide the leading-order behavior of the rare-event tails of $\mathcal{P}(\eta_r)$ and $\mathcal{P}(\Theta_r)$. Focussing on some low integer values of n and d , where simple explicit results can be derived, we have obtained the asymptotic tails of these probability distributions, at any finite time and scale, for the cases $\{n, d\} = \{0, 1\}$, $\{0, 3\}$ and $\{-1, 2\}$. We note that the scalings actually agree with a naive extension of those obtained from the regular saddle-point computation. This also gives the high-mass tail of the mass function of point-like singularities (i.e. Dirac peaks in the density field, which correspond to shock strengths in the one-dimensional case).

Then, we find that for $n < -1$ the very low density tail shows an exponential cutoff of the form $e^{-\eta_r^{(n+1)/2}}$, whereas for $n > -1$ there is no exponential falloff (but there could be a power-law decline). For the latter cases, in the quasi-linear regime, this part of the probability distribution $\mathcal{P}(\eta_r)$ corresponds to extremely rare underdensities and has a negligible weight, and around moderate fluctuations, $|\eta_r - 1| \ll 1$, the distribution shows a falloff on both sides of the mean $\langle \eta_r \rangle = 1$. In the highly nonlinear regime, this intermediate low-density regime disappears and low-density (and empty) regions are no longer rare. Then, one needs another method to describe the low-density part of the probability distribution at small scales.

Throughout this article, we have checked that our results agree with the two one-dimensional cases of white-noise initial velocity ($n = 0$) and Brownian initial velocity ($n = -2$), where many exact results are known, thanks to the Markovian properties shared by both cases, which allow a derivation of explicit formulae through specific methods. Note that these two cases are representative of the two classes of initial conditions, $-1 < n < 1$ and

$-3 < n < -1$, where the initial velocity is dominated by small/long wavelengths and which exhibit the different behaviors discussed above. Hence they provide a good check of the general methods presented in this article. In addition to the interest of the asymptotic behaviors obtained here, we can hope that they could serve as a bench-

mark to test other approximation schemes, devised to study additional quantities such as typical events. Moreover, since the approach developed in this paper is rather general - for instance it was already applied to the gravitational dynamics - it may also prove useful for other systems.

-
- [1] J. M. Burgers, *The nonlinear diffusion equation* (D. Reidel, Dordrecht, 1974).
- [2] S. Kida, *J. Fluid Mech.* **93**, 337 (1979).
- [3] J. Bec and K. Khanin, *Phys. Rep.* **447**, 1 (2007).
- [4] U. Frisch, *Turbulence* (Cambridge University Press, Cambridge, 1995).
- [5] E. Hopf, *Commun. Pure Appl. Mech.* **3**, 201 (1950).
- [6] J. D. Cole, *Quart. Appl. Math.* **9**, 225 (1951).
- [7] J.-D. Fournier and U. Frisch, *J. Mec. Theor. Appl.* **2**, 699 (1983).
- [8] S. N. Gurbatov, A. Malakhov, and A. Saichev, *Nonlinear random waves and turbulence in nondispersive media: waves, rays and particles* (Manchester University Press, 1991).
- [9] P. L. Doussal (2008), arXiv:0809.1192.
- [10] S. N. Gurbatov, A. I. Saichev, and S. F. Shandarin, *Mont. Not. Roy. Astron. Soc.* **236**, 385 (1989).
- [11] M. Vergassola, B. Dubrulle, U. Frisch, and A. Noullez, *Astron. Astrophys.* **289**, 325 (1994).
- [12] A. L. Melott, S. F. Shandarin, and D. H. Weinberg, *Astrophys. J.* **428**, 28 (1994).
- [13] S. N. Gurbatov, S. I. Simdyankin, E. Aurell, U. Frisch, and G. Toth, *J. Fluid Mech.* **344**, 339 (1997).
- [14] Z.-S. She, E. Aurell, and U. Frisch, *Commun. Math. Phys.* **148**, 623 (1992).
- [15] L. Frachebourg and P. A. Martin, *J. Fluid Mech.* **417**, 323 (2000).
- [16] Y. G. Sinai, *Commun. Math. Phys.* **148**, 601 (1992).
- [17] J. Bertoin, *Commun. Math. Phys.* **193**, 397 (1998).
- [18] P. Valageas, *J. Stat. Phys.* **134**, 589 (2009).
- [19] G. M. Molchan, *J. Stat. Phys.* **88**, 1139 (1997).
- [20] A. Noullez, S. N. Gurbatov, E. Aurell, and S. I. Simdyankin, *Phys. Rev. E* **71**, 056305 (2005).
- [21] U. Frisch, J. Bec, and E. Aurell, *Phys. Fluids* **17**, 081706 (2005).
- [22] P. J. E. Peebles, *Astrophys. J.* **263**, L1 (1982).
- [23] E. Komatsu, J. Dunkley, and M. R. N. et al., *ApJS* **180**, 330 (2009).
- [24] P. J. E. Peebles, *The large scale structure of the universe* (Princeton university press, Princeton, 1980).
- [25] Y. B. Zeldovich, *Astron. Astrophys.* **5**, 84 (1970).
- [26] F. Bernardeau, S. Colombi, E. Gaztañaga, and R. Scocimarro, *Phys. Rep.* **367**, 1 (2002).
- [27] S. Colombi, F. R. Bouchet, and L. Hernquist, *Astrophys. J.* **465**, 14 (1996).
- [28] M. Avellaneda and W. E, *Commun. Math. Phys.* **172**, 13 (1995).
- [29] M. Avellaneda, *Commun. Math. Phys.* **169**, 45 (1995).
- [30] P. Valageas (2009), arXiv:0903.0956.
- [31] M. H. Goroff, B. Grinstein, S.-J. Rey, and M. B. Wise, *Astrophys. J.* **311**, 6 (1986).
- [32] R. Kraichnan, *J. Fluid Mech.* **41**, 189 (1970).
- [33] Y. Kaneda, T. Ishihara, and K. Gotoh, *Phys. of Fluids* **11**, 2154 (1999).
- [34] P. Valageas, *Astron. Astrophys.* **476**, 31 (2007).
- [35] B. Grinstein and M. B. Wise, *Astrophys. J.* **320**, 448 (1987).
- [36] J. N. Fry, *Astrophys. J.* **279**, 499 (1984).
- [37] F. Bernardeau, *Astrophys. J.* **433**, 1 (1994).
- [38] F. Bernardeau and L. Kofman, *Astrophys. J.* **443**, 479 (1995).
- [39] P. Valageas, *Astron. Astrophys.* **382**, 412 (2002).
- [40] P. C. Martin, E. D. Siggia, and H. A. Rose, *Phys. Rev. A* **8**, 423 (1973).
- [41] R. Phythian, *J. Phys. A* **10**, 777 (1977).
- [42] R. V. Jensen, *J. Stat. Phys.* **25**, 183 (1981).
- [43] C. D. Dominicis, *J. Phys. Colloq.* **37**, 247 (1976).
- [44] J. Zinn-Justin, *Quantum field theory and critical phenomena* (Clarendon Press, Oxford, 1989).
- [45] P. Valageas, *Astron. Astrophys.* **465**, 725 (2007).
- [46] V. Gurarie and A. Migdal, *Phys. Rev. E* **54**, 4908 (1996).
- [47] H. C. Fogedby, *Phys. Rev. E* **57**, 4943 (1998).
- [48] G. Falkovich, I. Kolokolov, V. Lebedev, and A. Migdal, *Phys. Rev. E* **54**, 4896 (1996).
- [49] C.-Y. Mou and P. B. Weichman, *Phys. Rev. Lett.* **70**, 1101 (1993).
- [50] R. Kraichnan, *J. Fluid Mech.* **5**, 497 (1959).
- [51] E. Balkovsky, G. Falkovich, I. Kolokolov, and V. Lebedev, *Phys. Rev. Lett.* **78**, 1452 (1997).
- [52] L. Morichoni, *Phys. Rev. E* **79**, 046324 (2009).
- [53] F. Bernardeau, *Astrophys. J.* **392**, 1 (1992).
- [54] F. Bernardeau, *Astron. Astrophys.* **291**, 697 (1994).
- [55] P. Valageas, *Astron. Astrophys.* **337**, 655 (1998).
- [56] P. Valageas, *Astron. Astrophys.* **382**, 450 (2002).
- [57] U. Frisch, J. Bec, and B. Villone, *Physica D* **152-153**, 620 (2001).
- [58] J. Bec and U. Frisch, *Phys. Rev. E* **61**, 1395 (2000).
- [59] W. E, K. Khanin, A. Mazel, and Y. Sinai, *Phys. Rev. Lett.* **78**, 1904 (1997).
- [60] S. Boldyrev, T. Linde, and A. Polyakov, *Phys. Rev. Lett.* **93**, 184503 (2004).
- [61] In [30] the initial velocity correlation was normalized as $\langle u_0(q_1)u_0(q_2) \rangle = D \delta_D(q_1 - q_2)$, so that the normalization used in the present paper, given in Table I, corresponds to $D = 2$. Indeed, going from the velocity $u_0(q)$ to its radial component u_{0r} , which in this one-dimensional case writes $u_{0r} = [u_0(r) + u_0(-r)]/2$ (symmetric component), multiplies the two-point correlation by a factor $1/2$.